

PLATINUM(II) COMPOUNDS AND NUCLEOLAR STRESS

by

EMILY CATHERINE SUTTON

A DISSERTATION

Presented to the Department of Biology
and the Graduate School of the University of Oregon
in partial fulfillment of the requirements
for the degree of
Doctor of Philosophy

June 2020

DISSERTATION APPROVAL PAGE

Student: Emily Catherine Sutton

Title: Platinum(II) Compounds and Nucleolar Stress

This dissertation has been accepted and approved in partial fulfillment of the requirements for the Doctor of Philosophy degree in the Department of Biology by:

Alice Barkan	Chairperson
Victoria DeRose	Advisor
Eric Selker	Core Member
Michael Harms	Core Member
Tristan Ursell	Institutional Representative

and

Kate Mondloch	Interim Vice Provost and Dean of the Graduate School
---------------	--

Original approval signatures are on file with the University of Oregon Graduate School.

Degree awarded June 2020

DISSERTATION ABSTRACT

Emily Catherine Sutton

Doctor of Philosophy

Department of Biology

October 2020

Title: Platinum(II) Compounds and Nucleolar Stress

Platinum(II) chemotherapeutic agents represent a critical class of anticancer compounds. The clinical use of these compounds is limited by side effects and development of resistance. Despite these limitations, the three FDA approved Pt(II) drugs – cisplatin, carboplatin, and oxaliplatin – remain an important treatment option for many cancers. The molecular mechanisms of these drugs remain unresolved and are the subject of significant investigation. One area of investigation is the impact that Pt(II) compounds have on ribosome biogenesis and the nucleolus. Existing literature has shown that oxaliplatin, but not cisplatin or carboplatin, kill cancer cells via the ribosome biogenesis stress response. This work seeks to clarify the relationship between Pt(II) compounds and ribosome biogenesis stress, alternatively referred to as nucleolar stress. Chapter I provides background on Pt(II) chemotherapeutic agents, the nucleolus, and ribosome biogenesis. Chapter II uses a structure-activity approach to identify unique structural properties that are responsible for nucleolar stress induction as measured by the redistribution of the nucleolar protein nucleophosmin (NPM1) in A549 cells. Chapter III pairs NPM1 redistribution with pulse-chase radiolabeling assays and imaging of other

nuclear and nucleolar proteins to establish that reduced transcription of ribosomal RNA transcripts is an early step responsible for nucleolar stress induction by oxaliplatin.

Chapter IV summarizes existing methods that allow tracking of Pt(II) compounds in cells, and describes the development of an assay to identify binding sites of Pt(II) on DNA in cells. These analyses allow for a more comprehensive understanding of the relationship between Pt(II) compounds and nucleolar stress.

This dissertation contains published and unpublished co-authored material.

© 2020 Emily Catherine Sutton

CURRICULUM VITAE

NAME OF AUTHOR: Emily Catherine Sutton

GRADUATE AND UNDERGRADUATE SCHOOLS ATTENDED:

University of Oregon, Eugene, OR

University of Maryland College Park, College Park, MD

DEGREES AWARDED:

Doctor of Philosophy, Biology, 2020, University of Oregon

Bachelor of Science, Biology, 2011, University of Maryland College Park

AREAS OF SPECIAL INTEREST:

Molecular Biology

Nucleolar Stress

Platinum Chemotherapeutics

PROFESSIONAL EXPERIENCE:

Graduate Employee, University of Oregon, 2014-2020

Intern, Associate Scientist II, Qiagen, Inc, Gaithersburg, MD 2011-2013

Undergraduate Researcher, University of Maryland College Park, 2010-2011

GRANTS, AWARDS, AND HONORS:

Best Talk, ASBMB Emerging Roles of the Nucleolus Symposium, 2019

Fellow, Science Literacy Program, University of Oregon, 2018

NIH Training Grant, Molecular Biology and Biophysics, University of Oregon,
2016-2018

Borgen Adamson Memorial Scholarship, University of Oregon Institute of
Molecular Biology, 2014

PUBLICATIONS:

Sutton, Emily C., Christine E. McDevitt, Matthew V. Yglesias, Rachael M. Cunningham, and Victoria J. DeRose. "Tracking the Cellular Targets of Platinum Anticancer Drugs: Current Tools and Emergent Methods." *Inorganica Chimica Acta*, June 26, 2019, 118984.

McDevitt, Christine E., Matthew V. Yglesias, Austin M. Mroz, **Emily C. Sutton**, Min Chieh Yang, Christopher H. Hendon, and Victoria J. DeRose. "Monofunctional Platinum(II) Compounds and Nucleolar Stress: Is Phenanthriplatin Unique?" *JBIC Journal of Biological Inorganic Chemistry*, September 7, 2019.

Sutton, Emily C.*, Christine E. McDevitt*, Jack Y. Prochnau, Matthew V. Yglesias, Austin M. Mroz, Min Chieh Yang, Rachael M. Cunningham, Christopher H. Hendon, and Victoria J. DeRose. 2019. “Nucleolar Stress Induction by Oxaliplatin and Derivatives.” *Journal of the American Chemical Society* 141 (46): 18411–15. *co-first authors

Sutton, Emily C., Victoria J. DeRose. “Mechanisms of oxaliplatin-induced nucleolar stress”, *in preparation*

ACKNOWLEDGEMENTS

First and foremost I would like to thank my advisor, Dr. Victoria DeRose, for her mentorship and guidance over the years. I truly enjoyed to opportunity to work in a lab that was so collaborative and where I was able to explore my research interests. Your advice, scientific wisdom, and facilitation of a welcoming lab environment were essential to my success in graduate school. I would also like to thank my committee chair, Dr. Alice Barkan, and the rest of my committee – Dr. Eric Selker, Dr. Mike Harms, and Dr. Tristan Ursell – for their guidance and support, and for challenging me to develop a rigorous and fascinating research project.

Thanks also to the many members of the DeRose lab. Rachael Cunningham and Emily Reister, you were both formative in helping me feel welcome to the lab and helping me navigate the unfamiliar territory of academic life. Your warmth and mentorship will be remembered. Rachael, I will never forget the expert scientific and general guidance you shared with not just me but the whole lab. Emily, you were always able to provide perspective, insight, and sharp analysis. Christy and Matthew, thank you for being great co-authors and friends. Christy, I will miss listening to you explain your latest craft project while making buffers, laughing while writing papers in the conference room, and spontaneous heart-to-heart conversations. Matthew, your insights, good nature, and sense of humor were a welcome addition to the lab. To the many other current and former members of the lab – Dr. Kory Plakos, Dr. Alan Moghaddam, Dr. Anja Busseman, Geri Laudenbach, Anna Hickey, Valentina Guevara, Olive Anagu, Michael Shaw, Jack Prochnau, Regina Wirth, Hannah Pigg, Dillon Willis, and more – thank you for your contributions and your role in creating such a supportive research community over the years. To many others I encountered through research and teaching – Stu Johnson, Gabrielle Andrew, Annie Rogers, Dr. Stacey Wagner, Pete Batzel, Dr. Leslie Coonrod, Dr. Clay Small, Katie Pérez, Dr. Alan Kelly, Dr. Debbie Schlenoff, Dr. Amy Connolly, and many more – thank you for being a part of my grad school journey.

Thanks to my many Oregon friends and comrades who I was fortunate to know as a researcher, student, union member, roommate, and community member. There are far

too many of you to name here but the moments we shared sustained me, gave me hope for the future, and truly built a home for me here. Particular gratitude goes to Aleesa and Maria. I could not have picked more supportive and brilliant friends for my cohort. Our hang-outs, coffee check-ins, practice talks, and general camaraderie were a sustaining force for me throughout grad school. I will miss having you as colleagues, and I am so excited to see what comes next for both of you.

To my friends and family outside of Oregon – thank you for finding ways to support me from a distance. Caitlin, I am so glad that you got the chance to visit me out here and grateful for our very long phone calls. Allison, Meaghan, and Joy – the times we were able catch up were truly rejuvenating. Thanks to my family for their belief in me and for truly making me feel like a superstar for being the first in the family to get a PhD. Particular thanks go to my parents, John and Donna, my siblings Addie and Clark, my aunt Roberta, my cousins Ellie and Kristine, and my late grandmothers Shirl and Aurore. Addie and Clark, words cannot express how much I have missed you both over the last six years. Often when I was struggling here in Oregon and thought about quitting, I kept going because I wanted to make you both proud. Lastly, I want to thank Ricardo. Thank you for your unwavering faith in me and your steadfast support which took seemingly limitless forms. At certain points while finishing this dissertation, the conditions were so challenging that they were almost comical (multiple lab floods, broken equipment, a global pandemic, unprecedented wildfires, and more). Through all of it, sharing time and space with you has truly been a gift. I will forever cherish your thoughtfulness, care, and infinitely unique perspective on the world.

For Addie and Clark

TABLE OF CONTENTS

Chapter	Page
CHAPTER I: INTRODUCTION.....	1
Background	1
Differential Effects of Pt(II) Compounds.....	5
Ribosome biogenesis and the nucleolus.....	7
The Nucleolus and Cancer	10
Pt(II) Compounds and the Nucleolus	11
Bridge to Chapter II.....	13
CHAPTER II: NUCLEOLAR STRESS INDUCTION BY OXALIPLATIN AND DERIVATIVES	14
Nucleolar Stress Induction by Oxaliplatin and Derivatives	14
Bridge to Chapter III	24
CHAPTER III: MECHANISMS OF PLATINUM-INDUCED NUCLEOLAR STRESS	25
Introduction	25
Results	30
Onset of NPM1 redistribution	30
Oxaliplatin but not cisplatin causes inhibition of rRNA transcription	32
Inhibition of rRNA transcription coincides with NPM1 redistribution upon oxaliplatin treatment	36
Pol I inhibition and DNA damage	37
Cisplatin and oxaliplatin both result in downstream p53 stabilization.....	40
Nucleolar integrity following Pt(II) treatment.....	41
Discussion	44
Bridge to Chapter IV	47

Chapter	Page
CHAPTER IV: IDENTIFYING INTRACELLULAR TARGETS OF PT(II)	48
Introduction	48
Pt(II) Interactions with nucleic acids	49
Pt(II) Interactions with RNA.....	51
Pulldown Studies to Identify Pt(II) Interactions with DNA.....	53
Detection of Platinum Using Pre-tethered Fluorophores	58
Click chemistry for post-treatment tethering to platinum compounds.....	61
Review Conclusion	63
A Pulldown Assay for Platinated DNA Utilizing a Clickable Pt(II) Derivate.....	63
Bridge to Chapter V	69
CHAPTER V: CONCLUDING REMARKS.....	70
Summary	70
Future directions.....	71
APPENDIX A: SUPPLEMENTARY INFORMATION FOR CHAPTER 2	74
Supplementary Figures.....	74
Supplementary Tables.....	79
Materials and Methods	81
APPENDIX B: SUPPORTING INFORMATION FOR CHAPTER III	90
Materials and Methods:.....	90
Supplementary Figures:.....	93
APPENDIX C: SUPPORTING INFORMATION FOR CHAPTER IV	95
Materials and Methods	95
Supplementary Figures.....	97
REFERENCES CITED.....	98

LIST OF FIGURES

Figure	Page
1.1. Chemical structures of the three platinum(II) chemotherapeutics.....	1
1.2. Cellular uptake and aquation of cisplatin.....	3
1.3. Ribosome biogenesis and the nucleolus	11
2.1. Compounds tested for inducing nucleolar stress via NPM1 relocalization	16
2.2. Nucleolar stress induced by Pt(II) compounds	17
2.3. Quantification of NPM1 relocalization induced by Pt(II) compounds.....	19
2.4. Size and hydrophobicity correlate to stress induction	21
2.5. Measurements and structures of non stress-inducing compounds.....	23
3.1. Time of redistribution of NPM1 upon treatment with platinum compounds	32
3.2. NPM1 relocalization and inhibition of rRNA transcription at 90 minutes.....	35
3.3. NPM1 relocalization and inhibition of rRNA transcription at 3 hours.....	37
3.4. DNA damage and p53 stabilization after treatment with Pt(II).....	42
3.5. Fibrillarin imaging after treatment with Pt(II) compounds.....	41
4.1. Pt(II) anticancer drugs currently approved for use in the United States.....	49
4.2. Platinum click schematic	64
4.3. Platinum click pulldown gel	65
4.4. Schematic of <i>in cellulo</i> Pt(II) pulldown experiment.....	66
4.5. Relevant findings from pilot Pt(II) pulldown study.....	68
4.6. rDNA is not enriched in Pt(II) pulldown samples	69

Figure	Page
A.1. NPM1 assay and quantification scheme	74
A.2. Additional images for compounds tested.....	75
A.3. Volume and hydrophobicity data.....	76
A.4. Histograms of NPM1 intensity for individual nuclei.....	77
A.5. DFT-optimized structures of compounds	78
B.1. Perinucleolar γ H2AX foci are not observed in oxaliplatin treated cells	93
B.2. Fibrillarin staining at 6 and 24 hours of treatment with oxaliplatin.....	94
C.1. Sequencing of Pt(II) samples shows high frequency of non-unique reads	97

LIST OF TABLES

Table	Page
4.1. Methods used to detect Pt(II) binding sites on nucleic acids.....	52
4.2. Click-enabled Platinum(II) Derivatives	60
A.1. IC50 values in A549 cells of Pt(II) compounds at 24 hours.....	79
A.2. IC50 values in A539 cells at 48 hours	79
A.3. Volume and hydrophobicity data.....	80

CHAPTER I: INTRODUCTION

Background

The antiproliferative effects of platinum compounds were first observed by Loretta Van Camp and Barnett Rosenberg, who were studying the effects of electric fields on cell growth using the rod-shaped bacteria *Escherichia coli* (Rosenberg, Van Camp, and Krigas 1965). When *E. coli* were grown in an electrolysis chamber utilizing platinum electrodes, they were able to grow but not divide, resulting in long, filamentous bacteria. A series of carefully planned experiments determined that the causative agent was a chemical product generated in the medium by platinum electrodes, and later experiments narrowed the responsible agent down to the platinum(II) compound *cis*-diamminodichloroplatinate or $\text{Pt(II)Cl}_2(\text{NH}_3)_2$, later shortened to cisplatin (Figure 1.1) (Rosenberg et al. 1967). This property of inhibiting division but not growth resembled the effects of existing chemotherapeutic agents and suggested the compound's potential as an antitumor drug. Within a few years of these discoveries, the antitumor effects of cisplatin had been demonstrated in mice (Rosenberg et al. 1969).

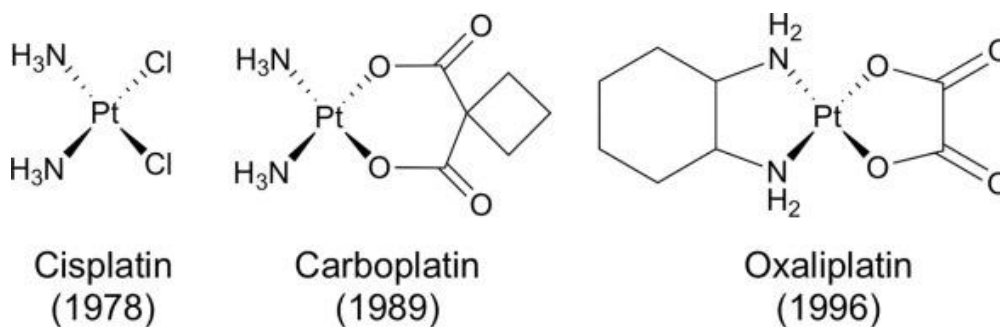


Figure 1.1: Chemical structures of the three platinum(II) chemotherapeutics that have been approved by the FDA, including year of approval.

When it first entered clinical trials, cisplatin was found to have significant side effects including kidney damage leading to renal failure (nephrotoxicity), nerve damage leading to hearing loss (ototoxicity), nausea, and vomiting. Methods were developed to mitigate these effects, particularly nephrotoxicity and nausea, but these complications remain a significant limitation in the use of cisplatin as a treatment option today. Despite these downsides, the drug was found to be extremely effective for a subset of cancers. It was approved by the U.S. Food and Drug Administration for use in testicular and ovarian cancer in 1979 (Wiltshaw 1979). Since its approval, it has drastically improved the prognosis for certain cancers and has proven to be beneficial as a co-treatment in combination with other chemotherapy drugs. It opened the world of drug discovery to heavy metal based drugs which were previously deemed too toxic for clinical use. This launched an era of research into other platinum drugs that might improve upon, replace, or complement the use of cisplatin in medicine (Kelland 2007; Johnstone, Suntharalingam, and Lippard 2016; Cheff and Hall 2017).

Cisplatin's mode of action became a topic of intense investigation. Within a couple decades of its approval, a general model was accepted for cisplatin's molecular mechanism. Cisplatin first enters cells via passive diffusion or through plasma membrane transporter proteins such as copper transporter-1 (CTR1). After the compound enters cells, its two chloride ligands are exchanged for water in an aquation reaction driven by the lower chloride concentration in cells (Wexselblatt, Yavin, and Gibson 2012). The non-labile ammine ligands remain on the platinum. This aquated species is the active form of the drug, which can interact with biomolecules including genomic DNA (Figure 1.2). These biomolecular interactions are responsible for the subsequent cytotoxic activity

of the drug. The canonical cytotoxic response is the DNA damage response (DDR). The Pt(II) lesion inhibits replication and ultimately leads to cell death (Jamieson and Lippard 1999; Chaney et al. 2005).

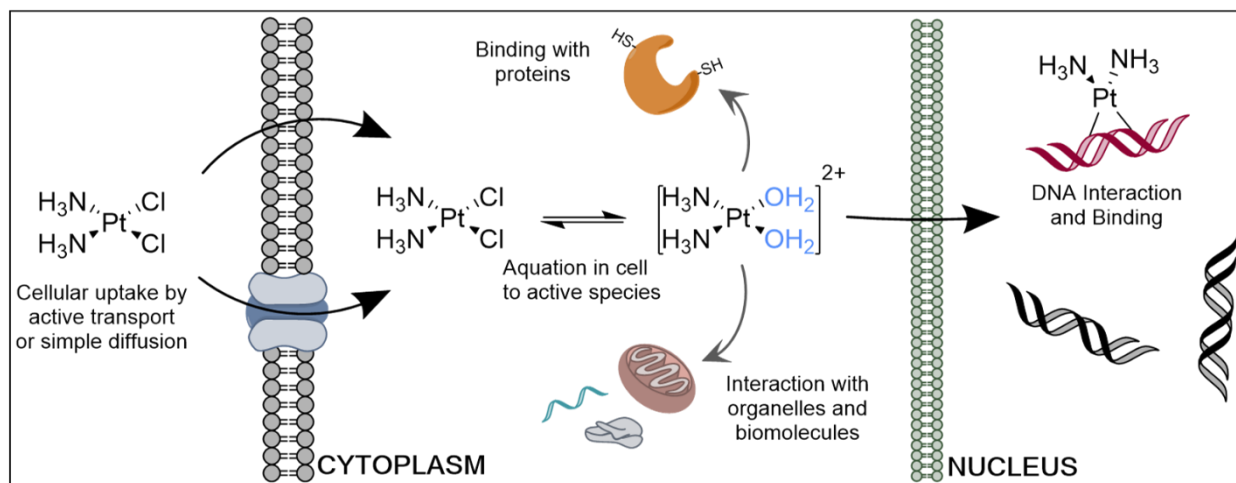


Figure 1.2: Cellular uptake and aquation of cisplatin. After transport into the cytoplasm, the chloride ligands are exchanged for aqua ligands. Aquated cisplatin interacts with many targets, including RNA and proteins in the cytoplasm. After entering the nucleus, it interacts with nuclear RNAs, proteins, and genomic DNA. This interaction with genomic DNA triggers the DNA damage response, which is the canonical mechanism of cell death upon cisplatin treatment. Diagram by Matthew Yglesias

Over the years, thousands of cisplatin analogs have been synthesized and evaluated for their potential use as chemotherapeutic agents (Kelland 2007). The vast majority of these did not pass initial stages of research, and of those that made it to clinical trials, only three have so far met standards for FDA approval. The first, carboplatin (Figure 1.1), was developed in attempt to mitigate side effects of cisplatin (Kelland 2007). Instead of the two chlorides as labile ligands, carboplatin possesses a bulkier cyclobutane dicarboxylate ligand that has slower substitution kinetics. The lesions formed by carboplatin are the same as those formed by cisplatin, with the two non-labile ammine ligands remaining on the Pt(II) after it is bound to molecules. This substitution of the labile ligands effectively reduces unwanted toxicity in a clinical setting. Fewer lesions

are formed at equimolar concentrations of these drugs, a consequence of the different aquation kinetics. This is believed to be a factor in limiting carboplatin's efficacy for certain types of cancer. For other types of cancer, such as some ovarian cancers, carboplatin and cisplatin have similar clinical efficacies (Kelland 2007).

The most recently FDA-approved Pt(II) drug is oxaliplatin (Figure 1.1). Oxaliplatin possesses both a different labile and non-labile ligand than cisplatin and carboplatin. The labile ligand is an oxalate and the non-labile ligand is a diaminocyclohexane (DACH). Oxaliplatin is effective for a different spectrum of cancers than the other two FDA-approved drugs and has a markedly different side effect profile. For instance, a common side effect of oxaliplatin is peripheral neuropathy, a type of neurotoxicity which is not seen as frequently with cisplatin and carboplatin. It has been used with relative success to treat colorectal cancer, especially in combination with the drug 5-fluorouracil (5-FU) (Kelland 2007).

Off-target effects and variable scopes of efficacy are only two barriers to the use of these drugs. Another key challenge is drug resistance. For example, it is not uncommon for tumors to become resistant to cisplatin (Kelland 2007; Johnstone, Suntharalingam, and Lippard 2016). This resistance may develop by preventing the drug from reaching biomolecular targets, or the cancer cells may develop ways to survive despite the compound reaching the target as normal. For instance, increased levels of proteins involved in Nucleotide Excision Repair (NER) may lead to cisplatin resistance in germ cell tumors (Welsh et al. 2004; Cierna et al. 2020; Kelland 2007; Köberle et al. 1999).

While these platinum compounds do have side effects and limitations, their collective utility in treating a variety of cancers has secured their place in the milieu of chemotherapeutics used in clinical cancer treatment regimens. Ongoing research continues to explore the possibility of new Pt(II) drugs which may treat a different range of cancers or have fewer side effects. Some investigations are underway to develop Pt(II) drugs that can be orally administered, a less invasive alternative to traditional intravenous injection (Kelland 2007; Johnstone, Suntharalingam, and Lippard 2016). By some estimates, Pt(II) compounds are still used in over half of chemotherapy regimens (Johnstone, Park, and Lippard 2014; Dyson and Sava 2006), either on their own or in co-treatment with other drugs. As research has continued on these drugs, a complex picture of their mechanisms of action has developed. For example, only a relatively small percentage of the Pt(II) that enters cells is believed to end up on genomic DNA, a necessary prerequisite to the DNA damage response. Studies have shown more accumulation of Pt(II) on RNA than DNA (Hostetter, Osborn, and DeRose 2012). In order to better understand how these ubiquitous drugs work, a more detailed description of their molecular mechanisms is necessary.

Differential Effects of Pt(II) Compounds

Why do these compounds have such differential efficacy? While a decent amount of clinical data exists to describe situations in which different Pt(II) drugs are useful, less is known about the underlying reasons for these differences. These Pt(II) compounds have quite similar structures for small molecule drugs, which makes their wide clinical differences even more intriguing. Differences in side effects and resistance profiles lack

comprehensive explanations at the molecular level (Kelland 2007). Thus, a greater understanding of the differences between these mechanisms is desired. What is known already about differences in these compounds with regard to their biomolecular behavior and mechanisms? Existing literature on the topic will be described below.

Most studies that have directly compared differences in the molecular mechanism between Pt(II) compounds have focused on the DNA damage response. The DDR encompasses a variety of signaling and repair pathways that are triggered by different types of DNA damage. Previous work has shown that in A2780 and CEM cells, fewer Pt(II) crosslinks were found on DNA after four hours of treatment with oxaliplatin compared to equimolar treatment with cisplatin (Faivre et al. 2003; J M Woynarowski et al. 2000; Jan M. Woynarowski et al. 1998). Some differences in the types of DDR activated by these drugs have also been demonstrated. Nucleotide excision repair (NER) and recombination repair do not discriminate between cisplatin and oxaliplatin lesions, but mismatch repair (MMR) does by detecting only cisplatin lesions (Chaney et al. 2005; Nehmé et al. 1999). In addition to differential effects on certain DDR pathways, cisplatin lesions increase the DNA binding affinity of several DNA-binding proteins and domains including High Mobility Group Box domain (HMGB), TATA-binding protein (TBP), and the HMGB analog Upstream Binding Factor (UBF) which is involved transcription by RNA Polymerase I (Pol I) (Chaney et al. 2005; Xiaoquan Zhai et al. 1998; Treiber et al. 1994; M. Wei et al. 2001). Cisplatin lesions increase these binding affinities more so than the DACH lesions induced by oxaliplatin (M. Wei et al. 2001). Differences have been observed in the ability of translesion DNA polymerases to bypass lesions made by oxaliplatin and cisplatin. These polymerases are better able to bypass oxaliplatin lesions

than cisplatin lesions (Chaney et al. 2005). A potential mechanism for this is suggested by *in vitro* studies showing that the protein HMG1 has an increased affinity for DNA with cisplatin, but not oxaliplatin, lesions. In addition to the studies showing less accumulation of Pt(II) in cells after oxaliplatin treatment than cisplatin treatment, Bruno et al have reported less DNA damage upon oxaliplatin treatment using the DNA damage marker γ H2AX (Bruno et al. 2017). Strikingly, they also showed that the DNA damage response may not be responsible for cell death upon oxaliplatin treatment, but that it may cause cell death by inducing ribosome biogenesis stress instead. With this evidence, a new model has emerged in which the DNA damage response may be responsible for cell death with carboplatin and cisplatin, but that the dominant driver of cytotoxicity upon treatment with oxaliplatin and phenanthriplatin — another Pt(II) compound currently under investigation as a potential therapeutic — is ribosome biogenesis stress.

Ribosome Biogenesis and the Nucleolus

The eukaryotic ribosome is a molecular machine comprised of two major subunits that translate mRNA into protein. Each ribosome is made from 4 ribosomal RNAs (rRNA) — 5S, 5.8S, 18S, and 28S — and dozens of ribosomal proteins. In order for the ribosome to be assembled, the rRNA must be transcribed and then processed into mature forms of rRNA. The rRNA and ribosomal proteins are then assembled into the two ribosomal subunits. These stages of rRNA transcription, rRNA processing, and ribosome assembly occur in a sub-nuclear organelle known as the nucleolus (Figure 1.3A).

The nucleolus is a prominent membraneless structure within the nucleus that was first observed microscopically over a century ago. In the 1960s, it was determined to be

the site of ribosome biogenesis. Ribosome biogenesis is the primary function of the nucleolus and the focus of most research into nucleolar function. The first step of ribosome assembly is the transcription of rRNA from rDNA by Pol I, facilitated by numerous transcription factors. The exception to this is the 5S rRNA transcript, which is transcribed separately in the nucleoplasm by RNA Polymerase III (Pol III). Over 200 copies of rDNA exist in the human genome, all located on the short arms of acrocentric chromosomes (Sanij and Hannan 2009; van Sluis and McStay 2015). Despite only some of these copies being transcriptionally active, rRNA transcription is believed to make up about 80% of total transcriptional activity in the cell. The rDNA is located in genetic regions known as nucleolar organizer regions (NORs). Genomic DNA is organized within the nucleus such that these NORs and rDNA are located within the nucleolus, which dissociates and re-forms each time a cell passes through the cell cycle. Nucleolar proteins diffuse throughout the cytoplasm as the cell approaches mitotic metaphase. These proteins aggregate to form what are known as “prenucleolar bodies” or PNBs, towards the end of mitosis. They then associate with the chromosomal NORs and resume transcription of rDNA by early G1-phase. By the end of G1, full nucleoli have re-formed around the NORs (Németh and Grummt 2018; Smirnov et al. 2016). Although typically described as a single organelle, multiple nucleoli are often visible in a variety of cell types. It is standard for them to exist in multiple aggregates, and possible that variations in nucleolar number may be indicative of abnormal ribosome biogenesis (Farley-Barnes et al. 2018).

Fully formed mammalian nucleoli are tripartite in structure (Figure 1.3B), with three visually distinct compartments that have been proposed to host different steps of

ribosome biogenesis (Pederson 2011; Hernandez-Verdun et al. 2010). The fibrillar center (FC) is the dense middle component of the nucleolus. It is surrounded by the dense fibrillar component (DFC), and both of these are located within the outermost granular component (GC). These three components are believed to be phase separated via liquid-liquid phase separation, meaning that they are immiscible liquids with segregated molecular components (similar to oil and water). The proposed model in which the subcompartments carry out different stages of ribosome biogenesis suggests that the assembly of ribosomes happens as the nascent ribosome exits the nucleolus, with early assembly (transcription and early processing) happening at the FC/DFC interface and late assembly (late processing) happening in the GC (Hernandez-Verdun et al. 2010).

However, it is also widely accepted that rRNA processing begins prior to termination of rRNA transcription. This overlap of functions in the GC, and evidence that the GC may be comprised of multiple domains (Pederson 2011), suggests that the strictly organized tripartite structure/function relationship described above may be more complicated than is sometimes described, although nucleolar organization remains critical to its function. This can be illustrated by regions of rRNA transcription identified by techniques such as EdU incorporation (van Sluis and McStay 2015).

The structure-function relationships between nucleolar organization and ribosome biogenesis also become extremely evident when there are disruptions in ribosome biogenesis. A process known as the ribosome biogenesis stress response, alternatively referred to as the nucleolar stress response in this text, is triggered upon perturbation of the biological processes that occur within the nucleolus. This response is thought to be a critical sensor of cellular stress. Disruptions that initiate this response include inhibition

of rRNA transcription and processing, blockage of ribosome assembly, rDNA damage, or direct disruption of nucleolar structure (Rubbi and Milner 2003; K. Yang, Yang, and Yi 2018; Boulon et al. 2010). Once the stress response is initiated, several proteins translocate from the nucleolus to the nucleoplasm, and nucleolar reorganization occurs. The translocation of proteins initiates the stabilization of the tumor suppressor protein p53, which results in downstream cell death or senescence. Recent work on this subject has increased interest in the nucleolus as a critical sensor for cellular stress signals and a potentially clinically relevant target for chemotherapeutics (Tsai and Pederson 2014; van Sluis and McStay 2014).

The Nucleolus and Cancer

A connection between the nucleolus and cancer has been recognized for almost as long as the nucleolus has been studied. Ribosome biogenesis is closely linked to the cell cycle, and aberrations in ribosome biogenesis can lead to increased cancer risk, which is highly influenced by dysregulation of the cell cycle (Tsai and Pederson 2014). Cancer cells often have higher rates of ribosome biogenesis, and cancer prognosis can be estimated by morphological observations of abnormal nucleoli (Derenzini, Montanaro, and Treré 2009; Derenzini, Montanaro, and Trerè 2017). Due to this and the involvement of nucleoli and ribosome biogenesis in a number of other signaling pathways related to cancer, interest has grown in potentially targeting ribosome biogenesis or the nucleolus more generally to treat cancer (Tsai and Pederson 2014; van Sluis and McStay 2014; Bruno et al. 2017).

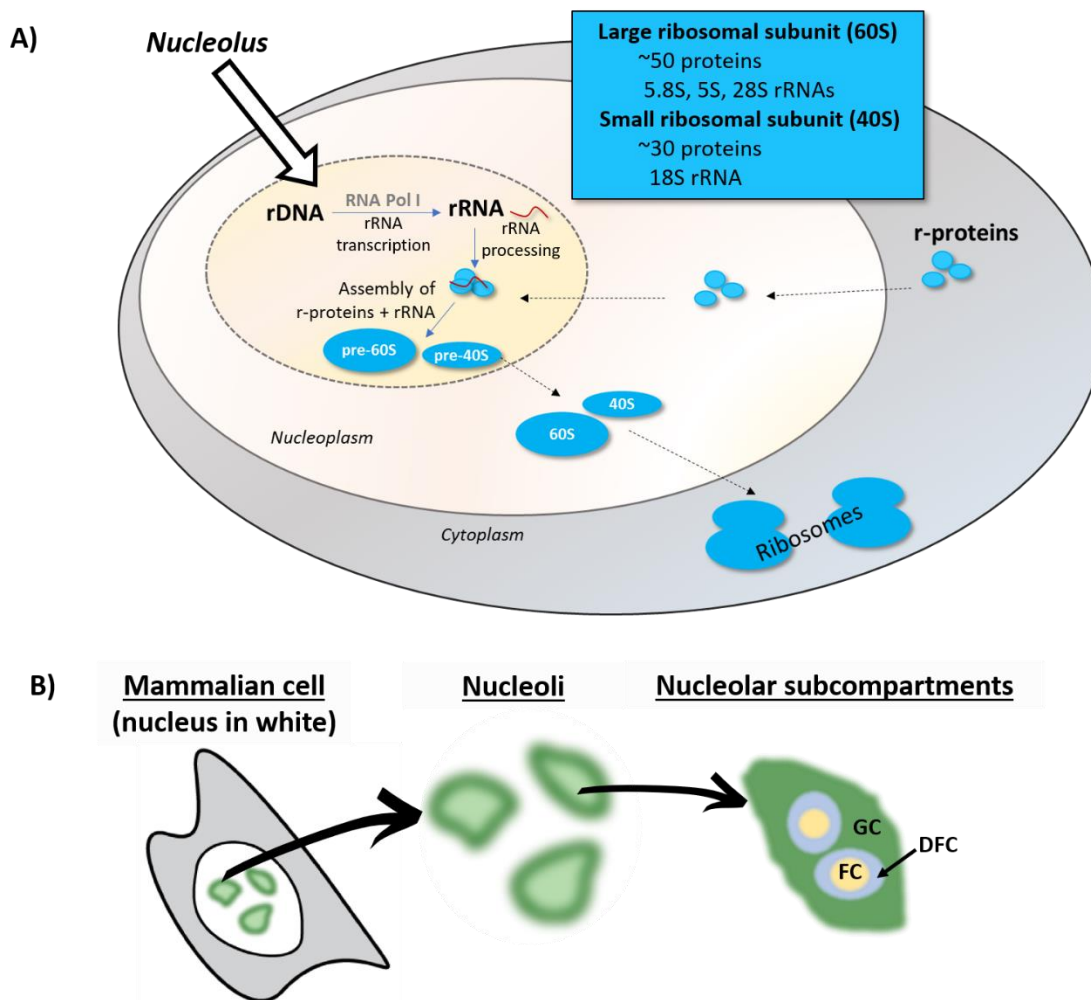


Figure 1.3: Ribosome biogenesis and the nucleolus A) Schematic of ribosome biogenesis, which occurs in the cell's nucleolus. rDNA is transcribed into pre-rRNA by Pol I. Pre-rRNA is processed into mature rRNA, which is then assembled with ribosomal proteins (r-proteins) into the large (60S) and small (40S) ribosomal subunits. B) Illustration of nucleoli in a cell and nucleolar subcompartments. FC = fibrillar center, GC = granular component, DFC = dense fibrillar center

Pt(II) Compounds and the Nucleolus

This nucleolus-cancer connection is particularly fascinating when considering the ways that Pt(II) compounds are also connected to the nucleolus. Using tools such as fluorescent clickable Pt(II) compounds, we have observed nucleolar localization of Pt(II) drug analogs in MDA-MB-461 cells (Wirth et al. 2015). Pt(II) accumulation on

ribosomes in *Saccharomyces cerevisiae* has also been observed (Plakos and DeRose 2017). Changes in levels of nucleolus-associated proteins occur in response to oxaliplatin treatment (Ozdian et al. 2017). As mentioned previously, Bruno et al have demonstrated that oxaliplatin's cytotoxic effect is likely to be driven by ribosome biogenesis stress (Bruno et al. 2017). The connection between these Pt(II) chemotherapeutic agents, the nucleolus and cancer raise many question and potential avenues of exploration, described in the next section.

Within this dissertation, I will address three main subtopics that have arisen from existing work on the topic of Pt(II) compounds and the nucleolus. The first concerns the chemical structure of nucleolar stress-inducing Pt(II) compounds. As only a subset of these compounds were previously reported to induce ribosome biogenesis stress, the following question will be addressed in Chapter II: What are the structural properties of Pt(II) compounds that are responsible for their ability to induce a nucleolar stress response? In this chapter specific structural requirements of Pt(II) compounds that are necessary to induce stress will be described. The second question concerns the differences in the biological responses induced by these drugs. Chapter III will address the following question: What biological mechanisms underlie the unique ability of just some of these Pt(II) compounds to cause nucleolar stress? In this chapter, Pol I inhibition will be identified as a key factor in the ability of oxaliplatin to induce nucleolar stress. Lastly, in Chapter IV I will discuss current and emerging tools that will allow the field to better identify the specific biomolecular targets of Pt(II) compounds and present a preliminary click-based pulldown assay to identify DNA targets of Pt(II) throughout the genome.

Bridge to Chapter II

In this chapter the importance and ubiquity of Pt(II) chemotherapeutic agents to the fields of medicine and biology has been established. Existing knowledge on the mechanisms of action of these compounds has been summarized and a need to better understand these mechanisms due to their clinical relevance has been emphasized. The connection between Pt(II) compounds and the nucleolus was discussed, including evidence that some Pt(II) compounds may induce cell death by the nucleolar stress response. Lastly, this chapter included a summary of the subtopics that will be addressed throughout this dissertation. In chapter II, experiments will be described in which a curated set of compounds was used demonstrate the requirement of specific structural features for Pt(II) compounds to cause nucleolar stress.

CHAPTER II: NUCLEOLAR STRESS INDUCTION BY OXALIPLATIN AND DERIVATIVES

This chapter contains published, co-authored material. This communication was co-authored by Christine E. McDevitt, Jack Prochnau, Matthew Yglesias, Austin Mroz, Min Chieh Yang, Rachael Cunningham, Christopher Hendon, and Victoria DeRose. CEM and ECS share co-first authorship. Contributions by ECS include initial investigation of differential nucleolar stress responses using NPM1 as a marker, experimental design and methodology, data collection, data interpretation and analysis, figure preparation, drafting of the initial manuscript, manuscript preparation, and addressing revisions.

Nucleolar Stress Induction by Oxaliplatin and Derivatives

The chemotherapeutic agent cisplatin has inspired the synthesis and investigation of thousands of Pt(II) analogs (Kelland 2007). Of these, only two other compounds — carboplatin and oxaliplatin — have met FDA standards for medical use. Until recently, it was believed that the cytotoxicity of these compounds could be attributed solely to their DNA crosslinking abilities and subsequent induction of the DNA Damage Response (DDR), a known trigger of apoptotic pathways (Wexselblatt, Yavin, and Gibson 2012). As the body of research on Pt(II) reagents has grown, a more complex picture has emerged of the mechanisms of action behind these ubiquitous drugs (Wexselblatt, Yavin, and Gibson 2012). A striking recent discovery is that oxaliplatin, but not cisplatin or carboplatin, causes cytotoxicity via disruptions in ribosome biogenesis rather than DDR (Bruno et al. 2017). Ribosome biogenesis occurs in the nucleolus, a conserved and highly structured organelle

in eukaryotes. Disruptions of the nucleolus or ribosome biogenesis trigger the nucleolar stress response, which leads to cell death or senescence via activation of the tumor suppressor p53. Because its molecular mechanisms are not yet fully understood, and due to its potential role as a chemotherapeutic target, this fascinating stress process is an area of intense interest in the fields of molecular biology and medicine (Tsai and Pederson 2014; Woods et al. 2015; Boulon et al. 2010; Farley-Barnes et al. 2018).

The specificity of oxaliplatin as a nucleolar stress inducer is intriguing when considered alongside other data indicating a relationship between Pt(II) compounds and the nucleolus.⁸ Post-treatment fluorescent labeling of clickable Pt(II) drug analogs has shown localization of these compounds to the nucleolus (Pickard and Bierbach 2013; Wirth et al. 2015), and there is significant evidence that Pt(II) compounds associate with ribosomes and ribosomal RNA (rRNA) (Plakos and DeRose 2017; Hostetter, Osborn, and DeRose 2012; Osborn et al. 2014; Melnikov et al. 2016; Rijal and Chow 2007; Saunders and DeRose 2016; Sutton, McDevitt, Yglesias, et al. 2019). The structural determinants and molecular mechanisms by which only specific Pt(II) compounds may cause a nucleolar stress response are not understood. Here, we explore properties of oxaliplatin and other Pt(II) compounds and find that a narrow window of derivatives is able to induce nucleolar stress. The results define a set of constraints for Pt(II) compounds to induce this unique cell death pathway.

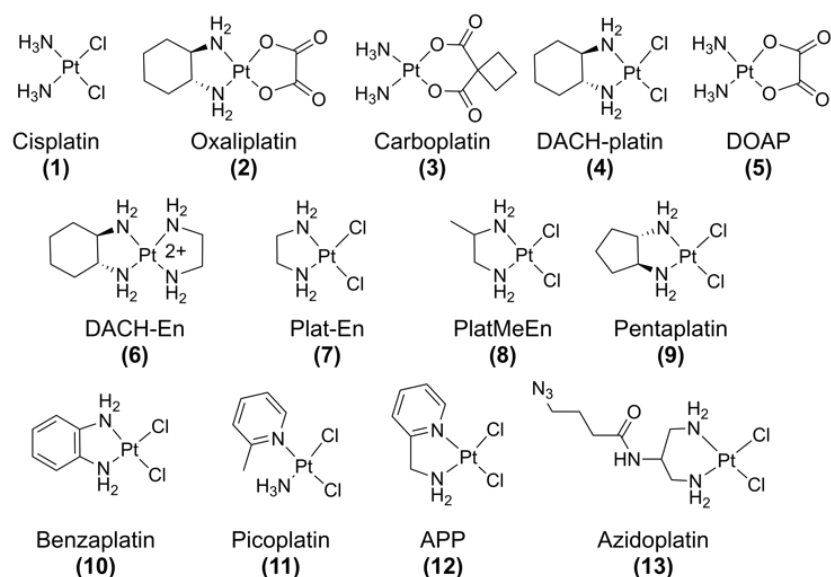


Figure 2.1: Compounds tested for inducing nucleolar stress via NPM1 relocalization in mammalian cells.

We selected Pt(II) compounds to test a variety of properties including steric bulk, hydrophobicity, crosslinking ability, and ligand orientation (Figure 2.1). The extent of nucleolar stress was measured by nucleophosmin (NPM1) imaging (Figure 2 and Figure A.1). Translocation of NPM1 from the granular component (GC) of the nucleolus to the nucleoplasm is a hallmark of the nucleolar stress response (Rubbi and Milner 2003; K. Yang et al. 2016). This translocation has been shown to be a necessary, but not sufficient, feature of p53-mediated cell death upon nucleolar stress (K. Yang et al. 2016), and thus is a robust and appropriate marker for nucleolar stress. A549 cells were selected for this study as they are well established to have a characteristic nucleolar stress response resulting in p53-mediated apoptosis (Bursac et al. 2014; Nicolas et al. 2016).

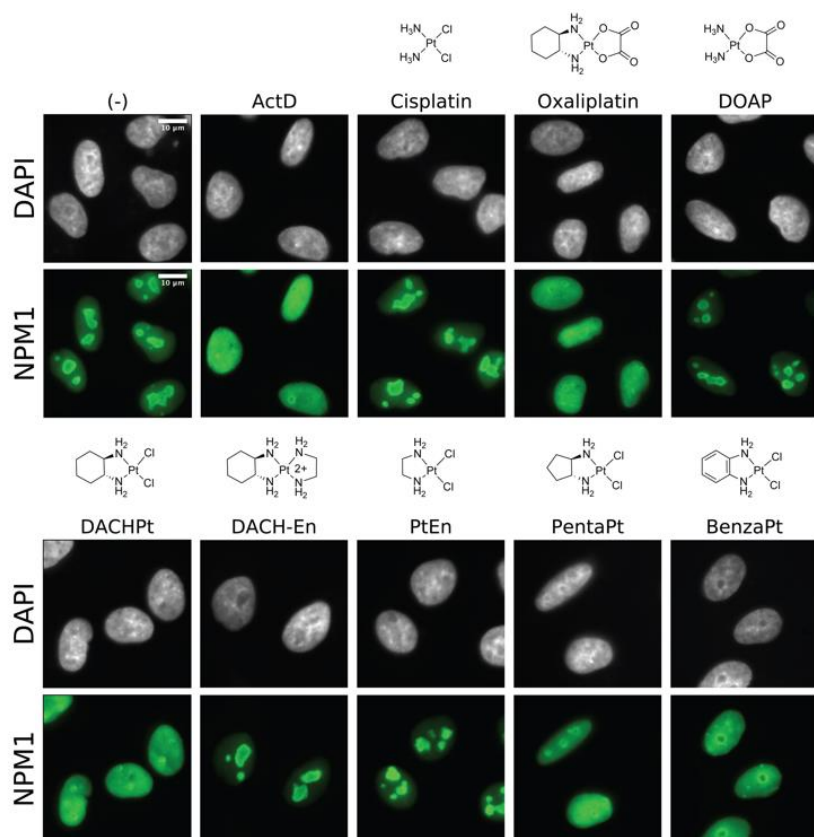


Figure 2.2: Nucleolar stress induced by Pt(II) compounds. NPM1 (green) relocation following 24-hr treatment in A549 cells. Treatment concentrations are 10 μ M except for Actinomycin D (5 nM). Scale bar = 10 μ m.

Cells were treated for 24 hours with a given compound prior to fixation and secondary immunofluorescence to detect NPM1 (Figure 2 and A.1). The extent of NPM1 redistribution was quantified using an image analysis pipeline (Figure A.1) to calculate the coefficient of variation (CV) of NPM1 intensity in each cell (Figure 2.3). The uniform distribution of NPM1 in cells undergoing nucleolar stress yields a low CV, as seen in positive control samples treated with known stress-inducer Actinomycin D (Figure 2.3). In addition to the observation of NPM1 redistribution, we noted a change in the shape of nucleoli from eccentrically shaped aggregates to round, sphere-like structures upon stress induction (Figure 2.2).

As predicted (Bruno et al. 2017; McDevitt et al. 2019), oxaliplatin (**2**) induces robust redistribution of NPM1, similar to the positive control, while NPM1 distribution in cisplatin (**1**) and carboplatin (**3**) treated cells more closely resembles that of the no-treatment control (Figure 2, Figure 2.3).

We note that for cisplatin-treated cells, a small amount of NPM1 redistribution was observed at this treatment concentration. This is likely because the 24-hour IC-50 value of cisplatin (12.8 μ M, Table A.1) is close to the treatment concentration, which may result in a subset of cisplatin-treated cells experiencing abnormal NPM1 distribution downstream of other cell death pathways, such as those mediated by the DDR (see footnote¹). Oxaliplatin, by contrast, shows robust NPM1 relocalization at treatment concentrations well below the IC-50 value (81.5 μ M, Table A.1), suggesting that nucleolar stress significantly precedes cell death pathways (Bruno et al. 2017). The observation of NPM1 relocalization well below IC-50 values was consistent with other stress-inducing compounds, including some compounds showing no toxicity at 24 hours despite extensive nucleolar stress (Table A.1). Thus, observation of nucleolar stress does not necessarily predict toxicity at 24 hours. In cases where no toxicity was observed at 24 hours, 48-hour IC-50 values were achieved. For this subset of compounds that was not sufficiently cytotoxic at 24 hours, stress induction did correlate with lower IC-50 values (Table A.2).

¹ Footnote: This model is supported by previously published data demonstrating that cisplatin causes significantly more DNA damage than oxaliplatin (Chaney et al. 2005; Faivre et al. 2003) and that DDR-mediated cell death occurs upon cisplatin treatment, but not oxaliplatin treatment (Bruno et al. 2017). Additionally, data from our lab shows that DNA damage occurs at early time points in cisplatin-treated cells, prior to any putative NPM1 relocation, whereas no such damage occurs prior to observed NPM1 distribution in oxaliplatin-treated cells (unpublished).

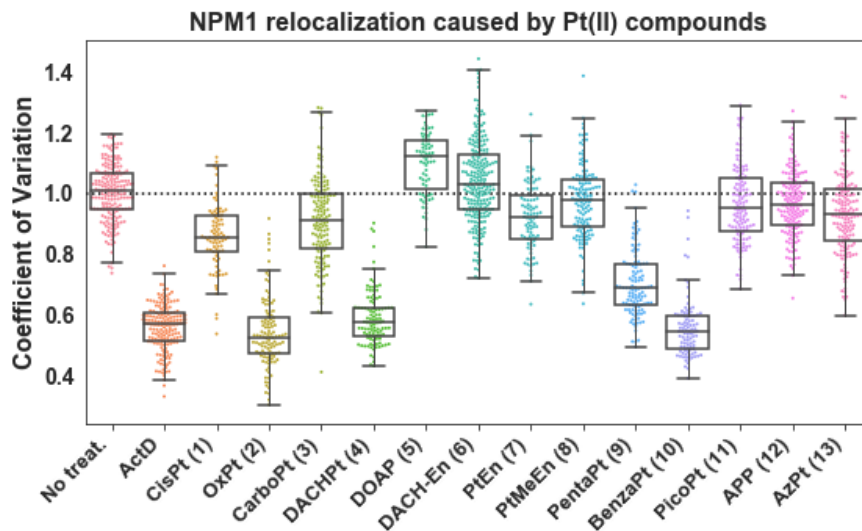


Figure 2.3: Quantification of NPM1 relocalization induced by Pt(II) compounds. Treatment conditions as in Figure 2.2; replicates and CV calculations as described in SI. For each treatment data set, boxes represent median, first, and third quartiles, and vertical lines are the range of data with outliers defined in the SI.

Oxaliplatin is distinct from cisplatin and carboplatin in both labile and non-labile Pt(II) ligands. The labile, chelating oxalate ligand of oxaliplatin delays aquation and therefore biomolecule crosslinking (Jerremalm et al. 2002) in comparison with cisplatin. We exchanged the labile and non-labile ligands of oxaliplatin and cisplatin with compounds **4** and **5**. We found that compound **4**, DACHPt, which has the non-labile DACH ligand of oxaliplatin and labile chloride groups of cisplatin, induces robust nucleolar stress. By comparison, **5**, or DOAP, which possesses the non-labile ammine ligands of cisplatin and the labile oxalic acid ligand of oxaliplatin, does not induce stress (Figures 2 and 3). The oxalic acid ligand alone also had no influence on NPM1 redistribution, nor did the DACH ligand by itself (Figure A.2, Figure A.3). From this, we concluded that the non-labile DACH ligand of oxaliplatin is responsible for the nucleolar stress response.

We next considered whether crosslinking of biomolecules by the Pt(II) compound is necessary for the induction of nucleolar stress. An alternate hypothesis is that the charged

Pt(II) acts as a targeting agent to facilitate transport of the DACH moiety to the nucleolus where it disrupts nucleolar processes without forming a Pt(II)-DACH lesion on a biomolecule. Compound **6**, DACH-En, retains the DACH ligand but is unable to form crosslinks with biomolecules due to replacement of the oxalic acid with an ethylenediamine ligand (Figure 2.1). This positively charged compound did not induce stress (Figure 2.2, Figure 2.3), suggesting that crosslinking of Pt(II) to cellular targets is necessary to induce a nucleolar stress response.

To refine requirements of the non-labile Pt(II) ligand that cause nucleolar stress, we examined the effects of steric bulk by testing **7**, **8** and **9**. Pt-En (**7**) possesses a non-labile ethylenediamine ligand. This small molecule did not induce stress in A549 cells (Figures 2 and 3), indicating that a chelating diamine ligand, a common feature between PtEn, DACHPt, and oxaliplatin, is not sufficient to induce stress. The addition of a methyl group to generate the bulkier PtMeEn (**8**), was also not sufficient to induce stress (Figure 2.3, Figure A.2, Figure A.3). Compound **9**, pentaplatin, possesses a five-membered ring that places its volume between the non-stress inducing PtMeEn and the stress-inducing six-membered DACHPt. Pentaplatin was found to induce nucleolar stress (Figure 2.1), although with a slightly higher resultant CV than positive controls or oxaliplatin (Fig. 3). These results suggest that bulk may be an important metric lending towards the ability of Pt(II) compounds to induce nucleolar stress. Using computed values for volume, we conclude that as a general trend, Pt(II) compounds with more steric bulk are more likely to induce nucleolar stress (Figure 2.4a, Y axis). Compound length, or steric reach, also generally appears to correlate with stress induction (Figure 2.4a, X axis). Some exceptions to this trend are discussed below.

The chair confirmation of the DACH ligand is not essential for stress induction. BenzaPt (10), in which the DACH cyclohexane is replaced with a planar aromatic ring (Figure 2.5B), also induces robust NPM1 redistribution (Figure 2.2 and Figure 2.3). Like DACHPt, BenzaPt is more hydrophobic than the simpler diam(m)ine compounds. To estimate the relatively hydrophobicity of our compounds of interest, we measured their water/octanol partition coefficients (Supplementary materials and methods). All of the stress-inducing compounds were found to be relatively hydrophobic (Figure 2.4b), leading to the conclusion that hydrophobicity, like steric bulk, positively correlates with stress induction. Similarly to steric bulk, however, exceptions to this trend were observed.

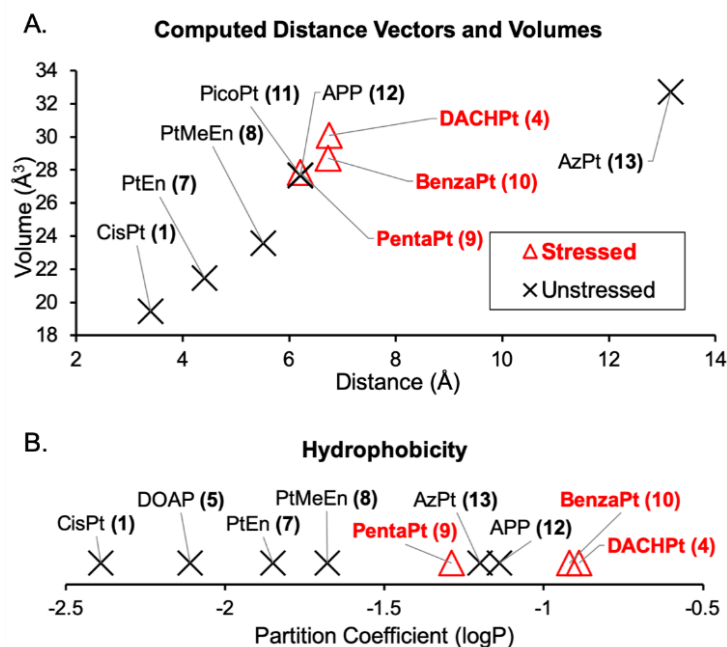


Figure 2.4: Size and hydrophobicity correlate with stress induction, with some exceptions. Compounds with a higher (less negative) partition coefficient are more hydrophobic than those with a lower (more negative) partition coefficient. Measurements and calculations are described in SI.

Compounds 11, 12, and 13 do not cause NPM1 relocation despite being similar or higher in terms of size and hydrophobicity to compounds that do cause nucleolar stress

(Figure 2.4). These exceptions may provide insight into the elements responsible for causing stress.

One particularly interesting comparison is between APP (**12**) (Zacharioudakis et al. 2017; Brunner and Schellerer 2003) and BenzaPt (**10**) (Figure 2.5A). These two Pt(II) compounds both have an aromatic ring, but differ in the orientation of the ring relative to the Pt(II), and by extension ring orientation relative to a biomolecule to which the compound is bound. While BenzaPt causes nucleolar stress, APP does not. Similarly, picoplatin (**11**) does not cause nucleolar stress despite having volume and reach similar to other compounds (Figure 2.4 and Figure 2.5). These results demonstrate a critical role for ring orientation in the ability of Pt(II) compounds to induce nucleolar stress.

The observation that azidoplatin (**13**) does not cause stress is of interest as this compound has extended volume and has previously been shown to localize to the nucleolus (Wirth et al. 2015). Thus, nucleolar localization, even when combined with relatively high hydrophobicity and larger bulk and length, is not sufficient to induce nucleolar stress.

Taken together, the results described provide significant insight into the structural determinants of nucleolar stress induction among Pt(II) compounds. We conclude that there is an important role for ligand orientation and a general correlation between steric bulk and stress induction (Figure 2.5).

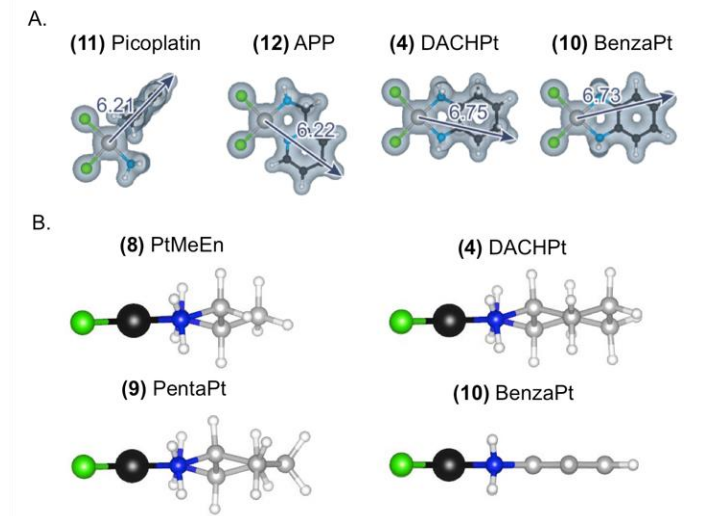


Figure 2.5: (A) Computed volume and distance measurements for non stress-inducing compounds 11 and 12 alongside stress-inducing compounds 4 and 10. (B) Ball and stick drawings of non stress-inducing compound 8 alongside stress-inducing 4, 9, and 10.

The differential responses induced by these compounds have clinical implications as the three currently FDA-approved Pt(II) chemotherapeutics are known to have different treatment and side effect profiles. Other important differences between these compounds have been observed in the literature. For example, oxaliplatin is noted to cause immunogenic cell death (ICD), while cisplatin does not (Siew et al. 2015; Englinger et al. 2019; Terenzi et al. 2016). Although this contrast is also observed in nucleolar stress, connections between ICD and nucleolar stress are not well-studied. Oxaliplatin has also been shown to cause changes in the size of neuronal nucleoli correlating with peripheral neuropathy (McKeage et al. 2001), a common side effect associated with oxaliplatin chemotherapy regimens. The relationship between nucleolar stress and platinum-induced neurotoxicity has not been explored. Additionally, there is some evidence that p53 mutations in colon cancer cell lines result in resistance to oxaliplatin-mediated cell death

(Toscano et al. 2007). This may be of interest given oxaliplatin's use in colon cancer treatments and p53's role in nucleolar stress- induced cell death.

Further study is warranted to provide clarification on the molecular mechanisms by which these compounds induce such different responses in the cell. For example, the stress-inducers may be interfering with progression of ribosome biogenesis (Rubbi and Milner 2003; Bursac et al. 2014), disrupting an intermolecular interaction of NPM1 that sequesters it in the nucleolus (K. Yang et al. 2016), altering biophysical properties of nucleic acids (Keck and Lippard 1992; Malina et al. 2007), or globally perturbing the biomolecular interactions that maintain nucleolar integrity. More work is needed to understand this fascinating biological stress process and to define the specific properties of Pt(II) compounds that cause it.

Bridge to Chapter III

In Chapter II, structural requirements for nucleolar stress induction by Pt(II) compounds were identified. Chapter III will examine the underlying biological mechanisms behind Pt(II) induced nucleolar stress.

CHAPTER III: MECHANISMS OF PLATINUM-INDUCED NUCLEOLAR STRESS

This chapter contains unpublished co-authored material by Emily C. Sutton and Victoria J. DeRose. ECS performed the experiments and data analysis, and VJD provided experimental and editorial guidance.

Introduction

The nucleolus is the site of ribosome biogenesis, a process that includes transcription of ribosomal RNA (rRNA) by RNA Polymerase I (Pol I), processing of rRNA, and assembly of ribosomal subunits. Nucleolar morphology can be used as a prognostic factor for tumor severity, and nucleolar size is correlated to node and receptor status in breast cancer as well as length of disease-free survival period (Derenzini, Montanaro, and Treré 2009). Functionally, ribosome biogenesis is closely associated with cellular processes such as the cell cycle, further linking the dysregulation of this process to cancer and other diseases (Tsai and Pederson 2014). While upregulated ribosome biogenesis is associated with cancer, inhibition of ribosome biogenesis can lead to activation of the tumor suppressor protein p53 via the nucleolar stress response. This has made both ribosome biogenesis and the nucleolus desirable targets for cytotoxic agents with potential chemotherapeutic applications (Pickard and Bierbach 2013; Woods et al. 2015; Bywater et al. 2012).

A few small molecules induce a cytotoxic nucleolar stress response by selectively inhibiting rRNA synthesis by Pol I. Actinomycin D (ActD) is known to selectively inhibit Pol I at low doses, an effect typically attributed to its propensity to target GC-rich regions

of DNA, including ribosomal DNA (rDNA). It is used effectively to treat specific types of tumors, but its clinical efficacy has been limited in scope (Tsai and Pederson 2014). BMH-21 was identified in a screen for compounds that induce a p53 response (Peltonen et al. 2010) and later found to inhibit Pol I (Peltonen et al. 2014). CX-5461 was identified in a screen for selective Pol I inhibitors (Drygin et al. 2011). The ability of BMH-21 to inhibit rRNA transcription is currently believed to be due to stalling of Pol I transcription followed by degradation of the Pol I subunit RPA194 (Peltonen et al. 2014; T. Wei et al. 2018). The mechanism of CX-5461 remains more elusive, with recent evidence suggesting that it may primarily exert its cytotoxic effects by way of topoisomerase II inhibition rather than Pol I inhibition as previously believed (Bruno et al. 2020; Haddach et al. 2012).

Pt(II) anticancer compounds have also been shown to disrupt nucleolar function. Until relatively recently, it was believed that all platinum-based chemotherapeutic agents, including cisplatin and oxaliplatin (Figure 3.1A), exerted their cytotoxic effects by triggering the DNA damage response (DDR) (Kelland 2007; Siddik 2003). In 2017, Bruno et al used an RNAi screening approach to conclude that while cisplatin acts via the canonical DDR, ribosome biogenesis inhibition was the primary mechanism of oxaliplatin cytotoxicity in cancer cells (Bruno et al. 2017). This distinction has been supported by later studies demonstrating more extensive redistribution of the protein nucleophosmin (NPM1) from the nucleolus to the nucleoplasm — a hallmark of the nucleolar stress response — upon treatment with oxaliplatin and derivatives (Sutton, McDevitt, Prochnau, et al. 2019). Because prior studies have suggested a more complex relationship between nucleolar stress processes and these platinum drugs, further

investigation into the differences between cisplatin and oxaliplatin with regard to their ability to disrupt nucleolar processes is warranted.

While no studies to date have been able to fully characterize how oxaliplatin might selectively induce ribosome biogenesis stress, its ability to do so is well documented in existing literature. Proteomics studies have shown changes in levels of proteins related to ribosome biogenesis upon oxaliplatin treatment (Ozdian et al. 2017). Robust oxaliplatin-induced redistribution of NPM1 has been demonstrated in multiple published studies (Bruno et al. 2017; McDevitt et al. 2019; Sutton, McDevitt, Prochnau, et al. 2019; Burger et al. 2010), and it has been shown to inhibit rRNA transcription and induce rearrangement of other nucleolar proteins at low doses (6.25 μM) in human fibrosarcoma cells (Burger et al. 2010).

The relationship between nucleolar stress induction and cisplatin is more complex. While there is some evidence for cisplatin's ability to affect ribosome biogenesis and other nucleolar processes, recent data and an evaluation of existing literature suggests these observed mechanisms may not be as clinically relevant as previously reported. Some examinations of cisplatin treatment in HeLa cells have demonstrated a reduction in rRNA synthesis by transcription run-on assay, along with redistribution of Pol I and Upstream Binding Factor (UBF), a transcription factor for Pol I (Jordan and Carmo-Fonseca 1998). Morphological changes in the nucleolus have been observed at early stages of cell death induced by high doses (40 μM) of cisplatin (Horky et al. 2001). Reduction of transcription follows colocalization of Pol I and coilin six hours after cisplatin treatment in HeLa cells, and this effect on transcription can be reversed by siRNA silencing of coilin (Gilder et al. 2011). Hamdane et al have shown that 30 μM of

cisplatin treatment leads to displacement of UBF from rDNA and inhibition of rRNA transcription in MEFs (Hamdane et al. 2015). One previously proposed model for cisplatin's apparent ability to interfere with Pol I transcription is that it Pt(II) lesions on DNA increase the binding affinity of transcription factors such as UBF, and consequently reduce the effective concentration of these transcription factors, thereby decreasing transcription of rRNA (Woods et al. 2015; Treiber et al. 1994). Interestingly, however, this effect is limited to the cisplatin DNA lesions, and the oxaliplatin DACH ligand does not yield this higher UBF binding affinity (Xiaoquan Zhai et al. 1998). Additional work examined the effect of these ligands on the DNA binding capacity of TATA binding protein (TBP) and High Mobility Group Box proteins (HMGBs). Both HMGBs and UBF are in the HMG box family of DNA binding proteins. For all proteins tested, the cisplatin ligand on DNA was found to yield higher protein binding than the DACH lesion that would be generated by oxaliplatin, whereas the DACH ligand did not have this effect (M. Wei et al. 2001). Given this data, if the UBF decoy model were correct, we would expect to see *more* inhibition of Pol I transcription with cisplatin treatment than oxaliplatin, as cisplatin lesions are more effective decoys than oxaliplatin lesions. Therefore, this model is contradicted by evidence that oxaliplatin has more of an impact on ribosome biogenesis than cisplatin (Bruno et al. 2017).

Cisplatin also does not induce the same robust level of NPM1 translocation as oxaliplatin does (Bruno et al. 2017; Sutton, McDevitt, Prochnau, et al. 2019). In sum, there is a clear difference between the ability of these highly similar platinum compounds to affect nucleolar processes. An overarching goal of research into these compounds is to better understand the mechanisms behind their differential efficacy and resistance

profiles, and recent evidence suggests it is decreasingly likely that any effects of cisplatin on nucleolar processes bear relevance to its clinical applications, with the inverse being true of oxaliplatin.

Oxaliplatin definitively has a more significant impact than cisplatin on ribosome biogenesis and nucleolar stress, but there has been no investigation into the potential mechanisms by which this difference may occur. Thus, further exploration of the mechanisms of action of these drugs and an examination of their ability to induce nucleolar stress is warranted. Previously, our lab has demonstrated some structural constraints for Pt(II) drugs to cause stress. The DACH ligand of oxaliplatin proved critical in determining the ability of Pt(II) compounds to induce stress, and while some changes to its size and aromaticity could be tolerated, compounds with different orientations of the DACH ring did not induce stress (Sutton, McDevitt, Prochnau, et al. 2019). This proved valuable in understanding what types of Pt(II) molecules can lead to this response, but the biological mechanism by which oxaliplatin-like Pt(II) compounds induce nucleolar stress and causes NPM1 redistribution is still not well understood. For example, Pt(II) compounds are known to cause DNA damage, which can cause nucleolar stress indirectly by inhibiting Pol I. This relationship between DNA damage and nucleolar stress has yet to be examined in the specific context of Pt(II)-induced nucleolar stress. Some previous work has closely examined the ability of oxaliplatin and cisplatin, among other chemotherapeutic compounds, to inhibit rRNA synthesis and processing as well as rearrangement of specific nucleolar proteins (Burger et al. 2010). However, these studies examined cisplatin's nucleolar effects at doses likely above clinical relevance, and did not directly link this Pt(II)-induced inhibition to p53 stabilization after treatment with

relevant Pt(II) doses. We sought to build on this work by utilizing similar techniques at time points and doses relevant to these critical processes. This paper marks a step forward in understanding which nucleolar processes do and do not cause Pt(II) induced nucleolar stress by carefully examining rRNA synthesis and processing alongside NPM1 redistribution at relevant time points, assessing DNA damage upon treatment at these time points, and further characterizing protein redistribution behavior in Pt(II) stress conditions. We find that rRNA transcription is inhibited at early time points by oxaliplatin, correlating with onset of NPM1 redistribution. We conclude that this inhibition is not caused by damage to ribosomal DNA. In addition, we find that NPM1 redistribution precedes the formation of canonical nucleolar caps as measured by fibrillarin.

Results

Onset of NPM1 redistribution

The protein NPM1 normally resides mainly in the periphery of the nucleolus and its relocalization to the nucleoplasm is a hallmark of the nucleolar stress response (Figure 3.1B). It has previously been shown that both cisplatin and oxaliplatin can cause redistribution of NPM1, but this requires much higher doses of cisplatin (100 μM) than oxaliplatin (6.25 μM) in the same cell lines (Burger et al. 2010). Additionally, there has been little exploration of the potential molecular events preceding NPM1 redistribution upon drug treatment. We had previously measured NPM1 redistribution after 24 hours of treatment (Sutton, McDevitt, Prochnau, et al. 2019). In order to directly compare both cisplatin and oxaliplatin and to initially bracket a time course for onset of NPM1

distribution, A549 cells were treated for 4, 8, and 12 hours with 10 μ M cisplatin or oxaliplatin. Cells were then fixed, permeabilized, and immunostained for NPM1 (Figure 3.1C, D). The extent of NPM1 redistribution was calculated as previously described (Sutton, McDevitt, Prochnau, et al. 2019; McDevitt et al. 2019) by determining the coefficient of variation (CV) of NPM1 pixel intensities within each nucleus. These CV values were then normalized to the average CV for a no-treatment control and plotted by treatment group (Figure 3.1E, F). A lower CV value indicates more broadly distributed NPM1 in the nucleoplasm, and more extensive nucleolar stress.

We determined that significant NPM1 translocation from the nucleolus is observed by 4 hours of treatment with oxaliplatin, and that the translocation becomes more extensive with time (Figure 3.1D, F). By contrast, at the same treatment concentration and time period, only a minor amount of NPM1 translocation occurs upon cisplatin treatment (Figure 3.1C, E). After oxaliplatin treatment, we observed rounding of the nucleoli as previously described (Sutton, McDevitt, Prochnau, et al. 2019). Also of note is the appearance of bulging regions of NPM1 around the periphery of many of the rounded nucleoli after oxaliplatin treatment (Figure 3.1D, white arrows). These features resemble “nucleolar caps”, or structures that have been reported to form after ribosomal DNA damage and other nucleolar stressors (Shav-Tal et al. 2005; Burger et al. 2010). Interestingly, NPM1 is not among the proteins previously reported to comprise nucleolar caps, with some studies expressly stating that nucleophosmin does not compartmentalize into nucleolar caps (Shav-Tal et al. 2005; Brodská et al. 2016). This rapid observable response with oxaliplatin treatment that includes NPM1 redistribution, morphological

features such as nucleolar rounding, and the appearance of putative nucleolar caps all raise interesting questions about the molecular processes behind them.

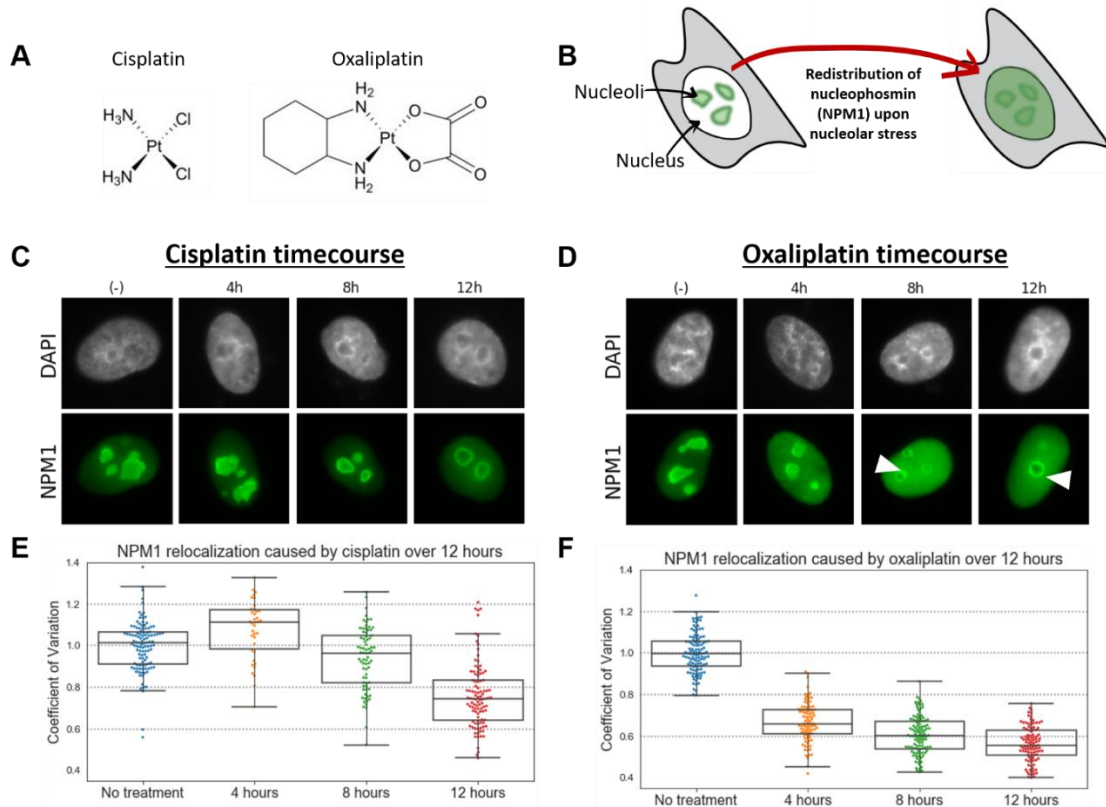


Figure 3.1: Time of redistribution of NPM1 upon treatment with platinum compounds. A) Structures of cisplatin and oxaliplatin. B) Schematic showing the redistribution of NPM1 from the periphery of the nucleolus to the nucleoplasm, a hallmark of the nucleolar stress response. C) Immunostaining of NPM1 (green) in A549 cells at 4, 8, and 12 hours after treatment with 10 μ M cisplatin. DAPI staining (grey) shows the nuclear DNA. D) Immunostaining of NPM1 in A549 cells at 4, 8, and 12 hours after treatment with 10 μ M oxaliplatin. Possible nucleolar cap-like structures indicated with arrows. E) Quantification of NPM1 relocalization after cisplatin treatment. F) Quantification of NPM1 relocalization after oxaliplatin treatment. A lower coefficient of variation (CV) indicates more extensive NPM1 redistribution and therefore more robust nucleolar stress. CV calculations, and boxplot presentation as described in the methods. For each treatment data set, boxes represent median, first, and third quartiles, and vertical lines are the range of data with outliers defined in the methods.

Oxaliplatin but not cisplatin causes inhibition of rRNA transcription

NPM1 redistribution is just one marker of nucleolar stress, and while it is a robust and ubiquitous marker, observation of this redistribution with accompanying morphological changes does not address the molecular mechanisms by which Pt(II) compounds might be inducing nucleolar stress. Several known triggers of nucleolar stress include inhibition of any of the stages of ribosome biogenesis, DNA damage, or direct perturbation of nucleolar structure (K. Yang et al. 2016; Rubbi and Milner 2003; Boulon et al. 2010). We sought to narrow down the potential causes of oxaliplatin-induced NPM1 redistribution by testing a number of processes known to affect it.

It has been established that inhibition of rRNA synthesis and processing are linked to nucleolar stress and NPM1 redistribution (Boulon et al. 2010). Prior studies of the influences of cisplatin and oxaliplatin on rRNA synthesis have yielded mixed results. Using pulse-chase approaches, it has been shown that both cisplatin and oxaliplatin can inhibit rRNA transcription but that neither affect rRNA processing. However, in these studies, cisplatin causes inhibition between 40-100 μ M, doses thought to be above clinical relevance (Burger et al. 2010, 2; Hamdane et al. 2015). Other studies have shown stark differences between cisplatin and oxaliplatin with regard to their ability to affect rRNA transcription. Using RT-qPCR, Bruno et al observed decreases in pre-rRNA levels after 30 minutes of treatment with oxaliplatin and Actinomycin D, followed by marked increases between 1-6 hours of continuous treatment. Treatment with cisplatin did not demonstrate this trend in pre-rRNA levels, which was used to support the conclusion that oxaliplatin acts as a ribosome biogenesis inhibitor like Actinomycin D, while cisplatin works by a different mechanism (namely, DNA damage).

To clarify the influence of cisplatin and oxaliplatin on rRNA transcription and processing and determine the relationship of NPM1 redistribution to these effects, we conducted pulse-chase radiolabeling experiments using a method previously described (Figure 3.2A) (Burger et al. 2010). After treatment of A549 cells with compounds for a fixed period, cells were incubated in Pt(II)-free medium containing ^{32}P -labeled phosphate for one hour, which would be incorporated into any newly synthesized RNA in the “pulse” step. Medium was then replaced with cold medium to track the processing fate of the newly synthesized RNA. Both the ^{32}P -labeled and total RNA were visualized. Low dose (5 nM) ActD is used as a positive control for Pol I transcription inhibition. NPM1 relocalization was measured at time points correlating to the beginning of the chase step.

At three hours of drug treatment, robust NPM1 relocalization is observed for both oxaliplatin and the positive control of ActD (Figure 3.2B,C). In addition, nucleolar rounding and nucleolar cap-like structures containing NPM1 are observed following treatment with both oxaliplatin and ActD (Figure 3.2B). These nucleolar changes are accompanied by inhibition of rRNA transcription but not processing in oxaliplatin and ActD-treated cells. Radiolabeled 47S and 28S bands are both significantly reduced in intensity in RNA labeled after oxaliplatin and ActD treatments in comparison to cisplatin-treated and untreated controls (Figure 3.2D,E). The simultaneous reduction of both of these transcripts indicates that rRNA transcription, but not processing, is being affected by these drugs, as a defect in RNA processing would be indicated by the reduction of the labeled 28S transcript, while 47S transcript levels would remain the same (or increase). Quantification (Figure 3.2E) shows that treatment with ActD almost completely eliminates both 47S pre-rRNA and the processed 28S transcripts. Following

oxaliplatin treatment, 47S levels are reduced to about 3% of the negative control and 28S levels reduced by about half. This level of inhibition of transcription is similar to that previously observed with 6 μM oxaliplatin treatment in X cells (Burger et al.) Cisplatin treatment, on the other hand, retained 65% of 47S transcript levels and 90% of 28S levels as compared to the negative control. Thus, both oxaliplatin and ActD inhibit rRNA transcription but not processing, whereas cisplatin has a much lesser effect. It can be concluded with reasonable confidence that the relatively small impact on rRNA transcription does not underlie cisplatin's cytotoxicity, for reasons that will be explored later in this paper.

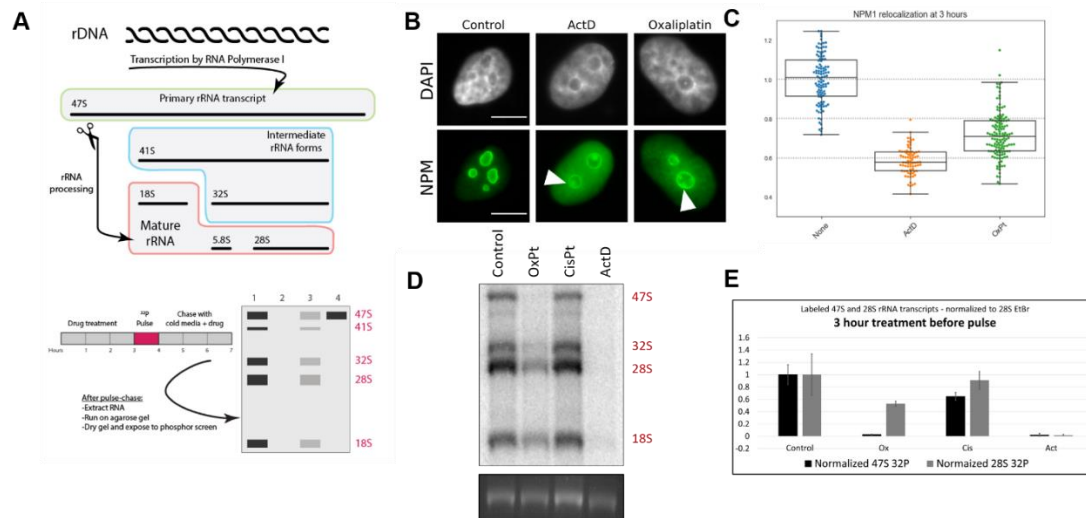


Figure 3.2: NPM1 relocalization and inhibition of rRNA transcription in A549 cells after 3 hours of treatment with platinum compounds. A) Schematic of rRNA processing and pulse chase experiment. B) NPM1 relocalization after 3 hours of treatment with 10 μM oxaliplatin and with positive control ActD (5 nM). Scale bar is 10 μm . Nucleolar cap-like structures indicated by arrows. C) Quantification of NPM1 relocalization 3 hours after treatment with 10 μM oxaliplatin or the positive nucleolar control of 5 nM ActD. D) Results of pulse chase experiment. Cells were treated with 10 μM of cisplatin or oxaliplatin, or 5 nM of ActD for 3 hours prior to the pulse step. Bottom frame shows total RNA (EtBr stain of 28S rRNA) while top image shows ³²P labeled rRNA. Transcript sizes are shown on the right. E) Quantification of pulse-chase data from the gel image in 2D. Error bars represent the standard deviation of two replicates separately treated in two separate wells of A549 cells on the same day.

Inhibition of rRNA transcription coincides with NPM1 redistribution upon oxaliplatin treatment

After establishing that rRNA transcription was significantly inhibited by oxaliplatin treatment, we wondered about the relationship between transcription inhibition and relocalization of NPM1. NPM1 is known to facilitate ribosome biogenesis, and depletion of NPM1 has been shown to inhibit pre-rRNA transcription (Scott and Oeffinger 2016). Thus we considered that NPM1 relocalization may precede transcription inhibition. To examine this more closely, we tested both NPM1 relocalization and rRNA synthesis at an earlier treatment timepoint of 90 minutes. At 90 minutes, many cells clearly display the nucleolar stress phenotype in NPM1 images, but not to the extent that is seen at later time points (Figure 3.3A). Many nuclei appear to be in an intermediate state in which NPM1 is partially translocated, with nucleoli that are not yet round (Figure 3.3A, third panel). A few nuclei do appear to have completely entered a nucleolar stress state, with complete translocation of NPM1 and completely rounded nucleoli (example in Figure 3.3A, fourth panel). This observation of intermediate levels of nucleolar stress following 90-minute oxaliplatin treatment is supported by the median CV value of around 0.9 (Figure 3.3B). Populations of cells undergoing extensive NPM1 translocation usually have median CV values below 0.7, as observed for the positive control of ActD and longer oxaliplatin treatment times (Figures 1 and 2). Transcriptional inhibition is clearly occurring at this time point after oxaliplatin treatment as observed by the reduction of transcript levels (Figure 3.3C, 3D). Oxaliplatin shows a reduction of primary transcript levels to about 60% of the control, and 28S transcripts to under 10% of control levels. This inhibition is not as extensive as the 3-hour time point, but the data supports that Pol I

inhibition precedes robust NPM1 redistribution or at least contemporaneously occurs with the redistribution.

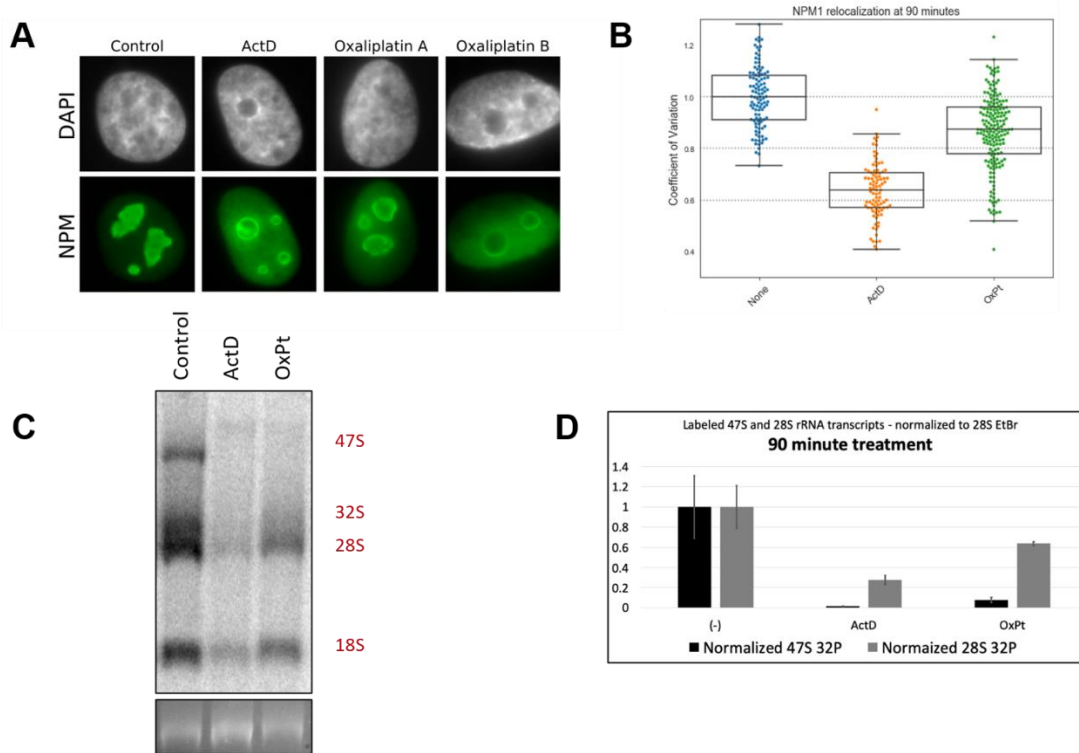


Figure 3.3: NPM1 relocation and inhibition of rRNA processing in A549 cells after 90 minutes of treatment with oxaliplatin. A) NPM1 relocation after 3 hours of treatment with 10 μ M oxaliplatin or 5 nM ActD. Two examples of oxaliplatin-treated cells illustrate the intermediate state of nucleolar stress that the cells are in at 90 minutes of treatment, with a range of cells showing various levels of NPM1 redistribution and nucleolar rounding. B) Quantification of NPM1 relocation at 90 minutes of treatment with oxaliplatin and ActD. C) Pulse chase experiment after 90 minutes treatment with ActD or oxaliplatin. D) Quantification of pulse-chase data from the gel image in 2D. Error bars represent the standard deviation of two replicates separately treated in two separate wells of A549 cells on the same day.

Pol I inhibition and DNA damage

It has been previously demonstrated that DNA damage can lead to the redistribution of NPM1 from the nucleolus to the nucleoplasm (Lee et al. 2005; Yang et al. 2016) and that Pol I inhibition can result from damage to ribosomal DNA (van Sluis and McStay 2017; Korsholm, Lund, and Larsen 2020; Larsen et al. 2014). Pt(II)

compounds are well known to form crosslinks and elicit a DNA damage response in cells (Chaney et al. 2005). Therefore, one possible mechanism by which oxaliplatin inhibits Pol I is as a secondary response to DNA damage. Previous work has shown that oxaliplatin forms fewer DNA lesions than cisplatin by 2-6 fold after 4 hours of treatment in A2780 and CEM cells as measured by atomic absorption spectroscopy (Jan M. Woynarowski et al. 1998; J M Woynarowski et al. 2000). Bruno et al observed γ H2AX foci in cisplatin, but not oxaliplatin treated cells in their 2017 study, further supporting their conclusion that cisplatin, but not oxaliplatin, causes cell death via DDR (Bruno et al. 2017). If oxaliplatin-induced nucleolar stress were caused by underlying DNA damage, we would expect excessive DNA damage induced by oxaliplatin relative to cisplatin, which is the opposite of what is currently reported in the literature. However, given the established ability of DNA damage to induce nucleolar stress, the possibility warranted investigation. We tested the hypothesis that the observed nucleolar and ribosome biogenesis stress responses to oxaliplatin correlated with oxaliplatin-induced DNA damage. We completed a time course from 3-5 hours and performed immunostaining with both NPM1 and γ H2AX. γ H2AX is a phosphorylated histone variant resulting from activation of the DDR signaling pathway ATM, and is a well-established marker that labels sites of DNA damage in cells (Bruno et al. 2017) (Figure 3.4A, 4B).

Nucleus-wide γ H2AX staining, concentrated in foci, was observed upon cisplatin treatment as expected (Figure 3.4A, 4B). Contrary to what was found in the Bruno paper, we did observe some γ H2AX staining with oxaliplatin treatment, although qualitatively this staining appeared to be less intense than the staining observed upon oxaliplatin treatment. There were very low levels of foci observed in the no treatment control and

with ActD treatment. NPM1 redistribution progressed as expected in both treatment conditions, with oxaliplatin displaying more extensive NPM1 relocalization than cisplatin at all three time points (Figure 3.4C).

The intensity of γ H2AX staining per nucleus was measured using an image analysis pipeline in the CellProfiler software (Carpenter et al. 2006). A “percent positive” value was calculated for each treatment condition relative to the no treatment control. A threshold was determined for a positive γ H2AX result based on the 90th percentile intensity value of the no treatment control for each time point. Nuclei in the experimental samples with integrated intensity levels higher than this were counted as positive for γ H2AX (Figure 3.4D). A higher percentage of cells were positive in cisplatin than oxaliplatin conditions. In conclusion, while our data do not support a complete lack of oxaliplatin-induced DNA damage, as reported by recent studies, or dramatic differences between the γ H2AX responses between these two drugs, they do suggest that cisplatin may be inducing a slightly more robust DDR than oxaliplatin. It is therefore unlikely that oxaliplatin’s strong nucleolar stress response is being caused by an upstream DDR.

In addition to nucleus-wide rRNA transcriptional silencing that can result from DNA damage (Larsen et al. 2014), a localized inhibition of Pol I within individual nucleoli can occur after damage to ribosomal DNA, marked by γ H2AX (Kruhlak et al. 2007). Other research has shown that upon targeted rDNA damage, nucleoli reorganize and form nucleolar caps which contain γ H2AX foci (van Sluis and McStay 2015). Among cells where nucleoli were clearly visible, this signature γ H2AX localization was not observed in any of the treatment conditions (Figure 3.4B). While a very small number

of cells came close to resembling this, they were not nearly as robust as what is reported in the literature (Figure S3), and represented a significant minority of cells, with only a few out of hundreds of observed cells resembling this phenotype (Figure S1). Among the few cells that did display γ H2AX foci near the nucleolus, foci were also observed throughout the nucleoplasm, suggesting that oxaliplatin is not disproportionately targeting nucleolus-associated DNA. So, in addition to oxaliplatin treated cells not having a whole genome increase in DNA damage causing NPM1 redistribution and Pol I inhibition, it is unlikely that rDNA damage specifically is causing these responses.

Cisplatin and oxaliplatin both result in downstream p53 stabilization

Mammalian cell death upon activation of the nucleolar stress response is mediated by stabilization of the tumor suppressor protein p53 (Rubbi and Milner 2003; Woods et al. 2015; Boulon et al. 2010; Pickard and Bierbach 2013). However, p53 can also be activated by a litany of other cellular stressors, including DNA damage (Boulon et al. 2010). We examined p53 stabilization by measuring the increase in p53 levels by Western blot (Figure 3.4D, 4E). Both cisplatin and oxaliplatin treatments show dose-dependent stabilization of p53 in A549 cells by 24 hours treatment time. At 3 hrs treatment, however, little p53 increase is observed with treatment of cisplatin, oxaliplatin, or ActD. Thus, although these compounds display different patterns of nucleolar changes at short time periods, they all have similar patterns of p53 stabilization, with little to no stabilization happening at 3 hours of treatment, but robust stabilization happening by 24 hours in a dose dependent manner.

Previous work has shown that cisplatin has a 24-hour IC-50 value of 12.8 μM in A549 cells, while oxaliplatin has a much higher 24-hour IC-50 value of 81.5 μM (Sutton, McDevitt, Prochnau, et al. 2019). Therefore, with 3-hour treatment at 10 μM concentrations for both compounds, oxaliplatin is causing robust nucleolar stress and Pol I inhibition at just 12% of the 24-hour IC-50 value, whereas cisplatin only displays minimal nucleolar stress at 78% of the 24-hour IC50 value. Both compounds cause robust p53 stabilization after 24 hours of treatment. These observations are in line with the prevailing idea that cisplatin causes cell death by DNA damage, whereas cell death caused by oxaliplatin involves nucleolar stress and, interestingly, selective inhibition of Pol I.

Nucleolar integrity following Pt(II) treatment

To further examine the properties of nucleolar structure affected by treatment with platinum compounds, we used immunofluorescence to observe the localization of fibrillarin, another critical nucleolar protein (Figure 3.5). Fibrillarin normally resides in the nucleolus in the dense fibrillar component (DFC). Fibrillarin-containing nucleolar caps form under conditions of nucleolar stress such as rDNA damage and inhibition of Pol I transcription (van Sluis and McStay 2017). Previous work has shown that both cisplatin and oxaliplatin result in formation of fibrillarin nucleolar caps at doses known to inhibit Pol I (Burger et al. 2010) which were, as described above, much higher for cisplatin (100 μM) than oxaliplatin (6.25 μM). Formation of these nucleolar caps upon oxaliplatin treatment would indicate that the robust NPM1 redistribution observed was occurring as part of a broader nucleolar disruption, which may involve the reorganization

and redistribution of many nucleolar proteins not limited to just NPM1 and would be similar to that induced by other nucleolar-stress inducing processes.

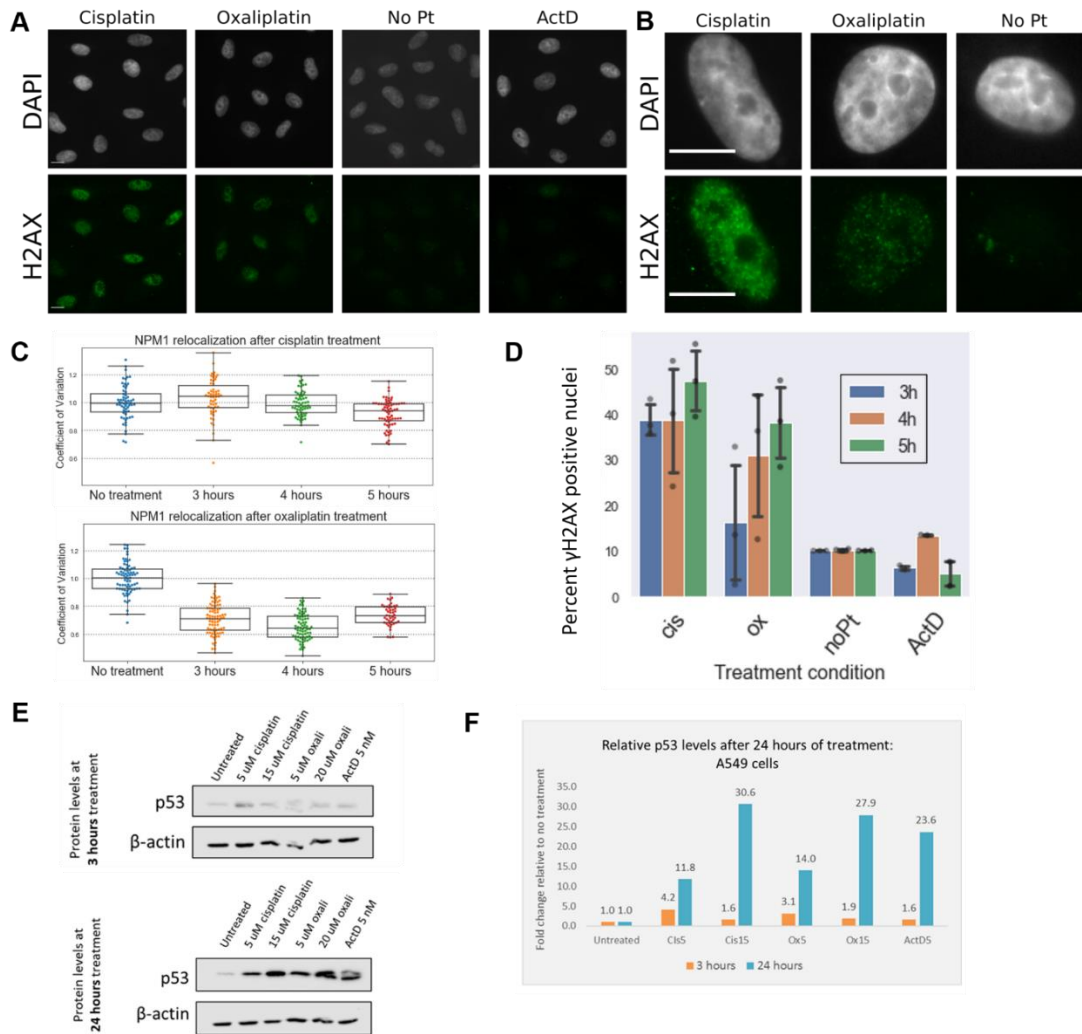


Figure 3.4: DNA damage and p53 stabilization after treatment with platinum(II) compounds. A) DNA damage, measured by γ H2AX immunofluorescence (green) after 5 hours of treatment with cisplatin and oxaliplatin. B) Representative single cell images of A549 cells after treatment with cisplatin and oxaliplatin. C) Quantification of NPM1 redistribution between 3-5 hours of treatment with cisplatin (top) and oxaliplatin (bottom). D) Quantification of γ H2AX positive nuclei, where the x axis represents the percent of nuclei scored as γ H2AX positive as described within the text. Imaging was conducted on 3 separate days, with the exception of ActD which was only tested on two days. A minimum of 50 cells were analyzed for each treatment group E) Western blot for p53 after Pt(II) treatment at 3 hours (top) and 24 hours (bottom). F) Quantification of p53 levels from Western blot from single testing day. All scale bars are 10 μ m

Interestingly, while cap-like structures were observed via NPM1 staining after just 3 hours of oxaliplatin treatment (Figure 3.2) and were continually observed up to 12 hours after treatment, fibrillar-in-containing nucleolar caps were not clearly detected after 6 hours of oxaliplatin treatment when observing fibrillar-in immunofluorescence (Figure 3.5A). Fibrillar-in-containing nucleolar caps were clearly observed as expected with the positive control of ActD (Figure 3.5A). With both oxaliplatin and ActD treatments, nucleoli became rounder and more fibrillar-in was detected in the nucleoplasm in comparison with the negative control. Fibrillar-in distribution in cisplatin treated cells largely resembled the negative control, with punctate foci observed in the nucleolus. Fibrillar-in nucleolar caps do appear in oxaliplatin-treated cells after 24 hours of treatment (Figure 3.5B, Figure B.2). Thus, nucleolar integrity is being altered after 3 hours oxaliplatin treatment, but clear formation of fibrillar-in-containing nucleolar caps does not occur until later timepoints. The timing of fibrillar-in nucleolar cap formation after oxaliplatin treatment suggests that the relocalization of NPM1 may play an earlier role in nucleolar disruption than fibrillar-in.

In sum, the imaging data from fibrillar-in confirms again that the nucleolus is more affected by oxaliplatin than cisplatin under similar conditions. It also suggests that NPM1 translocation is not occurring independently as a unique phenomenon separate from the behavior of other nucleolar proteins, but as part of a global change to nucleolar structure and one that precedes fibrillar-in localization into nucleolar caps.

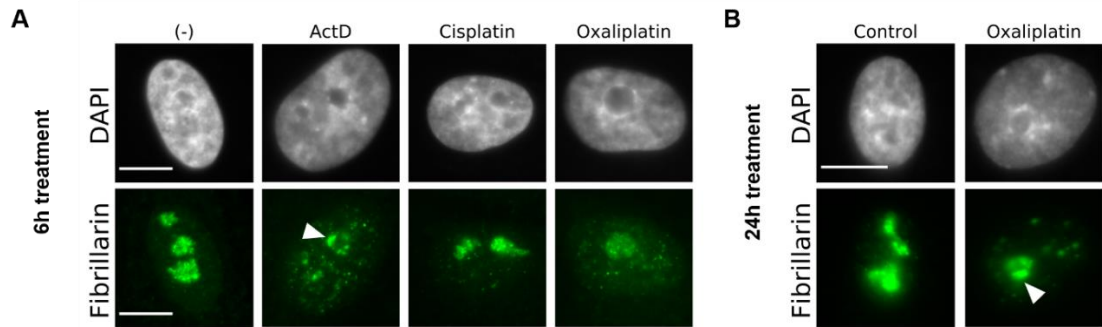


Figure 3.5: Fibrillarlin imaging after treatment with platinum compounds. Representative images of fibrillarlin immunostaining after 10 μ M treatment with Pt(II) compounds or 5 nM ActD for A) 6 hours or B) 24 hours. Nucleolar caps indicated by white arrow.

Discussion

The goal of this work was to better understand the effects of Pt(II) compounds on nucleolar stress related processes. While both oxaliplatin and cisplatin have been reported to influence nucleolar processes, these effects occur at relatively higher cisplatin treatment concentrations [Burger]. A recent report provides evidence that oxaliplatin causes cell death through a nucleolar stress response rather than through the DNA damage pathways long considered operative for cisplatin. This leads to a growing picture that while both compounds form lesions on DNA as well as other biomolecules, oxaliplatin acts primarily through an impact on the nucleolus. To further investigate how oxaliplatin impacts nucleolar processes and clarify its differences from cisplatin, we set out to directly compare the effects of these drugs on underlying biological processes that are associated with nucleolar stress. We focused on early treatment timepoints and examined redistribution of NPM1, performed pulse-chase assays to assess rRNA transcription and processing, observed DNA damage via γ H2AX imaging, and further observed changes in nucleolar structure by imaging fibrillarlin. These studies were

performed in A549 cells, which are well-characterized with respect to nucleolar stress pathways.

At equivalent doses, oxaliplatin, but not cisplatin, was found to significantly inhibit rRNA transcription and not processing. This inhibition happens after just 90 minutes of oxaliplatin treatment and is correlated with early translocation of NPM1 including formation of NPM1-associated nucleolar cap structures. Although fibrillarin is redistributed from the nucleolus by 6 hours of treatment with oxaliplatin, fibrillarin-containing nucleolar caps are not observed until later time points, well after robust redistribution of NPM1 is observed. Thus, oxaliplatin at low doses causes global perturbation of the nucleolus, accompanied by Pol I inhibition and likely not driven by DNA damage. Cisplatin does not cause any of these nucleolar changes under similar treatment conditions. Cisplatin does cause more robust γ H2AX appearance, consistent with a significant DNA damage response. Taken together, our data support a model in which the DDR is a predominant mechanism of cell death upon cisplatin treatment (Bruno et al. 2017). The data further indicate that prior observations of nucleolar responses at high cisplatin treatment concentrations (Burger et al. 2010; Jordan and Carmo-Fonseca 1998) are due to processes downstream of a primary DDR response.

Both cisplatin and oxaliplatin lead to p53 stabilization in A549 cells by 24 hr treatment, but neither compound shows p53 stabilization at the earlier timepoints. Both rRNA transcription inhibition caused by oxaliplatin, and DDR with cisplatin, may cause downstream p53 stabilization by different pathways (Burger et al. 2010) that have been established for nucleolar stress and for DDR in A549 cells.

Importantly, these observations open the possibility that oxaliplatin is a specific/selective RNA polymerase I inhibitor, in a class similar to BMH-21. Further studies might focus on which existing Pol I inhibitors oxaliplatin most closely resembles regarding the cellular behaviors it elicits. NPM1 redistribution should be considered in a broader context of nucleolar disorganization rather than strictly an independent phenomenon, and it is noteworthy that this phenomenon appears to precede the formation of nucleolar caps. The previously undescribed observation of NPM1 “cap-like” structures prior to the canonical caps formed with fibrillarin merits further investigation itself.

Previous work has shown a connection between rRNA processing and p53 stabilization alongside changes in nucleolar proteins (Burger et al. 2013). This connection had not been characterized previously with platinum compounds or with other compounds that primarily seem to induce nucleolar stress linked p53 stabilization via rRNA transcription inhibition. An interesting alternate explanation for lower amounts of DNA damage upon oxaliplatin treatment is that the relocalization of NPM1 is preventing a robust DNA damage response.

Many questions remain with regard to platinum compounds and their relationship to nucleolar stress. For example, how does oxaliplatin inhibit RNA Pol I? Several explanations are possible. It is possible that oxaliplatin directly inhibits Pol I by stalling in a manner similar to BMH-21, and ensuing degradation of Pol I subunits. Oxaliplatin may also prevent formation of the Pol I transcription complex in another manner. For instance, oxaliplatin might bind to and alter R-loops, which modulate transcription. In addition to specific questions remaining about the relationship of particular chemotherapeutic drugs to nucleolar stress, overarching questions about the

reorganization of the nucleolus remain. For example, what are the molecular steps governing nucleolar rearrangement following inhibition of rRNA transcription?

There may be a connection between this specific inhibition of Pol I by oxaliplatin and other processes which have shown differences between these compounds. For example, immunogenic cell death (ICD) has been shown to be more affected by oxaliplatin, and damage to the neurons via disruption of the neuronal nucleolus also appears more affected by oxaliplatin than cisplatin based on existing literature (McKeage et al. 2001; Terenzi et al. 2016). The questions above are critical to a better understanding the mechanisms of platinum-induced nucleolar stress and possible specific inhibition of Pol I by oxaliplatin. Exploration of this topic might lay the groundwork for a better clinical understanding of these drugs.

Bridge to Chapter IV

In this chapter, biological mechanisms underlying a Pt(II) induced nucleolar stress response were explored. Chapter IV will review existing methods to track and identify Pt(II) lesions on biomolecules, summarize results of studies using these methods, and describe the development of a click-based pulldown assay to enrich for Pt(II)-bound DNA in HeLa cells.

CHAPTER IV: IDENTIFYING INTRACELLULAR TARGETS OF PT(II)

This chapter includes previously published work from a review article that was co-authored by Christine E. McDevitt, Rachael Cunningham, Matthew Yglesias, and Victoria DeRose. It also includes data and preliminary conclusions from a DNA pulldown experiment that I developed, designed, and performed. The latter end of this experiment, including library preparation and data analysis, was performed by Emily Reister.

Introduction

Since the discovery and implementation of cisplatin as an anticancer compound, the mechanisms of action of platinum therapeutics (Figure 4.1) have been the topics of an immense body of research. Cellular pathways leading to antiproliferation, toxicity, side effects and resistance have all been subjects of intense study. Unraveling specific pathways is complicated by the pleiotropic responses induced by these relatively simple metal compounds. Identifying the range of targets of platinum compounds upon treatment in eukaryotic cells could aid in this goal, but represents a significant challenge. Unlike drugs with high specificity, these small metal compounds have many potential binding sites in cells including abundant potential primary ligands from amino acids and nucleobases as well as small molecules. In the context of a complex cellular environment, selectivity might be achieved by compartmentalization, accessibility, and other factors that are difficult to predict from *in vitro* work.

Recent advances in high-throughput and ‘omics’ methodologies provide new tools to approach complex questions such as comprehensive identification of small molecule targets in cells. In this review, we describe recent applications of these methods to identify cellular targets of Pt(II) anticancer compounds and their analogues. These include approaches for genome-wide detection of Pt-DNA and Pt-RNA adducts using high-throughput sequencing and various enrichment methods. Comprehensive proteomics-based methods to detect Pt-protein interactions in cells, and current results from those studies, are reviewed. We summarize synthetic tools, including recent literature on fluorescent probes used for platinum detection and click-enabled platinum derivatives for post-treatment labeling. It is our intent for the work described in this review to complement previously published reviews discussing molecular targets of Pt(II) anticancer compounds and methodologies to detect them (Chapman et al. 2011; Wexselblatt, Yavin, and Gibson 2012; White, Haley, and DeRose 2016).

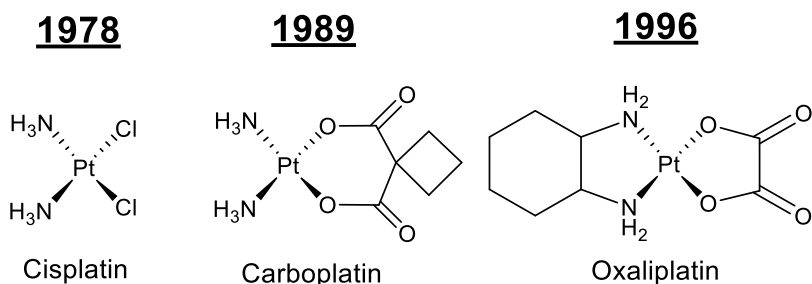


Figure 4.1: Pt(II) anticancer drugs currently approved for use in the United States. Included are years of FDA approval.

Pt(II) Interactions with nucleic acids

The most well-studied mechanism of action of Pt(II)-based chemotherapeutics is the formation of Pt(II) lesions on DNA, which can lead to inhibition of replication and

ultimately cell death via DNA damage response (DDR) pathways (Jamieson and Lippard 1999). Pt(II) lesions primarily form 1,2-intrastrand crosslinks on adjacent guanines, although they can also form 1,2-intrastrand crosslinks on AG dinucleotides, 1,3-intrastrand crosslinks on nonadjacent guanines, interstrand crosslinks, and monofunctional adducts (Jamieson and Lippard 1999). This pattern has been observed both *in vitro* and *in vivo*, and has been described in detail in existing reviews (Jamieson and Lippard 1999; Chaney et al. 2005; Wang and Lippard 2005). Studies on the in-cell interactions between Pt(II) and nucleic acids that do not focus on the DDR are extremely limited. With recent evidence that oxaliplatin in particular causes cell death via ribosome biogenesis stress rather than DNA damage (Bruno et al. 2017), the need for a better understanding of platinum's interactions with nucleic acids in cells has gained renewed interest.

Rather than focusing on the *in vitro* interactions of Pt(II) with nucleic acids and the propensity of these compounds to form particular types of adducts, this review will describe more recent methods employed to isolate and identify DNA and RNA targets of these drugs in a cellular context. The studies reviewed have used a combination of enzymatic, immunological, and chemical methods to approximate the location of these lesions following treatment *in vivo* or *in cellulo* (Table 4.1). Enzymatic methods leverage the features of platinum lesions which block polymerases (Grimaldi et al. 1994; McGurk et al. 2001) or protect regions of oligonucleotides from digestion (Dedduwa-Mudalige and Chow 2015). Primer extension assays use polymerases to extend primers on platinated template strands of DNA or RNA until they are blocked by platinum adducts, revealing lesions at polymerase stop sites. These methods can be coupled with a variety

of downstream methods including traditional sequencing gels, PCR, high throughput sequencing, and mass spectrometry. Recently, click-enabled Pt compounds have promised a more direct method of locating these lesions on DNA and RNA.

Pt(II) Interactions with RNA

There is abundant evidence for platinum accumulation on cellular RNA, and several *in vitro* studies of Pt-RNA interactions have shown propensity for GG and AG adducts as well as Pt-induced crosslinking in structured RNAs (Chapman et al. 2011; Saunders and DeRose 2016). Studies from our lab and others have utilized reverse transcriptase (RT) primer extension and sequencing gels (Table 4.1a) to probe for lesions on RNA isolated from platinum-treated bacteria and yeast (Hostetter, Osborn, and DeRose 2012; Osborn et al. 2014; Rijal, Bao, and Chow 2014; Rijal and Chow 2008). On yeast ribosomal RNA (rRNA), cisplatin-induced Pt binding sites were identified on the 18S helix (Hostetter, Osborn, and DeRose 2012), while both cisplatin and oxaliplatin lesions were described on the sarcin-ricin loop of rRNA (Osborn et al. 2014). Recently, this RT primer extension has been applied in a high throughput context to identify cisplatin adducts formed *in vivo* on yeast rRNA (Plakos and DeRose 2017), with several new sites being identified. These sites - located on helices 23, 24, 58, 80, and 89 of the yeast ribosome - were confirmed by traditional gel-based primer extension analysis.


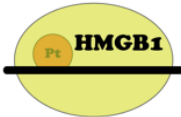
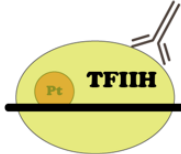
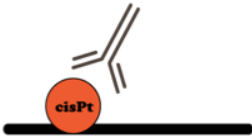

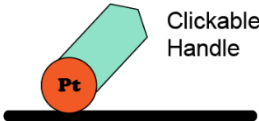
Method	Uses	References
a. Primer extension 	Sequencing gels to ID rRNA targets in yeast and bacteria	(Hostetter, Osborn, and DeRose 2012) (Osborn et al. 2014) (Rijal, Bao, and Chow 2014)
	High throughput ID of rRNA targets - yeast	(Plakos and DeRose 2017)
	High throughput ID of DNA lesions - human cell lines	(Hu et al. 2016; 2017) (Yimit et al. 2019) (Y. Yang et al. 2018) (Shu et al. 2016)
b. Pulldown - HMGB1 enrichment 	Enrichment of Pt sites prior to high throughput primer extension	(Shu et al. 2016)
c. Pulldown – IP of DNA damage repair proteins 	Enrichment prior to high throughput sequencing of repair sites	(Hu et al. 2016; 2017)
d. Pulldown – IP of GG adducts formed by cisplatin 	Pulldown of platinated DNA for microarray	(Powell et al. 2015)
	Enrichment prior to high throughput primer extension	(Hu et al. 2016; 2017)
e. Enzymatic and chemical probing 	Mapping sites on bacterial rRNA	(Dedduwa-Mudalige and Chow 2015)
f. Post treatment labeling - click chemistry 	In-gel fluorescent detection of Pt on yeast tRNA and rRNA	(Osborn et al. 2014)
	Fluorescent microscopy of Pt adducts in tissue culture	(Zacharioudakis et al. 2017); (Yao, Tracy, and Bierbach 2019); (Wirth et al. 2015); (Qiao et al. 2014); (Ding et al. 2013)

Table 4.1: Methods used to detect Pt(II) binding sites on nucleic acids

In bacteria, RT primer extension analysis has been used to assess the interaction of cisplatin and amino acid-modified platinum compounds with the 16S bacterial rRNA (Rijal, Bao, and Chow 2014). Adjacent to these polymerase-based enzymatic mapping methods, RNase and chemical probing techniques (Table 4.1e) have been used to reveal platination sites on bacterial rRNA hairpins (Dedduwa-Mudalige and Chow 2015). A 2016 study identified platinum binding sites on bacterial ribosomes following *in vitro* cisplatin treatment using X-ray crystallography (Melnikov et al. 2016), but the relevance of these findings to the formation of adducts *in vivo* is unknown. The DeRose lab has utilized click chemistry to identify *in vitro* Pt(II) binding to *S. cerevisiae* rRNA and tRNA (Osborn et al. 2014), described in more detail below.

Pulldown Studies to Identify Pt(II) Interactions with DNA

Recent studies have used pulldown techniques to enrich for platinum-bound genomic DNA prior to analysis with other methods (Y. Yu et al. 2018). Hu et al. utilized a high-throughput sequencing assay called “Damage-seq” which relies on immunoprecipitation enrichment of Pt-bound DNA (Table 4.1d) with an anti-Pt-DNA antibody followed by analysis of polymerase stop sites (Table 4.1a) (Hu et al. 2016). This assay was performed alongside Excision Repair Sequencing (XR-seq), which selects sequences from damaged fragments excised in Nucleotide Excision Repair (NER) using an antibody that recognizes Transcription Factor II H (anti-TFIIH, Table 4.1c). For Damage-seq, enrichment of Pt-bound DNA fragments was conducted via immunoprecipitation with a commercially available antibody raised against cisplatin-induced Pt-GG adducts. Following this enrichment, amplification of isolated DNA was

performed such that fragments with a platinum lesion resulted in a truncated amplification product (Table 4.1a). These samples are then subjected to high-throughput sequencing and analyzed. This Damage-seq method was conducted on human lymphocyte GM12878 cells that had been treated with 200 μ M cisplatin for 1.5 hours or 200 μ M oxaliplatin for 3 hours. Results from cisplatin-treated samples revealed uniform distribution of lesions on the genome correlating with GG dinucleotide frequency. The exception was a very slight enrichment at nucleosome centers, which the authors suggest protect lesions from repair. In contrast, XR-seq revealed a heterogeneous pattern of repair on the genome, with NER excision products disproportionately originating from sequences known to be located in active chromatin sites. Similar results were found from samples treated with oxaliplatin. In sum, the authors describe homogeneously distributed genome-wide platinum binding as measured by Damage-seq and heterogeneous patterns of genome repair as measured by XR-seq. From this, they conclude that the observed sites of platinum damage on the genome is mostly dictated by repair efficiency, rather than lesion formation. The same group later developed “high-sensitivity-Damage-seq” (Hu et al. 2017), or HS-Damage-seq, which is designed to deplete undamaged DNA fragments from the extracted genomic DNA prior to high-throughput sequencing. This technology was used to demonstrate that Pt adduct formation is generally reduced around certain transcription factor binding sites. The authors suggest that this is caused by occlusion of these sites by the transcription factors occupying them, effectively blocking cisplatin from accessing the sites. Damage-seq and XR-seq have been used in mouse models to generate cisplatin damage and repair maps in different mouse organs (Yimit et al. 2019),

and XR-seq has been used to map excision repair sites in mouse tissues after cisplatin treatment at different stages of the circadian cycle in mice (Y. Yang et al. 2018).

Shu et al. have recently developed a technology called “cisplatin-seq” (Shu et al. 2016). This is another high-throughput sequencing assay relying on the ability of Pt-DNA adducts to block polymerases. In this study, Pt-bound DNA was first enriched with a protein construct (Table 4.1b) derived from a high mobility group (HMG) box protein known to bind Pt-DNA lesions formed by cisplatin, HMGB1 (Chow, Barnes, and Lippard 1995). The construct was demonstrated via dot blotting to have a high affinity for both GG and AG crosslinks, in contrast to the commercially available cisplatin antibody which was biased towards GG crosslinks (Table 4.1d). HMGB-enriched fragments were amplified with DNA polymerase and analyzed via high throughput sequencing. Cisplatin sites were identified if a stop was measured in sequencing that was also within a sequence that was enriched via the HMGB1 pulldown. This cisplatin-seq method was applied to HeLa cells that had been treated for 3, 12, or 24 hours with 50 μ M cisplatin. An analysis of Pt(II) accumulation by chromosome distribution revealed an enrichment of platinum crosslinking sites on mitochondrial DNA relative to nuclear chromosomes. Within nuclear DNA, the researchers found relative enrichment in promoter regions and transcription termination sites, but determined that this enrichment could be attributed to a higher frequency of GG dinucleotides in those regions. Similarly, chromosomes found to have a relative enrichment of platinum lesions had a higher GG frequency. Interestingly, strong nucleosome signals were associated with higher crosslink frequency regardless of GG density. Higher crosslink frequency was also observed on sequences associated with non-histone DNA binding proteins. The authors suggest from

this correlation that these proteins protect crosslinking sites from NER, and that shielding from repair affects the accumulative pattern of lesions on the genome.

Powell et al. performed a microarray-based pulldown study using the anti-cisplatin antibody (Table 4.1d) (Powell et al. 2015). The antibody was used to enrich for both cisplatin- and oxaliplatin-damaged DNA in yeast and normal human dermal fibroblast cell culture, with treatment concentrations up to 1 mM. Enriched samples were analyzed via microarray and compared to an unenriched input sample. The human microarrays covered a randomly selected 10 Mbp section of chromosome 17, while the yeast microarray probed the whole genome. These results were examined in association with a ChIP-on-chip microarray dataset from yeast to correlate DNA damage maps with histone H3 acetylation changes, which are expected to be more abundant in regions of DNA damage. A low-resolution map of DNA damage was generated and revealed heterogeneous distribution of Pt-induced DNA damage, with some correlation to expected damage sites based on GG and AG sequence distributions. H3K9 acetylation patterns were found to be the same regardless of the type of damage.

Taken together, these high-throughput studies have confirmed an expected preference for platinum lesion formation on GG dinucleotides and more generally regions of high guanine frequency on the genome. They have also suggested that nucleosomes and DNA binding proteins may shield Pt(II) lesions from DNA repair machinery. A relationship between nucleosome positioning and the formation of Pt(II)-DNA lesions is supported by studies that have demonstrated either an overall increase (Han et al. 2016) or redistribution (Zacharioudakis et al. 2017) of Pt(II)-DNA lesions upon induction of a euchromatic state in cells using histone deacetylase inhibitors.

Beyond these general conclusions, these studies have revealed mixed results regarding the initial formation and accumulative patterns of Pt adducts. Several limitations have permeated these studies, with one major challenge being the enrichment of platinated fragments prior to sequencing. Some rely on the commercially available anti-cisplatin antibody for enrichment (ab103261, Abcam) (Hu et al. 2016; Powell et al. 2015). While this antibody recognizes the GG lesions formed by cisplatin and carboplatin, it has little to no immunoreactivity to AG adducts (Shu et al. 2016) and has not been demonstrated to recognize the adducts formed by oxaliplatin. Similarly, the HMG protein used by Shu et al. to enrich for platinated DNA has been shown to have a higher affinity for lesions formed by cisplatin than those formed by oxaliplatin (Chaney et al. 2005; M. Wei et al. 2001). Additionally, these methods were all developed using high concentrations of Pt compounds that are above clinical relevance. All rely on one or more “secondary properties” of the lesions, such as their ability to block polymerases, or the affinity of specific proteins or antibodies to Pt-damaged DNA. More direct methods such as those utilizing click chemistry to recognize and enrich for the Pt compounds themselves regardless of cargo have the potential to further our understanding of Pt accumulation on DNA genome-wide and nucleic acids more generally in the cell. The next sections will discuss ways to visually track Pt(II) compounds in the cell using fluorescent tags. These approaches can complement those that identify genomic and other nucleic acid binding sites in the cell.

Detection of Platinum Using Pre-tethered Fluorophores

Methods of spatially tracking platinum compounds in cells are important tools for understanding molecular targets and are complementary to high-throughput molecular approaches. Atom-based methods such as installation of a radioactive platinum atom, X-ray fluorescence, electron microscopy, NMR, and mass spectrometry can provide information on platinum location and binding partners and have been reviewed previously (White, Haley, and DeRose 2016). These methods, while useful for *in vitro* and non-cellular work, are difficult to apply to live cells. One approach for potential live-cell imaging is the tethering of a fluorophore directly onto the platinum compound.

Cisplatin, oxaliplatin, and carboplatin are small, low or no- carbon molecules (Figure 4.1) in contrast to most fluorophores. The attachment of a fluorophore to platinum compounds can give rise to differences in charge, lipophilicity, solubility, polarity, or reactivity from the parent platinum compounds, as noted previously by Wexselblatt et al. (Wexselblatt, Yavin, and Gibson 2012). For platinum compounds, small changes can result in large differences to toxicity. For example, the addition of a methyl or ethyl to the cyclohexane ring changes the toxicity of oxaliplatin derivatives (Galanski et al. 2004). Another example demonstrated by Rijal et al. showed altered binding specificities of different amino-acid modified platinum compounds towards 16S rRNA (Rijal, Bao, and Chow 2014). If such small changes can make large impacts in these examples, it would stand to reason that larger deviations, such as an added fluorophore, could significantly affect activity. Also of concern may be the assumption that the fluorescent ligand remains tethered to the platinum in the cell. Fluorescence detection only gives information on the location and presence of the fluorophore and not

the platinum itself. Fluorophores tethered through a monodentate ligand could be susceptible to trans-labilization (Wexselblatt, Yavin, and Gibson 2012).

Despite these limitations, platinum-tethered fluorophores have proved invaluable to platinum research and continue to be synthesized. There have been many new compounds that incorporate a fluorophore created within the last few years. Kitteringham et al. have created a carboplatin mimic with an incorporated BODIPY fluorophore and have imaged it in both cisplatin sensitive and resistant cells (Kitteringham et al. 2018). Kalayda et al. created an oxaliplatin mimic which has been functionalized with a fluorescein and used to study oxaliplatin resistance (Kalayda et al. 2017). A glucose and BODIPY conjugate has also been synthesized that shows enhanced uptake into cells (Ramu et al. 2018). Xue et al. created a BODIPY-incorporated platinum compound modified with a photosensitizer to induce reactive oxygen species (Xue et al. 2017). Yao et al. have also produced a cysteine-directed derivative using their click enabled, acridine-tethered compound **7** (Table 4.2) (Yao, Tracy, and Bierbach 2019). Additionally, platinum(IV) has been derivatized to release fluorophores from the axial positions to investigate payload release upon reduction. Some recent Pt(IV) derivatives utilize aggregation-induced emission for visualization (Yuan et al. 2014) and an EGFR-targeted platinum compound tethered to a fluorescein (Mayr et al. 2017). Fluorescent platinum probes have been valuable to the field and continue to be used to further study platinum accumulation and targets; however, the chemical concerns of the derivatives compared to the parent compounds have gone largely unaddressed. A more direct method, such as selectively tethering fluorophores to platinum compounds after native activity has already occurred, is highly desirable.

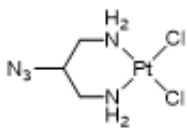
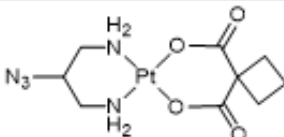
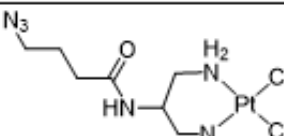
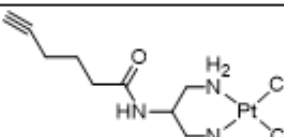
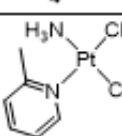
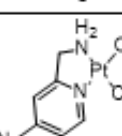
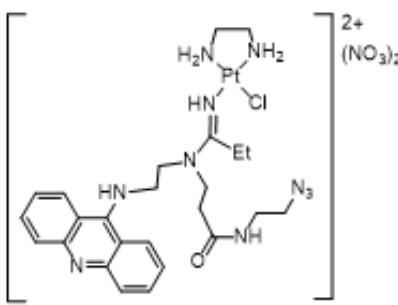
Structure	Use	Reference
 <p style="text-align: center;">1</p>	Library synthesis of carboplatin derivatives	(Urankar and Košmrlj 2010)
	Fluorescent labeling of DNA and ribosome	(Moghaddam et al. 2015)
	Protein target identification	(Cunningham and DeRose 2017)
 <p style="text-align: center;">2</p>	Synthesis of carboplatin derivatives	(Urankar and Košmrlj 2010)
	Toxicity	(Kitteringham et al. 2018)
 <p style="text-align: center;">3</p>	Protein target identification	(Cunningham and DeRose 2017)
	DNA pulldown	(Cunningham et al. 2018)
	Cellular imaging	(Wirth et al. 2015)
	Fluorescent labeling of DNA	(Wirth et al. 2015)
 <p style="text-align: center;">4</p>	Cellular Imaging	(Wirth et al. 2015)
 <p style="text-align: center;">5</p>	Fluorescent labeling of RNA, ribosomal RNA and tRNA	(Hostetter, Osborn, and DeRose 2012)
 <p style="text-align: center;">6</p>	Cellular imaging, gene expression, DNA binding	(Zacharioudakis et al. 2017)
 <p style="text-align: center;">7</p>	Synthesis of acridine derivatives	(Yao, Tracy, and Bierbach 2019)
	Cellular imaging	(Ding et al. 2013)
	DNA labeling	(Ding et al. 2013)
	Investigation of DNA and RNA synthesis, Cell cycle investigation	(Qiao et al. 2014)

Table 4.2: Click-enabled Platinum(II) Derivatives

Click chemistry for post-treatment tethering to platinum compounds

Click chemistry refers to reactions that are distinguished as being modular and high yielding (Kolb, Finn, and Sharpless 2001). A widely used bioorthogonal click reaction is azide-alkyne cycloaddition, either Cu-catalyzed (CuAAC) or strain-promoted (SPAAC). An azide group is easy to incorporate via a substitution reaction into many molecules of interest. The small size, biological inertness, and overall neutral charge have made it an enticing option for incorporation into platinum ligands. The installation of a small azide may have less influence on the localization or activity of the platinum compound than the installation of a large fluorophore. The selectivity of the CuAAC and SPAAC reactions for post-treatment labeling provide direct detection of the platinum compound.

There are currently a handful of available click-capable platinum compounds (Table 4.2). All of the compounds have been used for cellular work and for a variety of other applications. Kitteringham et al. determined the IC_{50} of the azide-modified compound **2**, which had similar toxicity to the parent carboplatin and much higher toxicity than the pre-tethered BODIPY conjugate mentioned above (Kitteringham et al. 2018; Urankar and Košmrlj 2010). Compound **1** originally synthesized by Urankar et al. has been used to label DNA as well as characterize cellular RNA targets in *S. cerevisiae* by Moghaddam et al. (Urankar and Košmrlj 2010; Moghaddam et al. 2015). It was also used for *in vitro* fluorescent protein labeling and an enzymatic assay (Cunningham and DeRose 2017) [40]. Compound **3** has been used to enrich for Pt-bound proteins for target identification in *S. cerevisiae* (Cunningham and DeRose 2017), in addition to its application to enrich for and fluorescently label Pt-bound DNA *in vitro* (Wirth et al.

2015; Cunningham et al. 2018). For a more comprehensive look at Pt binding in a cellular context, compound **3** and compound **4**, its alkyne derivative, were used in cellular imaging studies (Wirth et al. 2015). Compound **5**, another click chemistry enabled compound developed in the DeRose lab, was used to fluorescently label ribosomal RNA and tRNA from treated *S. cerevisiae* (Osborn et al. 2014). Zacharioudakis et al. synthesized compound **6** in order to determine localization of Pt-DNA adducts upon treatment with a histone deacetylase inhibitor (Zacharioudakis et al. 2017) and to investigate the effect of platinum on gene expression. Lastly, compound **7** was used by Qiao et al. to determine the cellular distribution of a Pt-acridine compound (Qiao et al. 2014). It has since been used to synthesize new derivatives that incorporate cysteine-directed moieties as described above. Compound **7** has been used to label proteins, investigate DNA and RNA synthesis after platinum introduction, and to fluorescently label DNA (Yao, Tracy, and Bierbach 2019; Qiao et al. 2014; Ding et al. 2013).

The click chemistry-enabled Pt compounds described above have been used to further understanding of Pt interactions in cells through the direct detection of the Pt reagent post-treatment, allowing for Pt localization that is theoretically unbiased from the influence of fluorophore properties. However, these compounds have all been restricted to the CuAAC reaction which requires a cytotoxic Cu(I) catalyst, or to strain-promoted reactions that require a non-cell permeable DIBO (Cañeque, Müller, and Rodriguez 2018). These properties have limited the use of click-enabled compounds for fluorescence imaging mainly to analysis in fixed cells. Further work into diversifying the click-capable platinum compounds to other types of bioorthogonal reactions may allow

expansion into live-cell imaging and other types of investigations based on post-treatment derivatization.

Review Conclusion

Upon entering a cell, platinum anticancer agents encounter an array of biomolecules. Despite the ubiquitous use of these drugs and their diverse clinical applications, the specific targets of cisplatin and its analogues in a cellular context remain elusive. Historically, attempts to understand the targeting profiles of these drugs have either relied on the examination of their extensive biological and clinical effects, or on highly specific *in vitro* structural studies. A growing body of research attempts to reconcile these disparate realms of study using unbiased, comprehensive high-throughput approaches towards target identification. So far in this chapter, work has been described which has begun to outline the patterns of platinum targeting and accumulation in the cell, as well as factors that determine in-cell binding specificity. Emergent methods and technologies were described that enable high-throughput identification of platinum targets. In the next section, development of a pulldown assay to enrich for Pt(II)-bound DNA will be described.

A Pulldown Assay for Platinated DNA Utilizing a Clickable Pt(II) Derivate

One potential application of the previously described clickable Pt(II) derivatives is identification of specific sequences of DNA that are bound to Pt(II). Using pulldown assays to identify the DNA targets of small molecules is a relatively recently developed strategy sometimes referred to as Chem-seq (Anders et al. 2014; Kapoor, Waldmann, and Ziegler 2016; Rodriguez and Miller 2014).

We sought to develop a Chem-seq assay that would identify Pt(II) targets on the genome utilizing the clickable Pt(II) compound 1,3-platin, (Figure 4.2A), or compound **1** in Table 4.2. Like other clickable azide compounds, this cisplatin analog can undergo a copper-catalyzed cycloaddition reaction to add an alkyne tagged molecule of interest such as a fluorophore or biotin (Figure 4.2B). The attachment of a biotin allows for the enrichment of Pt(II) bound biomolecules via biotin-streptavidin pull-down.

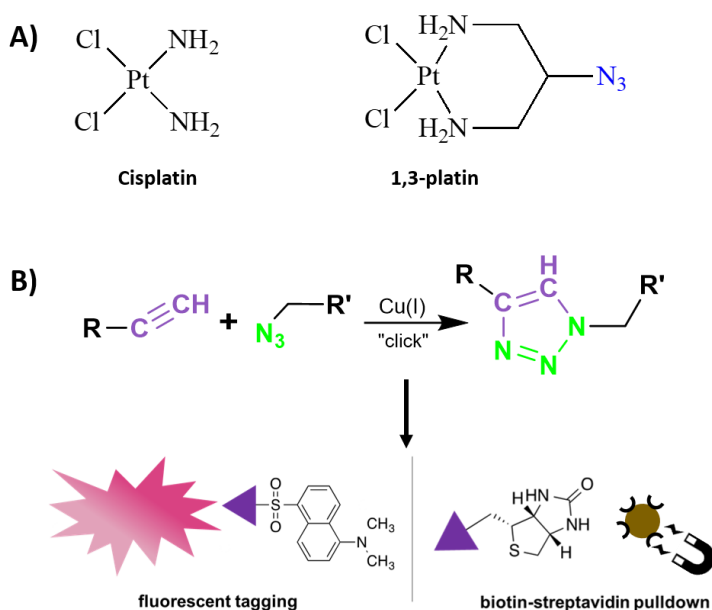


Figure 4.2: Click pull-down schematic A) Structures of cisplatin and its clickable analog 1,3-platin. B) The alkyne-azide cycloaddition reaction and two examples of molecules that can be appended via this reaction. Fluorescent tagging allows for visualization via microscopy or gel, and biotin allows for enrichment of bound molecules via pull-down.

To first establish the viability of this assay, we needed to verify that Pt(II) bound, biotin-clicked DNA could be enriched from a pool of platinated and unplatinated DNA. These initial experiments were conducted with compound **3** from Table 4.2, also known as azidoplatin. A DNA hairpin was platinated via azidoplatin treatment and subsequently clicked to biotin. Platinated, clicked hairpin was purified via HPLC. Platinated hairpin was mixed with an unplatinated long oligonucleotide and the mixture was incubated to

with magnetic streptavidin beads. After binding, beads were washed and remaining bound DNA was eluted off via heating in formamide. Samples were evaluated by acrylamide gel analysis.

Results showed specific binding of the platinated, clicked (biotinylated) DNA hairpin, which was successfully eluted off of the beads with formamide (Figure 4.3). No nonspecific binding of the unplatinated long oligonucleotide was observed, and this oligo appears to have completely been washed off the beads by the second wash step. We also needed to demonstrate that platinum and biotin were able to be removed from the DNA after enrichment so that the DNA can be used for downstream amplification and sequencing. We were able to demonstrate that after formamide elution, platinum and biotin can be removed from the DNA via thiourea reversal, leaving unplatinated DNA available for downstream sequencing.

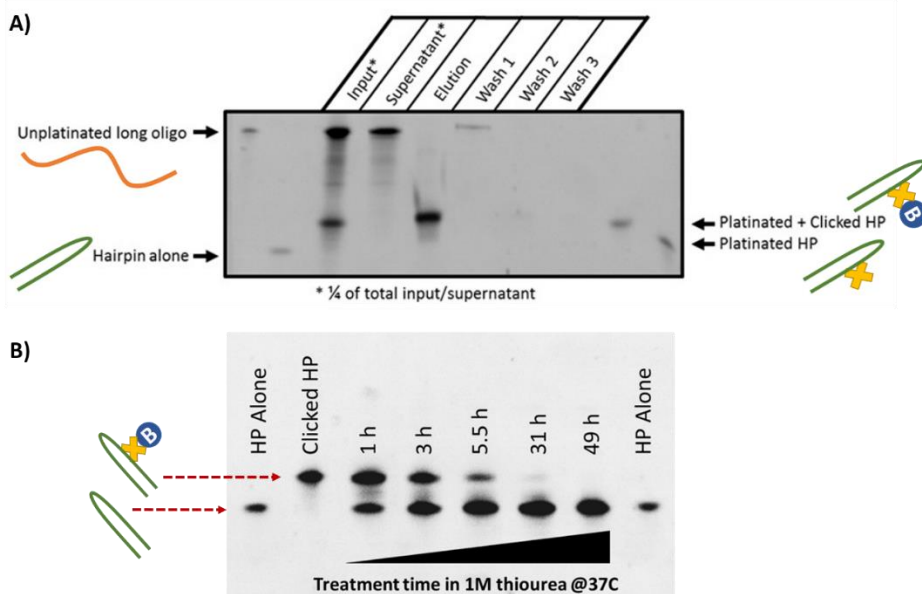


Figure 4.3: Platinum click pulldown gel A) Acrylamide gel demonstrating successful enrichment of platinated DNA hairpin (HP) from a mixed solution of platinated HP and unplatinated long oligo via biotin-streptavidin pulldown. Platinum molecule is indicated by yellow cross, biotin is indicated by blue circle. B) Acrylamide gel demonstrating successful removal of platinum from the hairpin after incubation for two days in 1M thiourea at 37C.

After establishing a protocol that could successfully enrich platinated DNA and remove this platinum, we proceeded to perform an *in cellulo* experiment to determine the DNA targets of this platinum compound on the genome of HeLa cells (Figure 4.4). HeLa cells were treated with 50 μM 1,3-platin for 30 hours. Genomic DNA was then isolated and fragmented to 150 bp fragments. A biotin click reaction was performed on fragmented DNA, and the platinum-bound fragments were enriched via streptavidin pulldown on magnetic beads. In total, 3 separate Pt(II) treatments were performed, and a DMF control treatment was also performed. Samples were taken from both the input and enriched fractions.

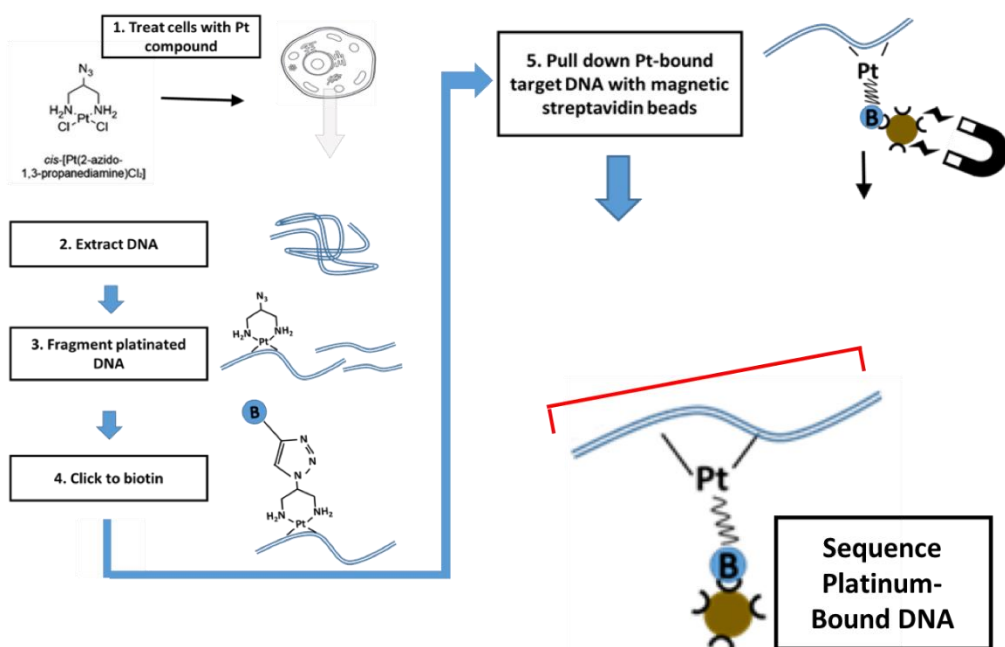


Figure 4.4: Schematic of *in cellulo* pulldown experiment to enrich and sequence Pt(II) bound DNA.

A summary of findings from this pilot DNA pulldown study is shown in Figures 4.5 and 4.6, with details of this analysis published in the dissertation of Dr. Emily Reister (Reister 2018). Pulldown yields were very low, likely due to infrequent binding of Pt(II)

on the genome. Due to these low yields, extra rounds of PCR amplification were performed to generate sequenceable libraries. Each pulldown sample yielded between 1 and 5 million usable reads. While this is lower than ideal for this type of study, analysis was performed to determine if we could at identify any highly platinum(II)-bound regions of DNA.

No significant difference in GC content was observed between the Pt(II) pulldown samples, the input, or the DMF treated control samples (Figure 4.5A). Further, no enrichment was found for adjacent guanines (Figure 4.5A). These results do not align with expectations and previous data supporting that Pt(II) would accumulate on guanine rich areas as well as preferentially accumulate on adjacent guanines (Hu et al. 2016; Shu et al. 2016; Powell et al. 2015). Whole genes were identified that had significant enriched sequences on average across the gene relative to the DMF control. Genes were considered that were not found in the DMF sample (or were found in very low amounts) that had at least 2 replicates with overlapping regions in enriched samples. Generally uniform distribution was observed throughout the genome, with a few peaks (Figure 4.5B). MACS2 analysis (Zhang et al. 2008) was performed and identified 86 significant peaks, with most enrichment at regions in highly repetitive sequences.

A)

Sample	GC%	GG Frequency
Platinum(II) Pulldown	40.4%	5.3%
Pulldown Input	41.2%	5.4%
DMF Pulldown	40.7%	5.6%

B)



Figure 4.5: Relevant findings from pilot Pt(II) pulldown study. A) No significant differences in GC content or frequency of adjacent guanines was observed between input, Pt(II) pulldown, and DMF control samples. B) Pt(II) read distribution across chromosomes shows minimal regional enrichment. Pulldown samples were compared to the input fractions, then to the pulldown control. Positive signals represent peaks that were shared between both Pt(II) samples are shown as positive signal. Although there are a few intense peaks (highlighted in red), hits are mostly distributed throughout the genome. Figures by Emily Reister.

One prediction was that we might see accumulation of Pt(II) on DNA associated with the nucleolus, due to the nucleolus-platinum connection described in Chapters I-III. To measure this, enrichment on rDNA was analyzed. Significant amounts of rDNA were found in pulled down Pt(II) samples, however there were also significant rDNA regions identified in DMF control samples (Figure 4.5C). Therefore, no rDNA enrichment was ultimately observed.

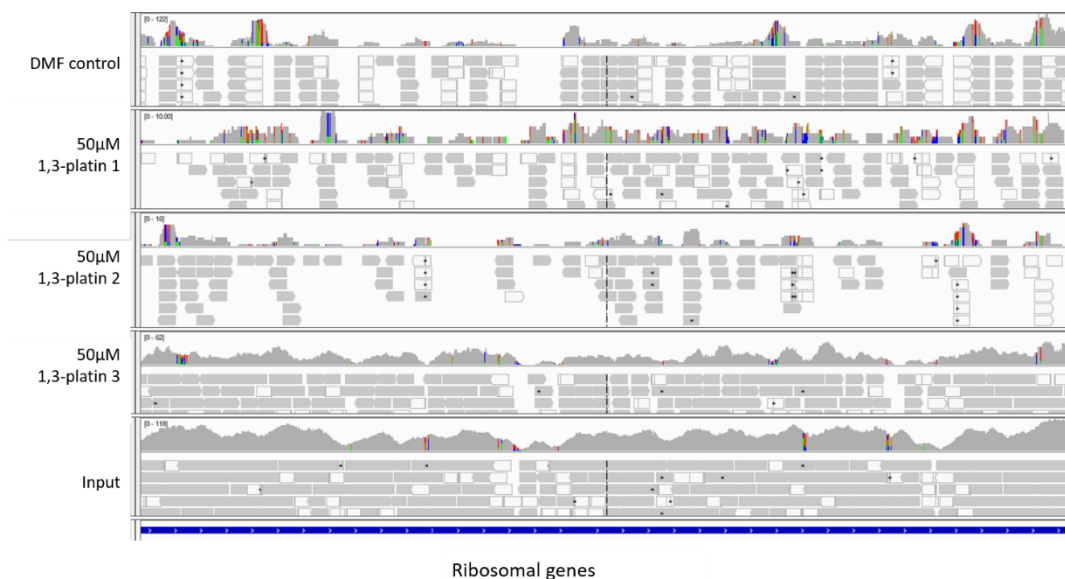


Figure 4.6: rDNA is not enriched in Pt(II) pull-down samples. Distribution of reads across ribosomal genes shows significant coverage, but the DMF control shows significant contamination of ribosomal DNA. Figure by Emily Reister.

This pilot study was primarily limited by low amounts of input DNA. Treating a larger amount of cells in follow-up studies would yield more total DNA and also larger amounts of DNA in the platinum-enriched samples. This would allow for more robust and accurate identification of Pt(II) targets.

Bridge to Chapter V

In this chapter, methods to detect Pt(II) compounds on biomolecules, particularly nucleic acids, were reviewed. Existing data from these methods was summarized and promising research that might improve upon these technologies was discussed. A pilot study to enrich for and sequence Pt(II) bound DNA using a clickable Pt(II) derivative was shown. In the next chapter, work from Chapters I-IV will be summarized and future directions will be discussed.

CHAPTER V: CONCLUDING REMARKS

Summary

Chapter I of this document introduced the topic of Pt(II) chemotherapeutic drugs by discussing the history of these compounds and literature on their potential mechanisms of action. Key background on the nucleolus and ribosome biogenesis was discussed. The relationship between the nucleolus, ribosome biogenesis, and cancer was established and an intriguing connection between Pt(II) drugs and the nucleolus was described. This chapter presented important questions that would be addressed throughout the dissertation, including why some Pt(II) compounds affect the nucleolus more than others, and which nucleolar processes might be affected by these drugs.

Chapter II built upon existing studies that highlighted the ability of a subset of Pt(II) compounds, including oxaliplatin but not cisplatin, to cause cell death via nucleolar stress rather than the canonical DNA damage response. Influential properties of Pt(II) compounds were investigated using redistribution of the nucleolar protein NPM1 as a marker of nucleolar stress. NPM1 assays were coupled to calculated and measured properties such as compound size and hydrophobicity, both of which were found to correlate positively with stress induction. The leaving group of oxaliplatin is not required for NPM1 redistribution. Interestingly, although changes in the size and aromaticity of oxaliplatin's DACH ligand can be tolerated, ring orientation appears critical for stress induction. The specificity of ligand requirements provides insight into the striking ability of only certain Pt(II) compounds to activate nucleolar processes.

In chapter III, inhibition of pre-rRNA transcription is identified as the primary cause of the nucleolar stress response upon oxaliplatin treatment. rRNA transcription and

processing is measured via pulse-chase assay at time points known to cause NPM1 redistribution. γ H2AX, a measure of DNA damage, was observed near these time points and p53 stabilization after treatments was measured. Fibrillarin, another nucleolar marker, was also observed. NPM1 redistribution and lowered pre-rRNA transcript levels are observed after short (1.5-3 hours) treatments with oxaliplatin, but not cisplatin. Broader nucleolar reorganization, including formation of nucleolar caps as observed with fibrillarin, is observed at later time points. Overall, these results further establish differences in nucleolar responses between cisplatin and oxaliplatin and establish Pol I inhibition by oxaliplatin as an underlying cause of these differences.

In chapter IV, established methods to identify biomolecular targets of platinum compounds were summarized, with a particular focus on nucleic acids. Click-enabled platinum compounds that can be used for post-treatment labeling were discussed. Development of a DNA pulldown method with these click-enabled compounds to identify the genomic targets of a Pt(II) drug analog was described. Preliminary sequencing results from a pilot study using this assay were presented.

Future directions

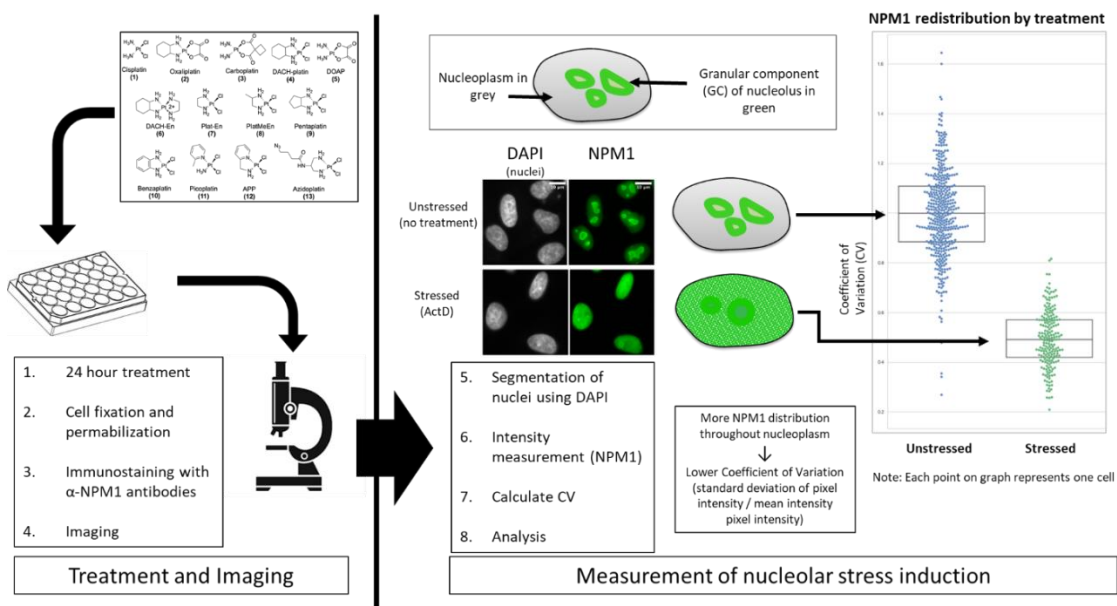
Throughout this document, the need for a better understanding of the mechanisms of action of Pt(II) chemotherapeutic agents has been clearly established. Many questions remain about the biological mechanisms of action of these drugs and their intracellular behavior on a molecular level. Are there properties of these compounds in addition to the ones described in Chapter II that can influence their ability to induce stress? Why is oxaliplatin a much more potent inhibitor of rRNA synthesis by Pol I? Oxaliplatin may be acting similarly to Pol I inhibitors such as BMH-21, which cause transcriptional stalling

and degradation of Pol I subunits. It may have a higher nucleolar uptake than cisplatin, or it may more robustly target rRNA and rDNA, leading to the disproportionate downstream effects on rRNA transcription. Tools such as the clickable Pt(II) analogs described in Chapter IV may help resolve these questions and are likely to prove valuable in developing a better understanding of the subcellular localization and behavior of these compounds. For example, the development of a clickable Pt(II) analog that can also induce nucleolar stress could be used as a basis of comparison with those that cannot, to see if the ability of Pt(II) compounds to induce stress correlated with differences in where they localize or which biomolecules they interact with in the cell. Would a more robust Chem-seq assay show accumulation of Pt(II) on rDNA? Do other Pt(II) compounds known to induce nucleolar stress, such as phenanthriplatin, also inhibit rRNA synthesis, and if so, is this inhibition via the same mechanism as oxaliplatin? Phenanthriplatin is a monofunctional adduct and induces nucleolar stress at much lower concentrations than oxaliplatin, so it is possible that it works by a different mechanism than oxaliplatin (McDevitt et al. 2019).

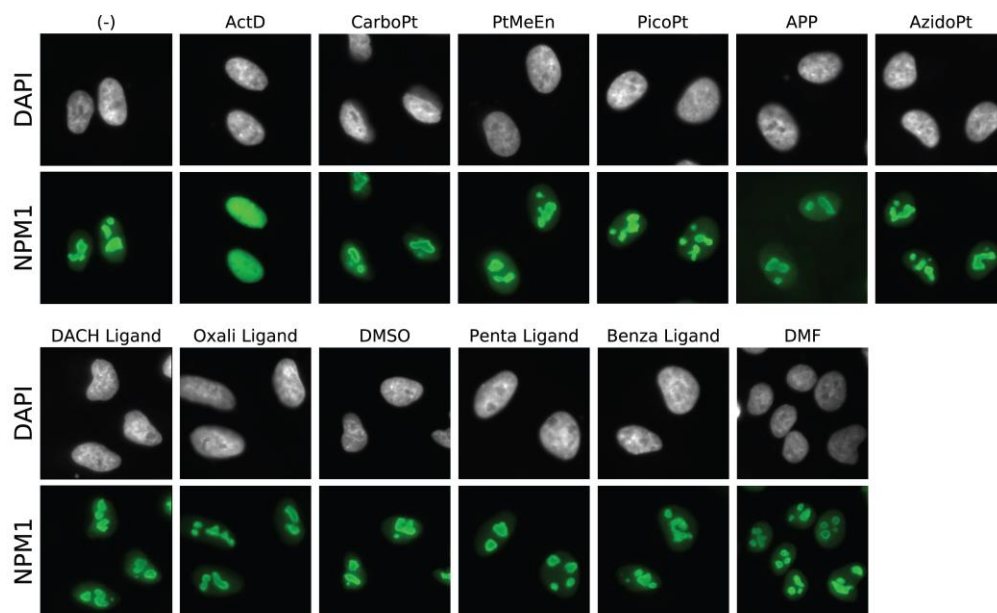
Overall, this work has marked a step forward in our understanding of the mechanisms of Pt(II) chemotherapeutic agents and their analogs, particularly in the context of the effects they have on the nucleolus and ribosome biogenesis. A more comprehensive explanation of these mechanisms may lead to a greater knowledge surrounding the efficacy of these drugs and the challenges faced in their clinical applications such as resistance and off-target effects. There may also be a link between the ability of certain Pt(II) compounds to induce ribosome biogenesis stress and the impact they have on other cellular phenomena such as Immunogenic Cell Death (ICD)

and peripheral neuropathy (Terenzi et al. 2016; McKeage et al. 2001). Further study into how Pt(II) compounds affect the nucleolus and ribosome biogenesis may even assist in the development of new chemotherapeutic agents or treatment strategies derived from these widely used compounds.

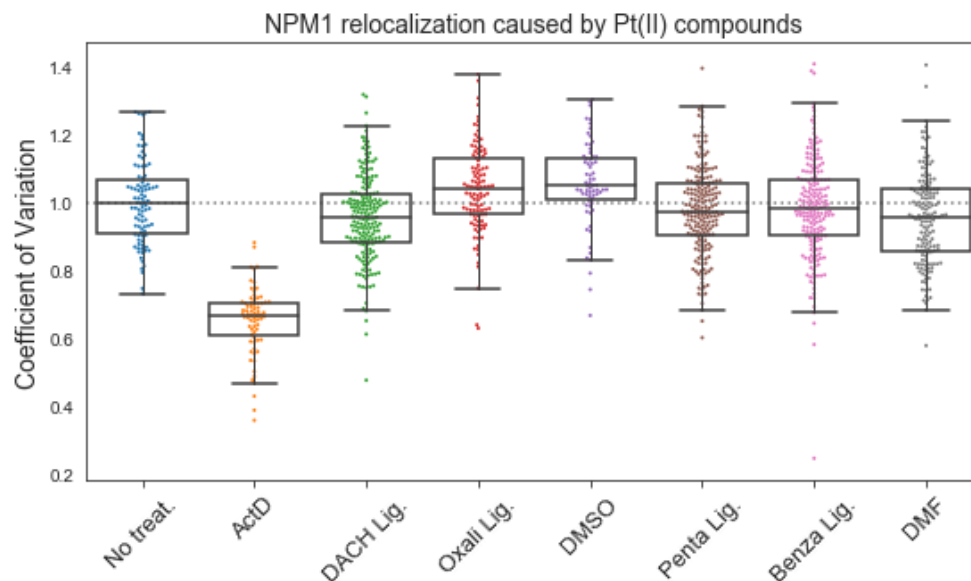
Supplementary Figures



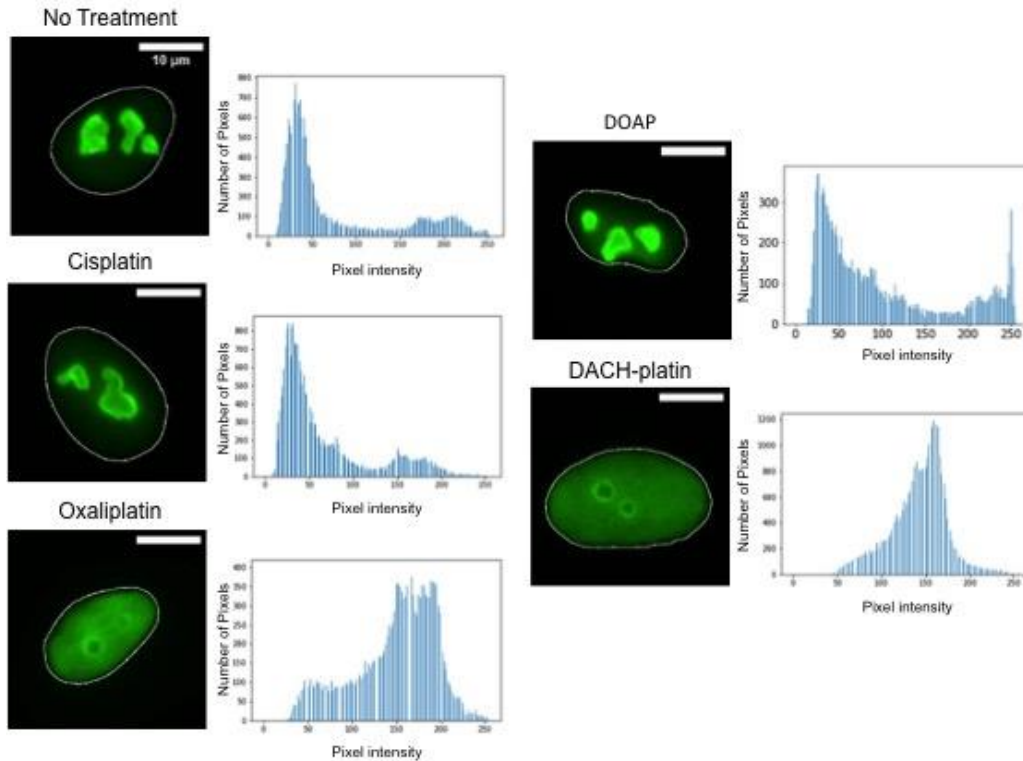
Supplementary Figure A.1. NPM1 assay and quantification scheme. A549 cells were seeded on coverslips treated for 24 hours with the selected compound. Cells were fixed, permeabilized, and stained with an α -NPM1 antibody as described in Materials and Methods section. After imaging, nuclei were segmented using DAPI staining and pixel intensity from NPM1 imaging was measured. The Coefficient of Variation (CV, standard deviation over mean), was calculated for each nucleus, normalized to the mean CV for the no treatment control on that day, and plotted as above with each nucleus represented by one point on the plot. An average CV of 1.0 indicates no stress, whereas a lower CV (around 0.6) indicates diffusion of NPM1 throughout the nucleoplasm, a positive indicator of nucleolar stress. Treatment data sets are represented by box plots, where the center, top, and bottom lines of boxes represent the median, first and third quartile respectively.



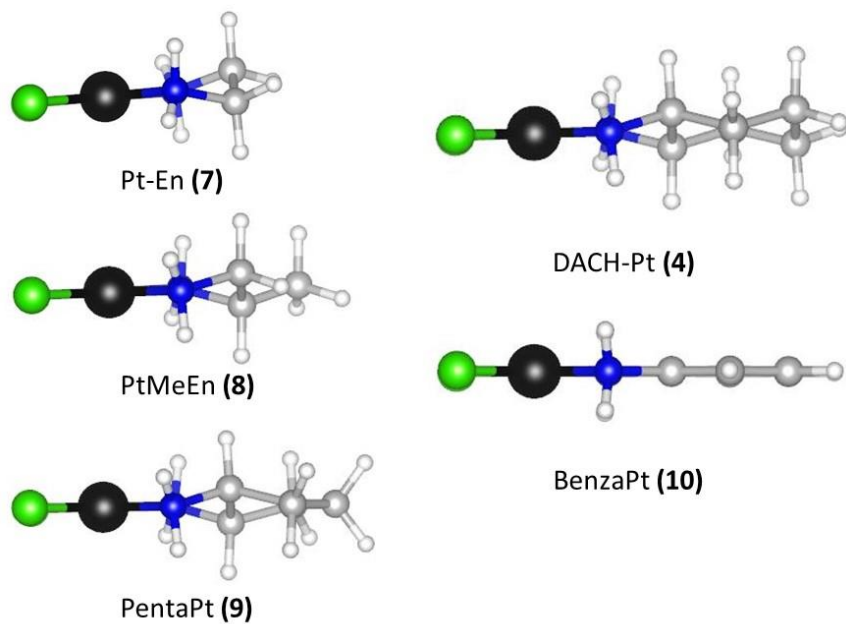
Supplementary Figure A.2. Additional images for compounds tested. Top row shows negative and positive (Actinomycin D) controls, and Pt(II) compounds **3**, **8**, **11**, **12**, and **13**, — respectively CarboPt, PtMeEn, PicoPt, APP, and AzidoPt— none of which caused nucleolar stress. Bottom row shows Pt(II)-free ligands of stress-inducing Pt(II) compounds and solvents used (DMSO and DMF). Ligands alone do not induce nucleolar stress, and neither do solvents. All treatments were performed for 24 hours. Pt(II) compound and ligand treatments were conducted at 10 μM , with the exception of Actinomycin D, which was 5 nM, and **3** (CarboPt), which was 20 μM .



Supplementary Figure A.3. Quantification of nucleolar stress induction for Pt(II)-free ligands and solvents used. CV quantification confirms that ligands alone do not induce nucleolar stress, and neither do solvents. All treatments were performed for 24 hours. Treatments were conducted at 10 μ M, with the exception of Actinomycin D, which was 5 nM. Treatment data sets are represented by standard box plots, where the center, top, and bottom lines of boxes represent the median, first and third quartile respectively. The vertical lines represent the range of data within 1.5xIQR of the lower and upper quartiles, where IQR is the difference between first and third quartile; points outside this range are considered outliers.



Supplementary Figure A.4. Histograms showing NPM1 intensity within a single nucleus in stressed and unstressed cells. X axis represents pixel intensity, and Y axis represents the number of pixels within a nucleus of the intensity on the X axis. Cells not undergoing nucleolar stress have a large number of low intensity pixels and a small number of high intensity pixels, indicating NPM1 is concentrated in the granular component of the nucleolus. Cells undergoing stress have a broader distribution of pixel intensities, with the histogram skewing towards high intensity, as NPM1 has redistributed throughout the entire nucleoplasm.



Supplemental Figure A.5. DFT-optimized structures of compounds illustrating the relative size of compounds and planarity of BenzaPt **10** relative to DACH-Pt **4**

Supplementary Tables

Table A.1. IC₅₀ values in A549 cells for selected compounds at 24 hours^a

Compound	IC ₅₀ (μM)
Oxaliplatin, 2	81.5±7
Cisplatin, 1	12.8±2
DACHplatin, 4	31.9±6
Pentaplatin, 9	37.5±5
Benzaplatin, 10	NR ^b
PlatEn, 7	46.1±6
PlatMeEn, 8	76.1±9
DOAP, 5	36.6±5
APP, 12	NR ^b

^aIC₅₀ values in A549 cells were determined after 24-hour treatment with indicated compound

^bNR=IC₅₀ value not reached, >500 μM

Table A.2. IC₅₀ values in A549 cells for selected compounds at 48 hours^a

Compound	IC ₅₀ (μM)
Oxaliplatin, 2	9.9±3.5
Cisplatin, 1	4.6±0.7
Benzaplatin, 10	6.9±0.7
APP, 12	36.9±4.3

^aIC₅₀ values in A549 cells were determined after 48-hour treatment with indicated compound

Table A.3. Volume and hydrophobicity data

Compound	Volume (Å ³)	Distance (Å)	logP
Cisplatin	19.46	3.40	-2.39±0.005
PlatMeEn	23.56	5.51	-1.68±0.014
PlatEn	21.47	4.41	-1.85±0.013
APP	27.66	6.21	-1.1±0.058
Picoplatin	27.69	6.21	-
Pentaplatin	27.85	6.21	-1.29±0.031
Benzaplatin	28.71	6.73	-0.92±0.038
DACH-platin	30.01	6.75	-0.89±0.011
Carboplatin	30.94	6.30	-
DACH-En	32.41	6.72	-
Azidoplatin	32.71	13.16	-1.2±0.059
Oxaliplatin	34.13	6.78	1.58±0.02

Materials and Methods

1. Cell culture and treatment

A549 human lung carcinoma cells (#CCL-185, American Type Culture Collection) were cultured at 37°C, 5% CO₂ in Dulbecco's Modified Eagle Medium (DMEM) supplemented with 10% Fetal Bovine Serum (FBS) and 1% antibiotic-antimycotic. Treatments were conducted on cells that had been grown for 11-25 passages to 70% confluency. Except where noted otherwise, treatments were conducted for 24 hours at 10 μM. Compounds were made into 5mM stocks on the day of treatment in 0.9% NaCl (cisplatin), DMF (**4, 7, 8, 10, 11, 12, 13, 14**), DMSO (**5**), or water (**1, 2, 3, 6**). Stock solutions were diluted into medium immediately prior to drug treatment.

2. Immunofluorescence

Cells to be imaged were grown on coverslips (Ted Pella product no 260368, Round glass coverslips, 10mm diam, 0.16-0.19mm thick) as described above. After treatment, cells were washed twice with phosphate buffered saline (PBS) and fixed for 20 minutes at room temperature in 4% paraformaldehyde in PBS. PFA was removed via aspiration and cells were then permeabilized with 0.5% Triton-X in PBS for 20 minutes at room temperature. Two ten-minute blocking steps were performed with 1% bovine serum albumin (BSA) in PBST (PBS with 0.1% Tween-20). Cells were incubated for one hour in primary antibody (NPM1 Monoclonal Antibody, FC-61991, from ThermoFisher, 1:200 dilution in PBST with 1% BSA) and 1 hour in secondary antibody (Goat Anti-Mouse IgG H&L Alexa Fluor® 488, ab150113, Abcam, 1:1000 dilution in PBST with 1% BSA), with 3 five minute wash steps using PBST between incubations, and were washed in the same manner again before mounting slides. Coverslips were mounted on slides with ProLong™ Diamond Antifade Mountant with DAPI (Thermo Fisher) according to manufacturer's instructions.

3. Cytotoxicity (MTT assay)

A549 cells were seeded in 24-well plates at a density of 5×10^4 cells/mL. The following day cells were treated with 0-750 μ M of compound in DMEM supplemented with 10% FBS and antibiotic-antimycotic. 24h after treatment, compound-containing medium was removed and cells washed twice with PBS. MTT in DMEM supplemented with 10% FBS and antibiotic-antimycotic was then added to cells and incubated for 3h. DMSO was used to dissolve the formazan crystals and absorbance at 595 nm was then determined using a Tecan microplate reader. Percent viability was determined by comparing to vehicle-treated control for each compound and IC₅₀ concentration calculated from triplicate measurements using the drc package in R (Ritz et al. 2015).

4. Image processing and quantification

Images were taken using a HC PL Fluotar 63x/1.3 oil objective mounted on a Leica DMi8 fluorescence microscope with Leica Application Suite X software. Quantification of NPM1 relocalization was performed in an automated fashion using a Python 3 script. Images were preprocessed in ImageJ (Rueden et al. 2017; Schindelin et al. 2012) to convert the DAPI and NPM1 channels into separate 16-bit greyscale images. Between 70 and 225 cells were analyzed for each treatment group. Nuclei segmentation was determined with the DAPI images using Li thresholding functions in the Scikit- Image Python package (van der Walt et al. 2014). The coefficient of variation (CV) for individual nuclei, defined as the standard deviation in pixel intensity divided by the mean pixel intensity, was calculated from the NPM1 images using the SciPy Python package. All data were normalized to the no-treatment control in each experiment. NPM1 imaging results for each compound were observed on a minimum of two separate testing days. Data are represented as boxplots generated using Seaborn within Python.

5. Synthesis

Materials

Cisplatin used for cell treatments was purchased from Strem Chemicals. Cisplatin used as a synthetic precursor was synthesized as described below. Oxaliplatin and carboplatin were purchased from TCI. Unless otherwise noted, all other compounds were purchased from Sigma Aldrich or TCI. Picoplatin and azidoplatin were synthesized as previously reported (Wirth et al. 2015).

Cisplatin (1)

Cisplatin was synthesized according to previously described methods by Dhara (Dhara, S.C. 1970) and reviewed (Wilson and Lippard 2014). Briefly, potassium tetrachloroplatinate (62.7 mg, 0.151 mmol, 1 eq) was dissolved in 180 μ L of water and stirred at 40°C. Potassium iodide (300 mg, 1.807 mmol, 12 eq) was dissolved separately in 500 μ L of water and warmed to 40°C. 250 μ L of the potassium iodide solution was added dropwise to the solution containing potassium tetrachloroplatinate. After addition of potassium iodide, the solution was warmed to 70°C. Once the solution reached 70°C it was removed from heat and cooled to room temperature. The solution was then filtered through celite. The filtrate was collected and used for the following reaction. A 2M solution of ammonium hydroxide in water (250 μ L) was added dropwise. The solution was allowed to stand for 30 minutes, filtered, and washed with ethanol (x1) and ether (x2). The solid was collected to yield 56.2 mg *cis*-diamminediiiodoplatinum(II). Silver sulfate (37 mg, 0.119 mmol, 1eq) was added to 5 mL of water. *Cis*-diamminediiiodoplatinum(II) (56.2 mg, 0.116 mmol, 1eq) was added slowly. The solution was heated to 80°C. The solution was stirred overnight. The silver iodide was filtered using celite and the filtrate collected. This solution was concentrated to 1.5 mL. Potassium chloride (174.6 mg, 2.34 mmol, 20 eq) was added to the solution and then heated to 80°C. The solution was stirred at 80°C for another 20 minutes and cooled to room temperature. The solution was filtered and washed with ethanol (x1) and ether (x2) to yield 23.5 mg (52%) *cis*-diamminedichloroplatinum(II). ¹H NMR (500 MHz, DMF-d7) δ 3.99 (s, 6H).

Cis-(*trans*-1,2-diaminocyclohexane)dichloride Platinum(II) (DACH-Pt) (4)

Cis-(trans(+/-)-1,2-diaminocyclohexane)dichloride Platinum(II) was prepared using general methods previously described (Wilson and Lippard 2014). Potassium tetrachloroplatinate (100.3 mg, 0.242 mmol, 1 eq) was dissolved in 4 mL of water. *Trans(+/-)-1,2-diaminocyclohexane* (29.1 mg, 0.255 mmol, 1eq) was added dropwise to the dark red solution and stirred for 7.5 hours. A yellow precipitate formed. The solution was filtered and washed with ice-cold methanol (x1) and acetone (x1). The yellow solid was then collected to yield 70 mg (76 %). ¹H NMR (500 MHz, DMF-d7) δ 5.59 (d, J = 7.4 Hz, 2H), 5.02 (s, 2H), 2.50 (qq, J = 11.2, 5.6, 3.8 Hz, 2H), 2.15 – 2.04 (m, 2H), 1.56 (dd, J = 7.7, 3.3 Hz, 2H), 1.48 (tt, J = 11.9, 5.6 Hz, 2H), 1.15 (qd, J = 11.9, 2.9 Hz, 2H). ¹⁹⁵Pt NMR (107 MHz, DMF-d7) δ -2270.32.

Cis-(diammine)oxalic acid Platinum(II) (DOAP) (5)

Cis-(diammine)oxalic acid Platinum(II) was prepared using general methods previously described (Wilson and Lippard 2014). Sodium oxalate was prepared by introducing excess sodium hydroxide to oxalic acid and filtering the resulting solid. *Cis-(diammine)diiodo platinum(II)* (92.3 mg, 0.193 mmol, 1 eq) was dissolved in 5 mL water. Silver nitrate (82mg, 0.4823 mmol, 2.5eq) was added and the reaction stirred overnight protected from light. The reaction was then filtered through celite and the filtrate collected. Sodium oxalate (26 mg, 0.194 mmol, 1 eq) was added to the filtrate and the reaction was stirred overnight and protected from light. The resulting light grey solid was filtered from the solution and washed with water (2x) and methanol (x2). Yield 33.3mg (54%). ¹H NMR (500 MHz, DMSO-d6) δ 4.27 (s, 6H). ¹³C NMR (126 MHz, DMSO-d6) δ 166.38. ¹⁹⁵Pt NMR (107 MHz, DMSO-d6) δ -1743.33.

Cis-(trans-1,2-diaminocyclohexane)1,2-ethylenediamine Platinum(II) (DACH-En) (6)

Cis-(trans(+/-)-1,2-diaminocyclohexane)dichloro platinum(II) (62 mg, 0.163 mmol, 1eq) was dissolved in 5 mL of water. 1,2-diaminoethane (32 mg, 0.533 mmol, 3.2eq) was added to the solution and refluxed for two days. The solution was then cooled room temperature over 24 hours. Solution was then evaporated to yield a yellow solid. ¹H NMR (500 MHz, Deuterium Oxide) δ 3.31

(t, $J = 5.8$ Hz, 1H), 3.05 (t, $J = 5.8$ Hz, 1H), 2.97 (s, 2H), 2.72 – 2.64 (m, 4H), 2.47 – 2.39 (m, 2H), 2.09 (dt, $J = 12.8, 2.0$ Hz, 2H), 1.67 – 1.60 (m, 2H), 1.41 – 1.28 (m, 2H), 1.20 (td, $J = 9.4, 8.9, 4.0$ Hz, 2H). ^{13}C NMR (126 MHz, D_2O) δ 61.17, 46.83, 40.43, 32.14, 23.92. ^{195}Pt NMR (107 MHz, D_2O) δ -3002.42. TOF MS ES+ for m/z $[(\text{M})]^{2+}$ $\text{C}_8\text{H}_{21}\text{Pt}$ calculated: 368.1414 found: 368.1403 ($[(\text{M})]^{2+}$).

Cis-(1,2-diaminoethylene)dichloride Platinum(II) (Plat-En) (7)

Cis-(1,2-diaminoethylene)dichloride Platinum(II) was prepared using general methods previously described (Wilson and Lippard 2014). Potassium tetrachloroplatinate (66 mg, 0.159 mmol, 1eq) was dissolved in 500 μL of water. 1,2-diaminoethane (9.36 mg, 0.156 mmol, 1eq) was added to the dark red solution and allowed to stir at room temperature for 12 hours. A yellow precipitate formed. The solution was filtered and washed with ice-cold 0.1M HCl (x1), ethanol (x1), and ether (x1). The yellow solid was collected to yield 27.5 mg (53%). ^1H NMR (500 MHz, DMF- d_7) δ 5.38 (s, 4H), 2.61 (s, 4H). ^{13}C NMR (126 MHz, DMF- d_7) δ 50.52. ^{195}Pt NMR (107 MHz, DMF- d_7) δ -2309.12.

Cis-(2,3-diaminopropane)dichloride Platinum(II) (Plat-MeEn) (8)

Cis-(2,3-diaminopropane)dichloride Platinum(II) was prepared according to previously reported methods and used as a mixture of isomers (Fanizzi et al. 1987). Potassium tetrachloroplatinate (34 mg, 0.082 mmol, 1eq) was dissolved in 1ml water and heated at 50 $^\circ\text{C}$. Excess potassium iodide (40 mg, 0.24 mmol, 3eq) was dissolved in 0.5 mL water and added dropwise to the platinum. The solution was stirred for 10 minutes and became black. To the stirring solution, 1,2-diamino propane (7 μL , 0.08 mmol, 1 eq) was added and the solution was stirred for 40 minutes. Yellow precipitate formed immediately. The solution was cooled to room temperature and filtered. The solid was washed with ice-cold ethanol (1x) and ether (1x).

The solid was dissolved in 2ml water and silver nitrate (28 mg, 0.16 mmol, 2eq) was added. The reaction was stirred for 2 days protected from light. The solution was filtered through celite and concentrated to 1ml. Excess potassium chloride (120 mg, 1.61 mmol, 20 eq) was added rapidly to the concentrated solution and the mixture was stirred at 50 °C for 1 hour. The resulting yellow solid was filtered and washed with methanol (1x) and ether (1x). ¹H NMR (500 MHz, DMF-*d*₇) δ 5.74 (s, 1H), 5.55 (d, *J* = 40.1 Hz, 2H), 5.22 (s, 1H), 3.30 – 3.17 (m, 1H), 2.89 – 2.80 (m, 1H), 2.66 (td, *J* = 8.2, 6.1, 3.1 Hz, 1H), 1.53 (d, *J* = 6.5 Hz, 3H). ¹³C NMR (126 MHz, DMSO) δ 56.00, 52.41, 16.38.

Cis-(trans-1,2-diaminocyclopentane)dichloride Platinum(II) (Penta-Pt) (9)

Cis-(trans-1*S*,2*S*-diaminocyclopentane)dichloride Platinum(II) was synthesized according to previously published methods (Garbutcheon-Singh et al. 2012). Potassium tetrachloroplatinate (101 mg, 0.243 mmol, 1eq) was dissolved in 2 mL of water. (1*S*, 2*S*)-trans-diaminocyclopentane dihydrochloride (43.1 mg, 0.249 mmol, 1eq) was added and stirring continued. 73 mg of 1,8-Diazabicyclo[5.4.0]undec-7-ene (DBU) (0.482 mmol, 2eq) was added to the solution. A yellow precipitate formed. The solution was filtered and washed with ethanol (x1) and ether (x2). The yellow solid was collected to yield 50.5 mg (57%). ¹H NMR (500 MHz, DMF-*d*₇) δ 5.18 (s, 2H), 5.00 (s, 2H), 3.41 – 3.31 (m, 2H), 2.16 (tdd, *J* = 9.6, 8.0, 5.3 Hz, 2H), 1.78 – 1.64 (m, 2H), 1.63 – 1.48 (m, 1H). ¹³C NMR (126 MHz, DMF-*d*₇) δ 70.21, 26.73, 23.93. ¹⁹⁵Pt NMR (107 MHz, DMF-*d*₇) δ -1987.96.

Cis-(1,2-phenylenediamine)dichloride Platinum(II) (Benza-Pt) (10)

Cis-(1,2-phenylenediamine)dichloride Platinum(II) was prepared using general methods previously described (Wilson and Lippard 2014). Potassium tetrachloroplatinate (103 mg, 0.248 mmol, 1eq) was dissolved in 1 mL of water. A dark red solution formed. 1,2-phenylenediamine (26.8 mg, 0.248 mmol, 1eq) was added and stirring continued for 6 hours. The solution was filtered and washed with ice-cold ethanol (x1) and ether (x2). The dark yellow/brown solid was collected

with a yield of 89.8 mg (96%). ^1H NMR (500 MHz, DMF- d_7) δ 7.72 (s, 2H), 7.46 (dd, $J = 5.9, 3.5$ Hz, 1H), 7.28 (dd, $J = 6.0, 3.4$ Hz, 1H). ^{13}C NMR (126 MHz, DMF- d_7) δ 144.76, 128.85, 127.36. ^{195}Pt NMR (107 MHz, DMF- d_7) δ -2199.18.

Cis-(2-aminomethylpyridine)dichloride Platinum(II) (APP) (12)

Cis-(2-aminomethylpyridine)dichloride Platinum(II) was synthesized according to previously described methods (Brunner and Schellerer 2003). A solution of 2-picolyamine (120 μL , 0.075 mmol, 1 eq) was made in 1.2 mL water. Potassium tetrachloroplatinate (55mg, 0.133 mmol, 2eq) was dissolved in 1.2 mL water. The platinum solution was added to the 2-picolyamine and the pH was adjusted to pH 5 using concentrated HCl. The reaction was stirred for 4 hours. The pH of the solution was adjusted during the reaction to be around pH 5-6 using 1 M NaOH. The resulting yellow solid was filtered and washed with water (2x) to yield 38.7 mg (89%). ^1H NMR (500 MHz, DMF- d_7) δ 9.43 (d, $J = 5.3$ Hz, 1H), 8.37 (t, $J = 7.7$ Hz, 1H), 7.91 (d, $J = 7.8$ Hz, 1H), 7.72 (t, $J = 6.7$ Hz, 1H), 6.42 (s, 2H), 4.55 (t, $J = 5.9$ Hz, 2H).

6. Measurement of partition coefficients

Water was mixed with octanol for 24 hours and left to stand for an additional 24 hours to obtain water-saturated octanol and octanol-saturated water that were used for determining partition coefficients. Measurements of the partition coefficients were performed using classical shake-flask method according to OECD guidelines (OECD 1995). Platinum complexes were dissolved in octanol-saturated water at concentrations between 0.5 mM and 5 mM. The octanol-saturated water mixtures were mixed with water-saturated octanol in a 1:1 ratio and vortexed for 30 minutes (OECD 1995; Wilson and Lippard 2012). The mixtures were then centrifuged and 0.5 mL samples of both phases were collected and quantified using RP-HPLC as described by Klose et al (Garbutcheon-Singh et al. 2012). An isocratic method was used for HPLC analysis with water and methanol. Methanol concentrations ranged from 10% to 30% with 30% being used for more hydrophobic compounds. The area of absorbance was used to calculate the ratio (P) of platinum in

octanol and water as this area is proportional to the concentration according to the Lambert-Beer law. The column was washed with 95% methanol 5% water between each octanol sample and equilibrated before the next sample was introduced. The stock solution of each platinum compound was compared to the total from octanol and water samples as a check of this method. This procedure to calculate logP was performed in triplicate and standard deviations were determined.

7. Computations

Computations were performed as previously reported (McDevitt et al. 2019). Briefly, compounds were optimized using density functional theory (DFT) in Gaussian09 (Frisch et al. 2016). Optimizations to geometry were performed using a RMS force convergence criterion of 10^{-5} hartree. The electronic wavefunction was minimized using GGA functional PBE (Perdew, Burke, and Ernzerhof 1996; 1997), with the DEF2TZP basis set. We did not explicitly include relativistic effects as these were not expected to impact the geometries of the compounds significantly (Pansini et al. 2017).

Two measures of size were used for the compounds: volume and longest vector between the platinum atom and the surface of the molecule. The vector represents the main steric component of the non-labile ligand of each compound to provide a direct comparison especially when comparing compounds that do not share the same aquation-labile ligand identity. In order to quantitatively assess the size of the molecules we used the presence of electric field, as derived from the electrostatic potential, to signify the location of the chemical system. DFT yields the electrostatic potential of the optimized, non-hydrolyzed compound structures and tools previously developed and reported were used to analyze the electrostatic potential of a chemical system (Butler, Hendon, and Walsh 2014). We used the same file format to analyze the electrostatic potential and the result was the electrostatic potentials of the optimized structures were computed by minimizing the electronic wavefunction using 500 eV planewave cutoff, a gamma only k-grid, and a PBE functional utilizing a plane-augmented wave (PAW) (Blöchl 1994; Kresse and Joubert 1999). basis

as implemented in the Vienna Ab Initio Software Package (Kresse and Furthmuller 1996; Kresse and Hafner 1993; 1994; Kresse and Joubert 1999).

All compounds were calculated in a sufficiently large computational box to minimize self-interaction. The electric field is the gradient of the electrostatic potential; therefore, the electric field includes the direction of the greatest increase in electrostatic potential. DFT calculations return electrostatic potential values on the order of 10^{-6} eV, therefore a change in less than 10^{-5} eV is considered negligible. This approach is based on previous atomic radii calculations which employ negligible change in electron density to assess the size of atoms. We used this measurement of the electric field and definition of the surface of the compound to find the total volume of the compounds as well as the longest vector from the platinum center to the farthest edge of the non-labile ligand.

APPENDIX B: SUPPORTING INFORMATION FOR CHAPTER III

Materials and Methods:

Cell culture and treatment - A549 human lung carcinoma cells (#CCL-185, American Type Culture Collection) were cultured at 37°C, 5% CO₂ in Dulbecco's Modified Eagle Medium (DMEM) supplemented with 10% Fetal Bovine Serum (FBS) and 1% antibiotic-antimycotic. Treatments were conducted on cells that had been grown for 11-25 passages to 70% confluency. Platinum compound treatments were conducted at 10 µM and Actinomycin D treatments were conducted at 5 nM. Platinum compounds were made into 5mM stocks on the day of treatment in 0.9% NaCl (cisplatin) or water (oxaliplatin). Stock solutions were diluted into media immediately prior to drug treatment.

Immunofluorescence - Cells to be imaged were grown on coverslips (Ted Pella product no 260368, Round glass coverslips, 10mm diam, 0.16-0.19mm thick) as described above. After treatment, cells were washed twice with phosphate buffered saline (PBS) and fixed for 20 minutes at room temperature in 4% paraformaldehyde in PBS. PFA was removed via aspiration and cells were then permeabilized with 0.5% Triton-X in PBS for 20 minutes at room temperature. Two ten-minute blocking steps were performed with 1% bovine serum albumin (BSA) in PBST (PBS with 0.1% Tween-20). Cells were incubated for one hour in primary antibody (NPM1 Monoclonal Antibody, FC-61991, from ThermoFisher, 1:200 dilution in PBST with 1% BSA; anti-Fibrillarin antibody ab4566 from Abcam, 1:500 dilution; anti-Phospho-Histone H2A.X, 14-9865-82, from ThermoFisher, 5 µg/mL) and 1

hour in secondary antibody (Goat Anti-Mouse IgG H&L Alexa Fluor® 488, ab150113, Abcam, 1:1000 dilution in PBST with 1% BSA), with 3 five minute wash steps using PBST between incubations, and were washed in the same manner again before mounting slides. Coverslips were mounted on slides with ProLong™ Diamond Antifade Mountant with DAPI (Thermo Fisher) according to manufacturer's instructions.

Pulse-chase - A549 cells were grown to 70% confluency in 6-well tissue culture plates as described in *Cell culture and treatment* section above. Cells were then treated for the indicated amount of time in DMEM supplemented with 10% FBS and 1X antibiotic-antimycotic with the drug of interest added. Prior to the pulse step, phosphate depletion was performed for 1 hour by switching regular medium for phosphate-free medium (including the previously mentioned FBS and antibiotic-antimycotic) which still contained the drug of interest. For the pulse step, medium was replaced with a solution of 15 $\mu\text{Ci/ml}$ ^{32}P orthophosphate made in phosphate-free medium (with FBS and antibiotic-antimycotic). After a 1-hour pulse step, medium was replaced with cold drug-containing DMEM as in the first step of treatment for a three-hour chase step. After this chase step, RNA was extracted from the cell, separated by size on an agarose gel and then visualized. The gels were visualized in two ways: 1) Total RNA that was visualized with an ethidium bromide stain and 2) only the radioactively labeled RNA that was produced during the pulse step was visualized. To achieve this, the gel was dried on Whatman paper using a gel dryer set for 2 hours at 70C, after which it was left on the gel dryer overnight at room temperature. The dried gel was exposed to a phosphor screen for 24 hours and the screen was imaged using a Storm phosphorimager. The amount of labeled RNA was quantified

by calculating the intensity of the gel bands in the images. The amount of radiolabeled RNA was normalized to the total RNA levels to control for the amount of total RNA that was loaded onto the gel. The amounts of the different RNA transcripts are shown in the graph as a fraction of the no treatment.

Western blotting - Cells were removed from tissue culture plates via trypsinization and subsequently lysed with RIPA buffer. Blocking step was performed in 5% milk in PBST from at room temperature from 1 hour to overnight. Blot was incubated at room temperature for 1 hour in primary antibody (1:500 NPM1 Monoclonal Antibody, FC-61991, from ThermoFisher, 1:1000 beta-Actin Monoclonal Antibody, AC-15, from ThermoFisher, both in 5% milk in PBST) and 1 hour in secondary antibody (1:10,000 Goat anti-Mouse IgG (H+L) Cross-Adsorbed Secondary Antibody, HRP, from ThermoFisher). Chemiluminescence was performed with SuperSignal West Pico Plus kit and the blot was rinsed 3 times for 1-5 minutes in PBST between incubation steps. The blot was imaged with Li-Cor imaging system and software.

Imaging and quantification - Images were taken using a HC PL Fluotar 63x/1.3 oil objective mounted on a Leica DMi8 fluorescence microscope with Leica Application Suite X software. Quantification of NPM1 relocalization was performed in an automated fashion using a Python 3 script. Images were preprocessed in ImageJ (Rueden et al. 2017; Schindelin et al. 2012) to convert the DAPI and NPM1 channels into separate 16-bit greyscale images. Nuclei segmentation was determined with the DAPI images using Li thresholding functions in the Scikit- Image Python package (van der Walt et al. 2014). The coefficient of variation (CV) for individual nuclei, defined as the standard deviation in

pixel intensity divided by the mean pixel intensity, was calculated from the NPM1 images using the SciPy Python package. All data were normalized to the no-treatment control in each experiment. Data are represented as boxplots generated using Matplotlib and Seaborn within Python.

Supplementary Figures:

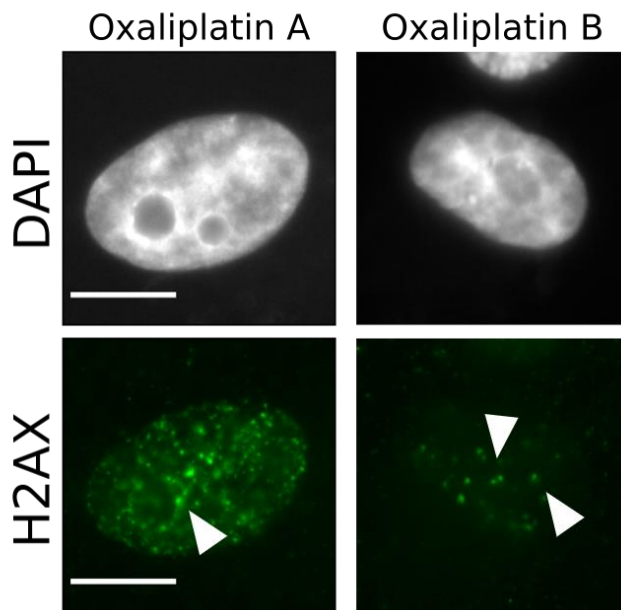


Figure B.1: Perinucleolar γ H2AX foci are not observed in oxaliplatin treated cells. γ H2AX foci have been previously reported to form in perinucleolar nucleolar caps after damage of ribosomal DNA. A small number (less than 1 in 40) of oxaliplatin treated nuclei showed γ H2AX foci around the periphery of the nucleolus, demonstrated in this figure. The low number of cells displaying nucleolar γ H2AX foci suggests that rDNA damage is likely not driving oxaliplatin-induced nucleolar reorganization. Scale bar 10 μ m

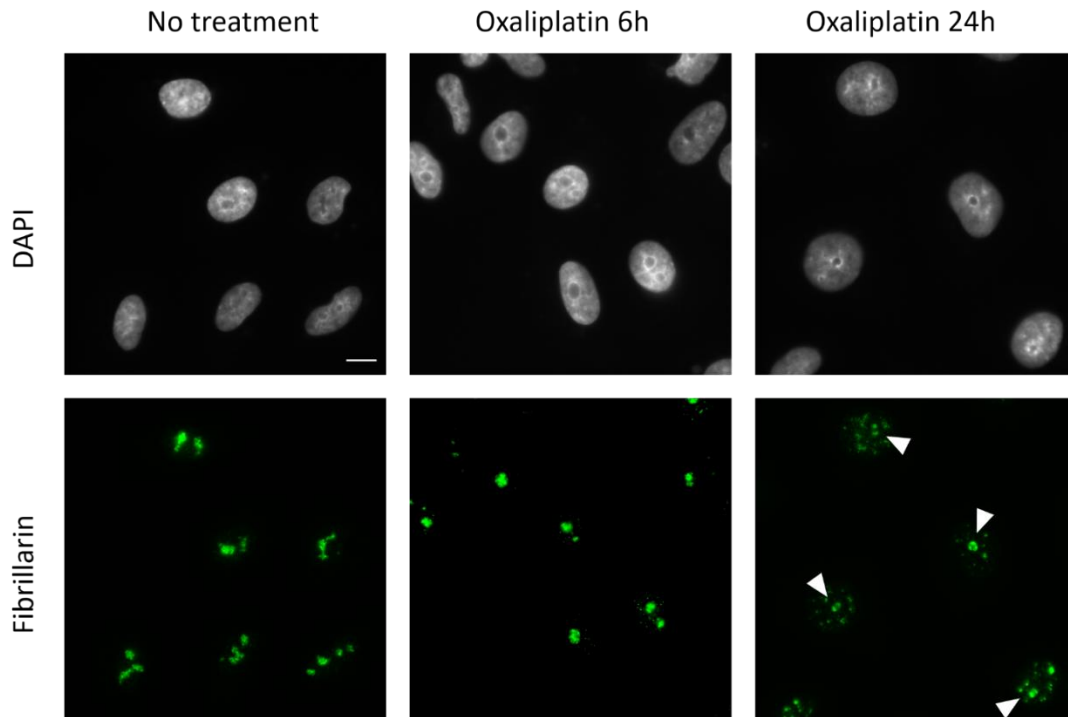


Figure B.2: Fibrillararin staining at 6 and 24 hours of treatment with oxaliplatin. Nucleolar caps are not observed at 6 hours of treatment, but are observed at 24 hours of treatment (indicated by white arrows). Nucleoli are rounded at 6 hours, as observed by both DAPI and fibrillararin staining, suggesting that nucleolar stress is occurring despite the lack of nucleolar caps at this time. Treatments were done at 10 μ M oxaliplatin

APPENDIX C: SUPPORTING INFORMATION FOR CHAPTER IV

Materials and Methods

Cell Culture – HeLa cells were grown in DMEM containing 10% FBS and 1% antibiotic/antimycotic solution. Cells were grown to ~80% confluence, then treated with either 50 μ M 1,3-Platin or DMF for 30 hours. DNA was extracted by Zymo extraction kit. DNA was sheared by sonication with Covaris M220: DNA sonicator to 150bp average fragment size.

Click Reaction – Purified, fragmented DNA was combined with 28.25mM PB, 1.5mM biotin alkyne, 75nM copper sulfate, 375nM tris(3-hydroxypropyltriazolylmethyl)amine, 1.5mM sodium ascorbate. Samples were incubated at 37°C overnight. DNA was purified with G25 and eluted in 50 μ L water.

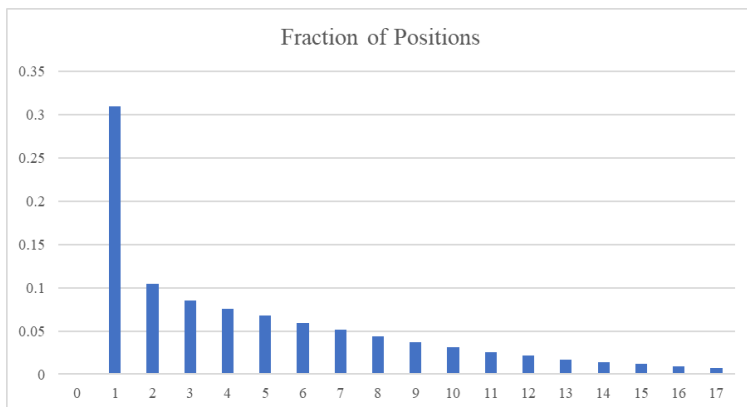
DNA pulldown – 2X Bind and wash buffer was prepared (2X Bind and wash buffer (10mM Tris HCl, 2M EDTA, 2M NaNO₃, pH 7.3). 20 μ L beads (Dynabeads MyOne Streptavidin C1 beads, Thermo Fisher) were aliquoted per sample. Beads were washed 3 times in 1mL 1X Bind and wash buffer (1M EDTA, 5mM Tris HCl, 1M NaNO₃, pH 7.3), then incubated on magnetic rack for 3 minutes between washes. Beads were then resuspended in 40 μ L 2X bind and wash buffer. 40 μ L DNA solution was added to the beads and incubated 15 minutes with gentle rotation. Samples were then placed on magnets and supernatant was removed and set aside. Beads were gently resuspended with 400 μ L 1X bind and wash butter then placed on magnet for 3 minutes. Supernatant was removed and set aside. Beads were then resuspended in 400 μ L 8M urea, gently pipetted, then set on magnet for 3 minutes. Supernatant was collected and set aside. Beads were then washed 3X in 400 μ L 1X bind and wash buffer (1M EDTA, 5mM Tris HCl, 100mM

NaNO₃, pH 7.3) allowing samples to sit on magnet for 3 minutes between washes and keeping the supernatant from each wash. To elute the DNA from the beads, 20µL formamide was added to each sample. Beads were incubated at 90°C for 3 minutes, then placed on magnet at room temperature for 3 minutes prior to removal of supernatant.

DNA precipitation after pulldown – Water was added to bring samples to a final volume of 400µL. To each sample, added 40µL 3M sodium acetate and 880µL ice cold ethanol. Samples were gently mixed, then incubated at -20°C for a minimum of 30 minutes. Samples were then spun at 14,000 rpm for 10 minutes and supernatant was removed. DNA pellet was dried under vacuum and each sample was resuspended in 10µL deionized water.

Sequencing library preparation – Sequencing libraries were prepared with KAPA HyperPlus library preparation kit according to manufacturer's instructions. Two extra rounds of PCR were performed due to low library yield. Samples were sequenced on the Illumina HiSeq 4000 with 150bp single-end reads. Upon receipt of data, adapters were removed with cutadapt, aligned with bowtie2 (Martin 2011; Langmead and Salzberg 2012). Samtools rmdups was used to remove PCR duplicates. Preliminary gene binding information was determined by counting genes with reads after pulldown with HTSeq-count, and then DESeq2. First run of peak calling was performed with MACS2 callpeaks (Zhang et al. 2008). A second software, HOMER, was subsequently used for peak calling, sample characterization, and gene and chromosome distribution (Heinz et al. 2010). Visualization was performed with CHIPseeker and clusterProfiler (G. Yu, Wang, and He 2015; G. Yu et al. 2012).

Supplementary Figures



Supplementary Figure C.1: Sequencing of Pt(II) samples shows high frequency of non-unique reads. After removing PCR duplicates, 31% of the reads in this experiment uniquely align, indicating this library was un-ideally low yielding. Ideally, a higher percentage of reads should align only to one position, and only a few should align to multiple. However, almost 70% of reads aligned to multiple positions in this experiment.

REFERENCES CITED

- Anders, Lars, Matthew G. Guenther, Jun Qi, Zi Peng Fan, Jason J. Marineau, Peter B. Rahl, Jakob Lovén, et al. 2014. “Genome-Wide Localization of Small Molecules.” *Nature Biotechnology* 32 (1): 92–96. <https://doi.org/10.1038/nbt.2776>.
- Blöchl, Peter E. 1994. “Projector Augmented-Wave Method.” *Physical Review. B, Condensed Matter* 50 (24): 17953–79. <https://doi.org/10.1103/physrevb.50.17953>.
- Boulon, Séverine, Belinda J. Westman, Saskia Hutten, François-Michel Michel Boisvert, and Angus I. Lamond. 2010. “The Nucleolus under Stress.” *Molecular Cell* 40 (2): 216–27. <https://doi.org/10.1016/j.molcel.2010.09.024>.
- Brodská, Barbora, Aleš Holoubek, Petra Otevřelová, and Kateřina Kuželová. 2016. “Low-Dose Actinomycin-D Induces Redistribution of Wild-Type and Mutated Nucleophosmin Followed by Cell Death in Leukemic Cells.” *Journal of Cellular Biochemistry* 117 (6): 1319–29. <https://doi.org/10.1002/jcb.25420>.
- Brunner, H, and K. -M Schellerer. 2003. “New Porphyrin Platinum Conjugates for the Cytostatic and Photodynamic Tumor Therapy.” *Inorganica Chimica Acta, Protagonists in Chemistry: Pierre Braunstein*, 350 (July): 39–48. [https://doi.org/10.1016/S0020-1693\(02\)01490-1](https://doi.org/10.1016/S0020-1693(02)01490-1).
- Bruno, Peter M, Yunpeng Liu, Ga Young Park, Junko Murai, Catherine E Koch, Timothy J Eisen, Justin R Pritchard, Yves Pommier, Stephen J Lippard, and Michael T Hemann. 2017. “A Subset of Platinum-Containing Chemotherapeutic Agents Kills Cells by Inducing Ribosome Biogenesis Stress.” *Nature Medicine* 23 (4): 461–471. <https://doi.org/10.1038/nm.4291>.
- Bruno, Peter M., Mengrou Lu, Kady A. Dennis, Haider Inam, Connor J. Moore, John Sheehe, Stephen J. Elledge, Michael T. Hemann, and Justin R. Pritchard. 2020. “The Primary Mechanism of Cytotoxicity of the Chemotherapeutic Agent CX-5461 Is Topoisomerase II Poisoning.” *Proceedings of the National Academy of Sciences* 117 (8): 4053–60. <https://doi.org/10.1073/pnas.1921649117>.
- Burger, Kaspar, Bastian Mühl, Thomas Harasim, Michaela Rohrmoser, Anastassia Malamoussi, Mathias Orban, Markus Kellner, et al. 2010. “Chemotherapeutic Drugs Inhibit Ribosome Biogenesis at Various Levels.” *Journal of Biological Chemistry* 285 (16): 12416–25. <https://doi.org/10.1074/jbc.M109.074211>.

- Burger, Kaspar, Bastian Mühl, Markus Kellner, Michaela Rohrmoser, Anita Gruber-Eber, Lukas Windhager, Caroline C Friedel, Lars Dölken, and Dirk Eick. 2013. "4-Thiouridine Inhibits RRNA Synthesis and Causes a Nucleolar Stress Response." *RNA Biology* 10 (10): 1623–30. <https://doi.org/10.4161/rna.26214>.
- Bursac, Sladana, Maja Cokaric Brdovcak, Giulio Donati, and Sinisa Volarevic. 2014. "Activation of the Tumor Suppressor P53 upon Impairment of Ribosome Biogenesis." *Biochimica et Biophysica Acta* 1842 (6): 817–30. <https://doi.org/10.1016/j.bbadis.2013.08.014>.
- Butler, Keith, Christopher Hendon, and Aron Walsh. 2014. "Electronic Chemical Potentials of Porous Metal-Organic Frameworks" 136: 2703–6.
- Bywater, Megan J., Gretchen Poortinga, Elaine Sanij, Nadine Hein, Abigail Peck, Carleen Cullinane, Meaghan Wall, et al. 2012. "Inhibition of RNA Polymerase I as a Therapeutic Strategy to Promote Cancer-Specific Activation of P53." *Cancer Cell* 22 (1): 51–65. <https://doi.org/10.1016/j.ccr.2012.05.019>.
- Cañeque, Tatiana, Sebastian Müller, and Raphaël Rodriguez. 2018. "Visualizing Biologically Active Small Molecules in Cells Using Click Chemistry." *Nature Reviews Chemistry* 2 (9): 202. <https://doi.org/10.1038/s41570-018-0030-x>.
- Carpenter, Anne E., Thouis R. Jones, Michael R. Lamprecht, Colin Clarke, In Han Kang, Ola Friman, David A. Guertin, et al. 2006. "CellProfiler: Image Analysis Software for Identifying and Quantifying Cell Phenotypes." *Genome Biology* 7 (10): R100. <https://doi.org/10.1186/gb-2006-7-10-r100>.
- Chaney, Stephen G., Sharon L. Campbell, Ekaterina Bassett, and Yibing Wu. 2005. "Recognition and Processing of Cisplatin- and Oxaliplatin-DNA Adducts." *Critical Reviews in Oncology/Hematology* 53 (1): 3–11. <https://doi.org/10.1016/j.critrevonc.2004.08.008>.
- Chapman, Erich G, Alethia A Hostetter, Maire F Osborn, Amanda L Miller, and Victoria J DeRose. 2011. "Binding of Kinetically Inert Metal Ions to RNA: The Case of Platinum(II)." *Metal Ions in Life Sciences* 9: 347–77.
- Cheff, Dorian M., and Matthew D. Hall. 2017. "A Drug of Such Damned Nature.1 Challenges and Opportunities in Translational Platinum Drug Research." *Journal of Medicinal Chemistry* 60 (11): 4517–32. <https://doi.org/10.1021/acs.jmedchem.6b01351>.
- Chow, Christine S., Carmen M. Barnes, and Stephen J. Lippard. 1995. "A Single HMG Domain in High-Mobility Group 1 Protein Binds to DNAs as Small as 20 Base Pairs Containing the Major Cisplatin Adduct." *Biochemistry* 34 (9): 2956–64. <https://doi.org/10.1021/bi00009a027>.

- Cierna, Zuzana, Vera Miskovska, Jan Roska, Dana Jurkovicova, Lucia Borszekova Pulzova, Zuzana Sestakova, Lenka Hurbanova, et al. 2020. "Increased Levels of XPA Might Be the Basis of Cisplatin Resistance in Germ Cell Tumours." *BMC Cancer* 20 (1): 17. <https://doi.org/10.1186/s12885-019-6496-1>.
- Cunningham, Rachael M., and Victoria J. DeRose. 2017. "Platinum Binds Proteins in the Endoplasmic Reticulum of *S. Cerevisiae* and Induces Endoplasmic Reticulum Stress." *ACS Chemical Biology* 12 (11): 2737–45. <https://doi.org/10.1021/acscchembio.7b00553>.
- Cunningham, Rachael M., Anna M. Hickey, Jesse W. Wilson, Kory J.I. Plakos, and Victoria J. DeRose. 2018. "Pt-Induced Crosslinks Promote Target Enrichment and Protection from Serum Nucleases." *Journal of Inorganic Biochemistry* 189 (December): 124–33. <https://doi.org/10.1016/j.jinorgbio.2018.09.007>.
- Dedduwa-Mudalige, Gayani N P, and Christine S Chow. 2015. "Cisplatin Targeting of Bacterial Ribosomal RNA Hairpins." *International Journal of Molecular Sciences* 16 (9): 21392–409. <https://doi.org/10.3390/ijms160921392>.
- Derenzini, Massimo, Lorenzo Montanaro, and Davide Trerè. 2009. "What the Nucleolus Says to a Tumour Pathologist." *Histopathology* 54 (6): 753–62. <https://doi.org/10.1111/j.1365-2559.2008.03168.x>.
- Derenzini, Massimo, Lorenzo Montanaro, and Davide Trerè. 2017. "Ribosome Biogenesis and Cancer." *Acta Histochemica* 119 (3). <https://doi.org/10.1016/j.acthis.2017.01.009>.
- Dhara, S.C. 1970. "A Rapid Method for the Synthesis of Cis-[Pt (NH₃)₂Cl₂]" 8: 193.
- Ding, Song, Xin Qiao, Jimmy Suryadi, Glen S. Marrs, Gregory L. Kucera, and Ulrich Bierbach. 2013. "Using Fluorescent Post-Labeling To Probe the Subcellular Localization of DNA-Targeted Platinum Anticancer Agents." *Angewandte Chemie International Edition* 52 (12): 3350–54. <https://doi.org/10.1002/anie.201210079>.
- Drygin, Denis, Amy Lin, Josh Bliesath, Caroline B. Ho, Sean E. O'Brien, Chris Proffitt, Mayuko Omori, et al. 2011. "Targeting RNA Polymerase I with an Oral Small Molecule CX-5461 Inhibits Ribosomal RNA Synthesis and Solid Tumor Growth." *Cancer Research* 71 (4): 1418–30. <https://doi.org/10.1158/0008-5472.CAN-10-1728>.
- Dyson, Paul J., and Gianni Sava. 2006. "Metal-Based Antitumour Drugs in the Post Genomic Era." *Dalton Transactions*, no. 16: 1929. <https://doi.org/10.1039/b601840h>.

- Englinger, Bernhard, Christine Pirker, Petra Heffeter, Alessio Terenzi, Christian R. Kowol, Bernhard K. Keppler, and Walter Berger. 2019. "Metal Drugs and the Anticancer Immune Response." *Chemical Reviews* 119 (2): 1519–1624. <https://doi.org/10.1021/acs.chemrev.8b00396>.
- Faivre, Sandrine, Denise Chan, Richard Salinas, Barbara Woynarowska, and Jan M. Woynarowski. 2003. "DNA Strand Breaks and Apoptosis Induced by Oxaliplatin in Cancer Cells." *Biochemical Pharmacology* 66 (2): 225–37. [https://doi.org/10.1016/S0006-2952\(03\)00260-0](https://doi.org/10.1016/S0006-2952(03)00260-0).
- Fanizzi, F. P., F. P. Intini, L. Maresca, G. Natile, R. Quaranta, M. Coluccia, L. Di Bari, D. Giordano, and M. A. Mariglió. 1987. "Biological Activity of Platinum Complexes Containing Chiral Centers on the Nitrogen or Carbon Atoms of a Chelate Diamine Ring." *Inorganica Chimica Acta* 137 (1): 45–51. [https://doi.org/10.1016/S0020-1693\(00\)87114-5](https://doi.org/10.1016/S0020-1693(00)87114-5).
- Farley-Barnes, Katherine I., Kathleen L. McCann, Lisa M. Ogawa, Janie Merkel, Yulia V. Surovtseva, and Susan J. Baserga. 2018. "Diverse Regulators of Human Ribosome Biogenesis Discovered by Changes in Nucleolar Number." *Cell Reports* 22 (7): 1923–34. <https://doi.org/10.1016/j.celrep.2018.01.056>.
- Frisch, MJ, HB Schlegel, GE Scuseria, MA Robb, JR Cheeseman, G Scalmani, V Barone, et al. 2016. *Gaussian09*. Gaussian Inc. Wallingford CT.
- Galanski, Markus, Afshin Yasemi, Susanna Slaby, Michael A. Jakupec, Vladimir B. Arion, Monika Rausch, Alexey A. Nazarov, and Bernhard K. Keppler. 2004. "Synthesis, Crystal Structure and Cytotoxicity of New Oxaliplatin Analogues Indicating That Improvement of Anticancer Activity Is Still Possible." *European Journal of Medicinal Chemistry* 39 (8): 707–14. <https://doi.org/10.1016/j.ejmech.2004.04.003>.
- Garbutcheon-Singh, K. Benjamin, Peter Leverett, Simon Myers, and Janice R. Aldrich-Wright. 2012. "Cytotoxic Platinum(II) Intercalators That Incorporate 1R,2R-Diaminocyclopentane." *Dalton Transactions* 42 (4): 918–26. <https://doi.org/10.1039/C2DT31323E>.
- Gilder, Andrew S, Phi M Do, Zunamys I Carrero, Angela M Cosman, Hanna J Broome, Venkatramreddy Velma, Luis a Martinez, and Michael D Hebert. 2011. "Coilin Participates in the Suppression of RNA Polymerase I in Response to Cisplatin-Induced DNA Damage." *Molecular Biology of the Cell* 22 (7): 1070–79. <https://doi.org/10.1091/mbc.E10-08-0731>.
- Grimaldi, Keith A., Simon R. McAdam, Robert L. Souhami, and John A. Hartley. 1994. "DNA Damage by Anti-Cancer Agents Resolved at the Nucleotide Level of a Single Copy Gene: Evidence for a Novel Binding Site for Cisplatin in Cells." *Nucleic Acids Research* 22 (12): 2311–17. <https://doi.org/10.1093/nar/22.12.2311>.

- Haddach, Mustapha, Michael K. Schwaebe, Jerome Michaux, Johnny Nagasawa, Sean E. O'Brien, Jeffrey P. Whitten, Fabrice Pierre, et al. 2012. "Discovery of CX-5461, the First Direct and Selective Inhibitor of RNA Polymerase I, for Cancer Therapeutics." *ACS Medicinal Chemistry Letters* 3 (7): 602–6.
<https://doi.org/10.1021/ml300110s>.
- Hamdane, Nouridine, Chelsea Herdman, Jean-Clement Mars, Victor Stefanovsky, Michel G Tremblay, and Tom Moss. 2015. "Depletion of the Cisplatin Targeted HMGB-Box Factor UBF Selectively Induces P53-Independent Apoptotic Death in Transformed Cells." *Oncotarget* 6 (29): 27519–36.
<https://doi.org/10.18632/oncotarget.4823>.
- Han, Chunhua, Amit Kumar Srivastava, Tiantian Cui, Qi-En Wang, and Altaf A. Wani. 2016. "Differential DNA Lesion Formation and Repair in Heterochromatin and Euchromatin." *Carcinogenesis* 37 (2): 129–38.
<https://doi.org/10.1093/carcin/bgv247>.
- Heinz, Sven, Christopher Benner, Nathanael Spann, Eric Bertolino, Yin C. Lin, Peter Laslo, Jason X. Cheng, Cornelis Murre, Harinder Singh, and Christopher K. Glass. 2010. "Simple Combinations of Lineage-Determining Transcription Factors Prime Cis-Regulatory Elements Required for Macrophage and B Cell Identities." *Molecular Cell* 38 (4): 576–89.
<https://doi.org/10.1016/j.molcel.2010.05.004>.
- Hernandez-Verdun, Danièle, Pascal Roussel, Marc Thiry, Valentina Sirri, and Denis L. J. Lafontaine. 2010. "The Nucleolus: Structure/Function Relationship in RNA Metabolism: Nucleolus." *Wiley Interdisciplinary Reviews: RNA* 1 (3): 415–31.
<https://doi.org/10.1002/wrna.39>.
- Horky, M, G Wurzer, V Kotala, M Anton, B Vojtěšek, J Vácha, and J Wesierska-Gadek. 2001. "Segregation of Nucleolar Components Coincides with Caspase-3 Activation in Cisplatin-Treated HeLa Cells." *Journal of Cell Science* 114 (Pt 4): 663–70.
- Hostetter, Alethia A, Maire F Osborn, and Victoria J DeRose. 2012. "Characterization of RNA-Pt Adducts Formed from Cisplatin Treatment of Saccharomyces Cerevisiae." *ACS Chem Biol.* 7 (1): 218–25.
<https://doi.org/10.1021/cb200279p.Characterization>.
- Hu, Jinchuan, Ogun Adebali, Sheera Adar, and Aziz Sancar. 2017. "Dynamic Maps of UV Damage Formation and Repair for the Human Genome." *Proceedings of the National Academy of Sciences*, June, 201706522.
<https://doi.org/10.1073/pnas.1706522114>.
- Hu, Jinchuan, Jason D Lieb, Aziz Sancar, Sheera Adar, Michael Leffak, and Pengbo Zhou. 2016. "Cisplatin DNA Damage and Repair Maps of the Human Genome at Single-Nucleotide Resolution." *PNAS* 113 (41): 11507–12.
<https://doi.org/10.1073/pnas.1614430113>.

- Jamieson, Elizabeth R, and Stephen J Lippard. 1999. "Structure, Recognition, and Processing of Cisplatin–DNA Adducts." *Medicinal Chemistry*.
<https://doi.org/10.1021/cr980421n>.
- Jerremalm, Elin, Pernilla Videhult, Gunvor Alvelius, William J. Griffiths, Tomas Bergman, Staffan Eksborg, and Hans Ehrsson. 2002. "Alkaline Hydrolysis of Oxaliplatin—Isolation and Identification of the Oxalato Monodentate Intermediate." *Journal of Pharmaceutical Sciences* 91 (10): 2116–21.
<https://doi.org/10.1002/jps.10201>.
- Johnstone, Timothy C, Ga Young Park, and Stephen J Lippard. 2014. "Understanding and Improving Platinum Anticancer Drugs--Phenanthriplatin." *Anticancer Research* 34 (1): 471–76.
- Johnstone, Timothy C., Kogularamanan Suntharalingam, and Stephen J. Lippard. 2016. "The Next Generation of Platinum Drugs: Targeted Pt(II) Agents, Nanoparticle Delivery, and Pt(IV) Prodrugs." *Chemical Reviews* 116 (5): 3436–86.
<https://doi.org/10.1021/acs.chemrev.5b00597>.
- Jordan, Peter, and Maria Carmo-Fonseca. 1998. "Cisplatin Inhibits Synthesis of Ribosomal RNA in Vivo." *Nucleic Acids Research* 26 (12): 2831–36.
<https://doi.org/10.1093/nar/26.12.2831>.
- Kalayda, Ganna V., Maximilian Kullmann, Markus Galanski, and Sabrina Gollos. 2017. "A Fluorescent Oxaliplatin Derivative for Investigation of Oxaliplatin Resistance Using Imaging Techniques." *JBIC Journal of Biological Inorganic Chemistry* 22 (8): 1295–1304. <https://doi.org/10.1007/s00775-017-1502-z>.
- Kapoor, Shobhna, Herbert Waldmann, and Slava Ziegler. 2016. "Novel Approaches to Map Small Molecule–Target Interactions." *Bioorganic & Medicinal Chemistry* 24 (15): 3232–45. <https://doi.org/10.1016/j.bmc.2016.05.020>.
- Keck, Michael V., and Stephen J. Lippard. 1992. "Unwinding of Supercoiled DNA by Platinum-Ethidium and Related Complexes." *Journal of the American Chemical Society* 114 (9): 3386–90. <https://doi.org/10.1021/ja00035a033>.
- Kelland, Lloyd. 2007. "The Resurgence of Platinum-Based Cancer Chemotherapy." *Nature Reviews. Cancer* 7 (8): 573–84. <https://doi.org/10.1038/nrc2167>.
- Kitteringham, Eolann, Dan Wu, Shane Cheung, Brendan Twamley, Donal F. O'Shea, and Darren M. Griffith. 2018. "Development of a Novel Carboplatin like Cytoplasmic Trackable near Infrared Fluorophore Conjugate via Strain-Promoted Azide Alkyne Cycloaddition." *Journal of Inorganic Biochemistry* 182 (May): 150–57.
<https://doi.org/10.1016/j.jinorgbio.2018.02.010>.

- Köberle, Beate, John R.W. Masters, John A. Hartley, and Richard D. Wood. 1999. "Defective Repair of Cisplatin-Induced DNA Damage Caused by Reduced XPA Protein in Testicular Germ Cell Tumours." *Current Biology* 9 (5): 273–78. [https://doi.org/10.1016/S0960-9822\(99\)80118-3](https://doi.org/10.1016/S0960-9822(99)80118-3).
- Kolb, Hartmuth C., M. G. Finn, and K. Barry Sharpless. 2001. "Click Chemistry: Diverse Chemical Function from a Few Good Reactions." *Angewandte Chemie (International Ed. in English)* 40 (11): 2004–21.
- Kresse, G, and J Furthmüller. 1996. "Efficient Iterative Schemes for Ab Initio Total-Energy Calculations Using a Plane-Wave Basis Set" 54: 11169.
- Kresse, G, and J Hafner. 1993. "Ab Initio Molecular Dynamics for Liquid Metals" 47: 558.
- Kresse, G., and J. Hafner. 1994. "Ab Initio Molecular-Dynamics Simulation of the Liquid-Metal--Amorphous-Semiconductor Transition in Germanium." *Physical Review B* 49 (20): 14251–69. <https://doi.org/10.1103/PhysRevB.49.14251>.
- Kresse, G, and D Joubert. 1999. "From Ultrasoft Pseudopotentials to the Projector Augmented-Wave Method" 59: 1758.
- Kruhlak, Michael, Elizabeth E. Crouch, Marika Orlov, Carolina Montaña, Stanislaw A. Gorski, André Nussenzweig, Tom Misteli, Robert D. Phair, and Rafael Casellas. 2007. "The ATM Repair Pathway Inhibits RNA Polymerase I Transcription in Response to Chromosome Breaks." *Nature* 447 (7145): 730–34. <https://doi.org/10.1038/nature05842>.
- Langmead, Ben, and Steven L Salzberg. 2012. "Fast Gapped-Read Alignment with Bowtie 2," 4.
- Larsen, Dorthe H., Flurina Hari, Julie A. Clapperton, Myriam Gwerder, Katrin Gutsche, Matthias Altmeyer, Stephanie Jungmichel, et al. 2014. "The NBS1–Treacle Complex Controls Ribosomal RNA Transcription in Response to DNA Damage." *Nature Cell Biology* 16 (8): 792–803. <https://doi.org/10.1038/ncb3007>.
- Malina, Jaroslav, Olga Novakova, Marie Vojtiskova, Giovanni Natile, and Viktor Brabec. 2007. "Conformation of DNA GG Intrastrand Cross-Link of Antitumor Oxaliplatin and Its Enantiomeric Analog." *Biophysical Journal* 93 (11): 3950–62. <https://doi.org/10.1529/biophysj.107.116996>.
- Martin, Marcel. 2011. "Cutadapt Removes Adapter Sequences from High-Throughput Sequencing Reads." *EMBnet.Journal* 17 (1): 10–12. <https://doi.org/10.14806/ej.17.1.200>.

- Mayr, Josef, Sonja Hager, Bettina Koblmüller, Matthias H. M. Klose, Katharina Holste, Britta Fischer, Karla Pelivan, et al. 2017. "EGFR-Targeting Peptide-Coupled Platinum(IV) Complexes." *JBIC Journal of Biological Inorganic Chemistry* 22 (4): 591–603. <https://doi.org/10.1007/s00775-017-1450-7>.
- McDevitt, Christine E., Matthew V. Yglesias, Austin M. Mroz, Emily C. Sutton, Min Chieh Yang, Christopher H. Hendon, and Victoria J. DeRose. 2019. "Monofunctional Platinum(II) Compounds and Nucleolar Stress: Is Phenanthriplatin Unique?" *JBIC Journal of Biological Inorganic Chemistry*, September. <https://doi.org/10.1007/s00775-019-01707-9>.
- McGurk, Claire J, Peter J McHugh, Michael J Tilby, Keith A Grimaldi, and John A Hartley. 2001. "Measurement of Covalent Drug-DNA Interactions at the Nucleotide Level in Cells at Pharmacologically Relevant Doses." In *Methods in Enzymology*, 340:358–76. Elsevier. [https://doi.org/10.1016/S0076-6879\(01\)40431-9](https://doi.org/10.1016/S0076-6879(01)40431-9).
- McKeage, M J, T Hsu, D Screnci, G Haddad, and B C Baguley. 2001. "Nucleolar Damage Correlates with Neurotoxicity Induced by Different Platinum Drugs." *British Journal of Cancer* 85 (8): 1219–25. <https://doi.org/10.1054/bjoc.2001.2024>.
- Melnikov, Sergey V, Dieter Soll, Thomas A Steitz, and Yury S Polikanov. 2016. "Insights into RNA Binding by the Anticancer Drug Cisplatin from the Crystal Structure of Cisplatin-Modified Ribosome." *Nucleic Acids Research* 44 (10): 4978–87. <https://doi.org/10.1093/nar/gkw246>.
- Moghaddam, Alan D., Jonathan D. White, Rachael M. Cunningham, Andrea N. Loes, Michael M. Haley, and Victoria J. DeRose. 2015. "Convenient Detection of Metal–DNA, Metal–RNA, and Metal–Protein Adducts with a Click-Modified Pt(II) Complex." *Dalton Trans.* 44 (8): 3536–39. <https://doi.org/10.1039/C4DT02649G>.
- Nehmé, A, R Baskaran, S Nebel, D Fink, S B Howell, J Y J Wang, and R D Christen. 1999. "Induction of JNK and C-Abl Signalling by Cisplatin and Oxaliplatin in Mismatch Repair-Proficient and -Deficient Cells." *British Journal of Cancer* 79 (7–8): 1104–10. <https://doi.org/10.1038/sj.bjc.6690176>.
- Németh, Attila, and Ingrid Grummt. 2018. "Dynamic Regulation of Nucleolar Architecture." *Current Opinion in Cell Biology* 52: 105–11. <https://doi.org/10.1016/j.ceb.2018.02.013>.
- Nicolas, Emilien, Pascaline Parisot, Celina Pinto-Monteiro, Roxane de Walque, Christophe De Vleeschouwer, and Denis L. J. Lafontaine. 2016. "Involvement of Human Ribosomal Proteins in Nucleolar Structure and P53-Dependent Nucleolar Stress." *Nature Communications* 7 (June): 11390. <https://doi.org/10.1038/ncomms11390>.

- OECD. 1995. *Test No. 107: Partition Coefficient (n-Octanol/Water): Shake Flask Method, OECD Guidelines for the Testing of Chemicals, Section 1*. Paris: OECD Publishing. <https://www.oecd-ilibrary.org/content/publication/9789264069626-en>.
- Osborn, Maire F, Jonathan D White, Michael M Haley, and Victoria J DeRose. 2014. “Platinum-RNA Modifications Following Drug Treatment in *S. Cerevisiae* Identified by Click Chemistry and Enzymatic Mapping.” *ACS Chemical Biology*, no. 11. <https://doi.org/10.1021/cb500395z>.
- Ozdian, Tomas, Dusan Holub, Zuzana Maceckova, Lakshman Varanasi, Gabriela Rylova, Jiri Rehulka, Jana Vaclavkova, et al. 2017. “Proteomic Profiling Reveals DNA Damage, Nucleolar and Ribosomal Stress Are the Main Responses to Oxaliplatin Treatment in Cancer Cells.” *Journal of Proteomics* 162 (June): 73–85. <https://doi.org/10.1016/j.jprot.2017.05.005>.
- Pansini, F, A Neto, M de Campos, and de Aquino R. 2017. “Effects of All-Electron Basis Sets and the Scalar Relativistic Corrections in the Structure and Electronic Properties of Niobium Clusters” 121 (30): 5728–34.
- Pederson, T. 2011. “The Nucleolus.” *Cold Spring Harbor Perspectives in Biology* 3 (3): a000638–a000638. <https://doi.org/10.1101/cshperspect.a000638>.
- Peltonen, Karita, Lauren Colis, Hester Liu, Sari Jäämaa, Henna M. Moore, Juulia Enbäck, Pirjo Laakkonen, et al. 2010. “Identification of Novel P53 Pathway Activating Small-Molecule Compounds Reveals Unexpected Similarities with Known Therapeutic Agents.” Edited by Joseph Alan Bauer. *PLoS ONE* 5 (9): e12996. <https://doi.org/10.1371/journal.pone.0012996>.
- Peltonen, Karita, Lauren Colis, Hester Liu, Rishi Trivedi, Michael S. Moubarek, Henna M. Moore, Baoyan Bai, Michelle A. Rudek, Charles J. Bieberich, and Marikki Laiho. 2014. “A Targeting Modality for Destruction of RNA Polymerase I That Possesses Anticancer Activity.” *Cancer Cell* 25 (1): 77–90. <https://doi.org/10.1016/j.ccr.2013.12.009>.
- Perdew, JP, K Burke, and M Ernzerhof. 1996. “Generalized Gradient Approximation Made Simple” 77: 3865–68.
- . 1997. “Errata: Generalized Gradient Approximation Made Simple” 78: 1396.
- Pickard, Amanda J., and Ulrich Bierbach. 2013. “The Cell’s Nucleolus: An Emerging Target for Chemotherapeutic Intervention.” *ChemMedChem* 8 (9): 1441–49. <https://doi.org/10.1002/cmdc.201300262>.
- Plakos, Kory, and Victoria J. DeRose. 2017. “Mapping Platinum Adducts on Yeast Ribosomal RNA Using High-Throughput Sequencing.” *Chemical Communications* 53 (95): 12746–49. <https://doi.org/10.1039/C7CC06708A>.

- Powell, James Rees, Mark Richard Bennett, Katie Ellen Evans, Shirong Yu, Richard Michael Webster, Raymond Waters, Nigel Skinner, and Simon Huw Reed. 2015. "3D-DIP-Chip: A Microarray-Based Method to Measure Genomic DNA Damage." *Scientific Reports* 5 (1). <https://doi.org/10.1038/srep07975>.
- Qiao, Xin, Song Ding, Fang Liu, Gregory L. Kucera, and Ulrich Bierbach. 2014. "Investigating the Cellular Fate of a DNA-Targeted Platinum-Based Anticancer Agent by Orthogonal Double-Click Chemistry." *JBIC Journal of Biological Inorganic Chemistry* 19 (3): 415–26. <https://doi.org/10.1007/s00775-013-1086-1>.
- Ramu, Vanitha, Srishti Gautam, Aditya Garai, Paturu Kondaiah, and Akhil R. Chakravarty. 2018. "Glucose-Appended Platinum(II)-BODIPY Conjugates for Targeted Photodynamic Therapy in Red Light." *Inorganic Chemistry* 57 (4): 1717–26. <https://doi.org/10.1021/acs.inorgchem.7b02249>.
- Reister, Emily. 2018. "High-Throughput Sequencing for Investigation of RNA Targets of Pt(II) Chemotherapy Drugs." Doctoral Dissertation, Eugene, OR: University of Oregon.
- Rijal, Keshab, Xun Bao, and Christine S. Chow. 2014. "Amino Acid-Linked Platinum(II) Analogues Have Altered Specificity for RNA Compared to Cisplatin." *Chemical Communications* 50 (30): 3918–20. <https://doi.org/10.1039/C3CC49035A>.
- Rijal, Keshab, and Christine S. Chow. 2007. "A New Role for Cisplatin: Probing Ribosomal RNA Structure." *Chemical Communications* 0 (1). <https://doi.org/10.1039/B816633A>.
- . 2008. "A New Role for Cisplatin: Probing Ribosomal RNA Structure." *Chem. Commun.*, no. 1: 107–9. <https://doi.org/10.1039/B816633A>.
- Ritz, Christian, Florent Baty, Jens C. Streibig, and Daniel Gerhard. 2015. "Dose-Response Analysis Using R." *PLOS ONE* 10 (12): e0146021. <https://doi.org/10.1371/journal.pone.0146021>.
- Rodriguez, Raphaël, and Kyle M Miller. 2014. "Unravelling the Genomic Targets of Small Molecules Using High-Throughput Sequencing." *Nature Reviews Genetics* 15 (12): 783–96. <https://doi.org/10.1038/nrg3796>.
- Rosenberg, Barnett, Loretta Van Camp, Eugene Grimley, and Andrew Thomson. 1967. "The Inhibition of Growth or Cell Division in Escherichia Coli by Different Ionic Species of Platinum (IV) Complexes." *The Journal of Biological Chemistry* 242 (6): 1347–52.
- Rosenberg, Barnett, Loretta Van Camp, and Thomas Krigas. 1965. "Inhibition of Cell Division in Escherichia Coli by Electrolysis Products from a Platinum Electrode." *Nature* 205 (4972): 698–99. <https://doi.org/10.1038/205698a0>.

- Rosenberg, Barnett, Loretta Van Camp, James E. Trosko, and Virginia H. Mansour. 1969. "Platinum Compounds: A New Class of Potent Antitumour Agents." *Nature* 222 (5191): 385–86. <https://doi.org/10.1038/222385a0>.
- Rubbi, Carlos P., and Jo Milner. 2003. "Disruption of the Nucleolus Mediates Stabilization of P53 in Response to DNA Damage and Other Stresses." *EMBO Journal* 22 (22): 6068–77. <https://doi.org/10.1093/emboj/cdg579>.
- Rueden, Curtis T., Johannes Schindelin, Mark C. Hiner, Barry E. DeZonia, Alison E. Walter, Ellen T. Arena, and Kevin W. Eliceiri. 2017. "ImageJ2: ImageJ for the next Generation of Scientific Image Data." *BMC Bioinformatics* 18 (1): 529. <https://doi.org/10.1186/s12859-017-1934-z>.
- Sani, Elaine, and Ross D. Hannan. 2009. "The Role of UBF in Regulating the Structure and Dynamics of Transcriptionally Active RDNA Chromatin." *Epigenetics* 4 (6): 374–82. <https://doi.org/10.4161/epi.4.6.9449>.
- Saunders, Adam M., and Victoria J DeRose. 2016. "Beyond Mg²⁺: Functional Interactions between RNA and Transition Metals." *Current Opinion in Chemical Biology, Biocatalysis and biotransformation * Bioinorganic chemistry*, 31 (April): 153–59. <https://doi.org/10.1016/j.cbpa.2016.02.015>.
- Schindelin, Johannes, Ignacio Arganda-Carreras, Erwin Frise, Verena Kaynig, Mark Longair, Tobias Pietzsch, Stephan Preibisch, et al. 2012. "Fiji: An Open-Source Platform for Biological-Image Analysis." *Nature Methods* 9 (7): 676–82. <https://doi.org/10.1038/nmeth.2019>.
- Scott, Daniel, and Marlene Oeffinger. 2016. "Nucleolin and Nucleophosmin: Nucleolar Proteins with Multiple Functions in DNA Repair." [Http://Dx.Doi.Org/10.1139/Bcb-2016-0068](http://Dx.Doi.Org/10.1139/Bcb-2016-0068) 94 (5): 419–32. <https://doi.org/10.1139/bcb-2016-0068>.
- Shav-Tal, Yaron, Janna Blechman, Xavier Darzacq, Cristina Montagna, Billy T. Dye, James G. Patton, Robert H. Singer, and Dov Zipori. 2005. "Dynamic Sorting of Nuclear Components into Distinct Nucleolar Caps during Transcriptional Inhibition." *Molecular Biology of the Cell* 16 (5): 2395–2413. <https://doi.org/10.1091/mbc.e04-11-0992>.
- Shu, Xiaoting, Xushen Xiong, Jinghui Song, Chuan He, and Chengqi Yi. 2016. "Base-Resolution Analysis of Cisplatin-DNA Adducts at the Genome Scale." *Angewandte Chemie International Edition* 55 (46): 14246–49. <https://doi.org/10.1002/anie.201607380>.
- Siddik, Zahid H. 2003. "Cisplatin: Mode of Cytotoxic Action and Molecular Basis of Resistance." *Oncogene* 22 (47): 7265–79. <https://doi.org/10.1038/sj.onc.1206933>.

- Siew, Yin-Yin, Soek-Ying Neo, Hui-Chuing Yew, Shun-Wei Lim, Yi-Cheng Ng, Si-Min Lew, Wei-Guang Seetoh, See-Voon Seow, and Hwee-Ling Koh. 2015. "Oxaliplatin Regulates Expression of Stress Ligands in Ovarian Cancer Cells and Modulates Their Susceptibility to Natural Killer Cell-Mediated Cytotoxicity." *International Immunology* 27 (12): 621–32. <https://doi.org/10.1093/intimm/dxv041>.
- Sluis, Marjolein van, and Brian McStay. 2014. "Ribosome Biogenesis: Achilles Heel of Cancer?" *Genes & Cancer* 5 (5–6): 152–53.
- . 2015. "A Localized Nucleolar DNA Damage Response Facilitates Recruitment of the Homology-Directed Repair Machinery Independent of Cell Cycle Stage." *Genes & Development* 29 (11): 1151–63. <https://doi.org/10.1101/gad.260703.115>.
- . 2017. "Nucleolar Reorganization in Response to RDNA Damage." *Current Opinion in Cell Biology* 46: 81–86. <https://doi.org/10.1016/j.ceb.2017.03.004>.
- Smirnov, Evgeny, Matúš Hornáček, Lubomír Kováčik, Tomáš Mazel, Adam Schröfel, Silvie Svidenská, Magdalena Skalníková, Eva Bartová, Dušan Cmarko, and Ivan Raška. 2016. "Reproduction of the FC/DFC Units in Nucleoli." *Nucleus* 7 (2): 203–15. <https://doi.org/10.1080/19491034.2016.1157674>.
- Sutton, Emily C., Christine E. McDevitt, Jack Y. Prochnau, Matthew V. Yglesias, Austin M. Mroz, Min Chieh Yang, Rachael M. Cunningham, Christopher H. Hendon, and Victoria J. DeRose. 2019. "Nucleolar Stress Induction by Oxaliplatin and Derivatives." *Journal of the American Chemical Society* 141 (46): 18411–15. <https://doi.org/10.1021/jacs.9b10319>.
- Sutton, Emily C., Christine E. McDevitt, Matthew V. Yglesias, Rachael M. Cunningham, and Victoria J. DeRose. 2019. "Tracking the Cellular Targets of Platinum Anticancer Drugs: Current Tools and Emergent Methods." *Inorganica Chimica Acta*, June, 118984. <https://doi.org/10.1016/j.ica.2019.118984>.
- Terenzi, Alessio, Christine Pirker, Bernhard K. Keppler, and Walter Berger. 2016. "Anticancer Metal Drugs and Immunogenic Cell Death." *Journal of Inorganic Biochemistry* 165 (December): 71–79. <https://doi.org/10.1016/j.jinorgbio.2016.06.021>.
- Toscano, Florent, Béatrice Parmentier, Zineb El Fajoui, Yann Estornes, Jean-Alain Chayvialle, Jean-Christophe Saurin, and Jacques Abello. 2007. "P53 Dependent and Independent Sensitivity to Oxaliplatin of Colon Cancer Cells." *Biochemical Pharmacology* 74 (3): 392–406. <https://doi.org/10.1016/j.bcp.2007.05.001>.
- Treiber, D K, X Zhai, H M Jantzen, and J M Essigmann. 1994. "Cisplatin-DNA Adducts Are Molecular Decoys for the Ribosomal RNA Transcription Factor HUBF (Human Upstream Binding Factor)." *Proceedings of the National Academy of Sciences of the United States of America* 91 (12): 5672–76. <https://doi.org/10.1073/pnas.91.12.5672>.

- Tsai, Robert Y L, and Thoru Pederson. 2014. "Connecting the Nucleolus to the Cell Cycle and Human Disease." *FASEB Journal : Official Publication of the Federation of American Societies for Experimental Biology* 28 (8): 3290–96. <https://doi.org/10.1096/fj.14-254680>.
- Urankar, Damijana, and Janez Košmrlj. 2010. "Preparation of Diazenecarboxamide–Carboplatin Conjugates by Click Chemistry." *Inorganica Chimica Acta* 363 (14): 3817–22. <https://doi.org/10.1016/j.ica.2010.07.031>.
- Walt, Stéfan van der, Johannes L. Schönberger, Juan Nunez-Iglesias, François Boulogne, Joshua D. Warner, Neil Yager, Emmanuelle Gouillart, and Tony Yu. 2014. "Scikit-Image: Image Processing in Python." *PeerJ* 2 (June): e453. <https://doi.org/10.7717/peerj.453>.
- Wang, Dong, and Stephen J. Lippard. 2005. "Cellular Processing of Platinum Anticancer Drugs." *Nature Reviews Drug Delivery* 4 (4): 307–20. <https://doi.org/10.1038/nrd1691>.
- Wei, M, S M Cohen, A P Silverman, and S J Lippard. 2001. "Effects of Spectator Ligands on the Specific Recognition of Intrastrand Platinum-DNA Cross-Links by High Mobility Group Box and TATA-Binding Proteins." *The Journal of Biological Chemistry* 276 (42): 38774–80. <https://doi.org/10.1074/jbc.M106374200>.
- Wei, Ting, Saman M. Najmi, Hester Liu, Karita Peltonen, Alena Kucerova, David A. Schneider, and Marikki Laiho. 2018. "Small-Molecule Targeting of RNA Polymerase I Activates a Conserved Transcription Elongation Checkpoint." *Cell Reports* 23 (2): 404–14. <https://doi.org/10.1016/j.celrep.2018.03.066>.
- Welsh, Carey, Roger Day, Claire McGurk, John R.W. Masters, Richard D. Wood, and Beate Köberle. 2004. "Reduced Levels of XPA, ERCC1 and XPF DNA Repair Proteins in Testis Tumor Cell Lines: NER Proteins in Testis Tumor Cells." *International Journal of Cancer* 110 (3): 352–61. <https://doi.org/10.1002/ijc.20134>.
- Wexselblatt, Ezequiel, Eylon Yavin, and Dan Gibson. 2012. "Cellular Interactions of Platinum Drugs." *Inorganica Chimica Acta* 393: 75–83. <https://doi.org/10.1016/j.ica.2012.07.013>.
- White, Jonathan D., Michael M. Haley, and Victoria J. DeRose. 2016. "Multifunctional Pt(II) Reagents: Covalent Modifications of Pt Complexes Enable Diverse Structural Variation and In-Cell Detection." *Accounts of Chemical Research* 49 (1): 56–66. <https://doi.org/10.1021/acs.accounts.5b00322>.

- Wilson, Justin J., and Stephen J. Lippard. 2012. "In Vitro Anticancer Activity of Cis-Diammineplatinum(II) Complexes with β -Diketonate Leaving Group Ligands." *Journal of Medicinal Chemistry* 55 (11): 5326–36. <https://doi.org/10.1021/jm3002857>.
- . 2014. "Synthetic Methods for the Preparation of Platinum Anticancer Complexes." *Chemical Reviews* 114 (8): 4470–95. <https://doi.org/10.1021/cr4004314>.
- Wiltshaw, Eve. 1979. "Cisplatin in the Treatment of Cancer." *Platinum Metals Review* 23 (3): 90–97.
- Wirth, Regina, Jonathan D. White, Alan D. Moghaddam, Aurora L. Ginzburg, Lev N. Zakharov, Michael M. Haley, and Victoria J. DeRose. 2015. "Azide vs. Alkyne Functionalization in Pt(II) Complexes for Post-Treatment Click Modification: Solid State Structure, Fluorescent Labeling, and Cellular Fate." *Journal of the American Chemical Society*, no. Ii: jacs.5b09108. <https://doi.org/10.1021/jacs.5b09108>.
- Woods, Simone J., Katherine M. Hannan, Richard B. Pearson, and Ross D. Hannan. 2015. "The Nucleolus as a Fundamental Regulator of the P53 Response and a New Target for Cancer Therapy." *Biochimica et Biophysica Acta (BBA) - Gene Regulatory Mechanisms* 1849 (7): 821–29. <https://doi.org/10.1016/j.bbagr.2014.10.007>.
- Woynarowski, J M, S Faivre, M C Herzig, B Arnett, W G Chapman, A V Trevino, E Raymond, et al. 2000. "Oxaliplatin-Induced Damage of Cellular DNA." *Molecular Pharmacology* 58 (5): 920–27. <https://doi.org/10.1124/MOL.58.5.920>.
- Woynarowski, Jan M., William G. Chapman, Cheryl Napier, Maryanne C. S. Herzig, Paul E. Juniewicz, Alex V. Trevino, Eric Raymond, et al. 1998. "Sequence- and Region-Specificity of Oxaliplatin Adducts in Naked and Cellular DNA." *Molecular Pharmacology* 54 (5): 770–77. <https://doi.org/10.1124/mol.54.5.770>.
- Xiaoquan Zhai, ‡, § Holger Beckmann ‖, § Hans-Michael Jantzen ⊥ and, and ‡ John M. Essigmann*. 1998. "Cisplatin–DNA Adducts Inhibit Ribosomal RNA Synthesis by Hijacking the Transcription Factor Human Upstream Binding Factor†." <https://doi.org/10.1021/BI981708H>.
- Xue, Xuling, Chengcheng Zhu, Huachao Chen, Yang Bai, Xiangchao Shi, Yang Jiao, Zhongyan Chen, Yupeng Miao, Weijiang He, and Zijian Guo. 2017. "A New Approach to Sensitize Antitumor Monofunctional Platinum(II) Complexes via Short Time Photo-Irradiation." *Inorganic Chemistry* 56 (7): 3754–62. <https://doi.org/10.1021/acs.inorgchem.6b02148>.

- Yang, Kai, Ming Wang, Yuzheng Zhao, Xuxu Sun, Yi Yang, Xie Li, Aiwu Zhou, et al. 2016. "A Redox Mechanism Underlying Nucleolar Stress Sensing by Nucleophosmin." *Nature Communications* 7 (November): 13599. <https://doi.org/10.1038/ncomms13599>.
- Yang, Kai, Jie Yang, and Jing Yi. 2018. "Nucleolar Stress: Hallmarks, Sensing Mechanism and Diseases." *Cell Stress* 2 (6): 125–40. <https://doi.org/10.15698/cst2018.06.139>.
- Yang, Yanyan, Ogun Adebali, Gang Wu, Christopher P. Selby, Yi-Ying Chiou, Naim Rashid, Jinchuan Hu, John B. Hogenesch, and Aziz Sancar. 2018. "Cisplatin-DNA Adduct Repair of Transcribed Genes Is Controlled by Two Circadian Programs in Mouse Tissues." *Proceedings of the National Academy of Sciences* 115 (21): E4777–85. <https://doi.org/10.1073/pnas.1804493115>.
- Yao, Xiyuan, Christopher M. Tracy, and Ulrich Bierbach. 2019. "Cysteine-Directed Bioconjugation of a Platinum(II)–Acridine Anticancer Agent." *Inorganic Chemistry* 58 (1): 43–46. <https://doi.org/10.1021/acs.inorgchem.8b02717>.
- Yimit, Askar, Ogun Adebali, Aziz Sancar, and Yuchao Jiang. 2019. "Differential Damage and Repair of DNA-Adducts Induced by Anti-Cancer Drug Cisplatin across Mouse Organs." *Nature Communications* 10 (1). <https://doi.org/10.1038/s41467-019-08290-2>.
- Yu, Guangchuang, Li-Gen Wang, Yanyan Han, and Qing-Yu He. 2012. "ClusterProfiler: An R Package for Comparing Biological Themes Among Gene Clusters." *OMICS: A Journal of Integrative Biology* 16 (5): 284–87. <https://doi.org/10.1089/omi.2011.0118>.
- Yu, Guangchuang, Li-Gen Wang, and Qing-Yu He. 2015. "ChIPseeker: An R/Bioconductor Package for ChIP Peak Annotation, Comparison and Visualization." *Bioinformatics* 31 (14): 2382–83. <https://doi.org/10.1093/bioinformatics/btv145>.
- Yu, Yang, Pengcheng Wang, Yuxiang Cui, and Yinsheng Wang. 2018. "Chemical Analysis of DNA Damage." *Analytical Chemistry* 90 (1): 556–76. <https://doi.org/10.1021/acs.analchem.7b04247>.
- Yuan, Youyong, Ryan T. K. Kwok, Ben Zhong Tang, and Bin Liu. 2014. "Targeted Theranostic Platinum(IV) Prodrug with a Built-In Aggregation-Induced Emission Light-Up Apoptosis Sensor for Noninvasive Early Evaluation of Its Therapeutic Responses in Situ." *Journal of the American Chemical Society* 136 (6): 2546–54. <https://doi.org/10.1021/ja411811w>.

Zacharioudakis, Emmanouil, Poonam Agarwal, Alexandra Bartoli, Nathan Abell, Lavaniya Kunalingam, Valérie Bergoglio, Blerta Xhemalce, Kyle M. Miller, and Raphaël Rodriguez. 2017. "Chromatin Regulates Genome Targeting with Cisplatin." *Angewandte Chemie* 129 (23): 6583–87. <https://doi.org/10.1002/ange.201701144>.

Zhang, Yong, Tao Liu, Clifford A. Meyer, Jérôme Eeckhoute, David S. Johnson, Bradley E. Bernstein, Chad Nusbaum, et al. 2008. "Model-Based Analysis of ChIP-Seq (MACS)." *Genome Biology* 9 (9): R137. <https://doi.org/10.1186/gb-2008-9-9-r137>.